

EUROPEAN ORGANISATION FOR NUCLEAR RESEARCH (CERN)



Submitted to: Phys. Rev. D.



CERN-PH-EP-2015-247
17th March 2018

Search for dark matter produced in association with a Higgs boson decaying to two bottom quarks in pp collisions at $\sqrt{s} = 8$ TeV with the ATLAS detector

ATLAS Collaboration

Abstract

This article reports on a search for dark matter pair production in association with a Higgs boson decaying to a pair of bottom quarks, using data from 20.3 fb^{-1} of pp collisions at a center-of-mass energy of 8 TeV collected by the ATLAS detector at the LHC. The decay of the Higgs boson is reconstructed as a high-momentum $b\bar{b}$ system with either a pair of small-radius jets, or a single large-radius jet with substructure. The observed data are found to be consistent with the expected Standard Model backgrounds. Model-independent upper limits are placed on the visible cross-sections for events with a Higgs boson decaying into $b\bar{b}$ and large missing transverse momentum with thresholds ranging from 150 GeV to 400 GeV. Results are interpreted using a simplified model with a Z' gauge boson decaying into different Higgs bosons predicted in a two-Higgs-doublet model, of which the heavy pseudoscalar Higgs decays into a pair of dark matter particles. Exclusion limits are also presented for the mass scales of various effective field theory operators that describe the interaction between dark matter particles and the Higgs boson.

1 Introduction

Although dark matter (DM) contributes a large component of the mass-energy of the universe, its properties and interactions with known particles remain unknown [1]. In light of this unsolved puzzle, searches for DM pair-produced at collider experiments provide important information complementary to direct and indirect detection experiments in order to determine whether a signal observed experimentally indeed stems from DM [2].

The leading hypothesis suggests that most of the DM is in the form of stable, electrically neutral, massive particles, i.e., Weakly Interacting Massive Particles [3]. This scenario gives rise to a potential signature at a proton-proton collider where one or more Standard Model (SM) particles, “X”, is produced and detected, recoiling against missing transverse momentum (with magnitude E_T^{miss}) associated with the non-interacting DM. Recent searches at the Large Hadron Collider (LHC) consider “X” to be a hadronic jet [4, 5], heavy-flavor jet [6, 7], photon [8, 9], or W/Z boson [10, 11]. The discovery of the Higgs boson h [12, 13] provides a new opportunity to search for DM production via the $h + E_T^{\text{miss}}$ signature [14–16]. In contrast to most of the aforementioned probes, the visible Higgs boson is unlikely to have been radiated from an initial-state quark or gluon, and the signal would give insight into the structure of DM coupling to SM particles.

Two approaches are commonly used to model generic processes yielding a final state with a particle X recoiling against a system of non-interacting particles. One option is to use non-renormalizable operators in an effective field theory (EFT) framework [17], where particles that mediate the interactions between DM and SM particles are too heavy to be produced directly in the experiment and are described by contact operators. Alternatively, simplified models that are characterized by a minimal number of renormalizable interactions, and hence explicitly include the particles at higher masses, can be used [18]. The EFT approach is more model-independent, but is not valid when a typical momentum transfer of the process approaches the energy scale of the contact operators that describe the interaction. Simplified models do not suffer from these concerns, but include more assumptions by design and are therefore less generic. The two approaches are thus complementary and both are included in this analysis.

2 Signal models and analysis strategy

Using the EFT approach, a set of models described by effective operators at different dimensions is considered, as shown in Figure 1(a). Following the notation in Ref. [14], the effective operators in ascending order of their dimensions are:

$$\lambda |\chi|^2 |H|^2 \quad (\text{Scalar DM, dimension-4}) \quad (1)$$

$$\frac{1}{\Lambda} \bar{\chi} i \gamma_5 \chi |H|^2 \quad (\text{Fermionic DM, dimension-5}) \quad (2)$$

$$\frac{1}{\Lambda^2} \bar{\chi}^\dagger \partial^\mu \chi H^\dagger D_\mu H \quad (\text{Scalar DM, dimension-6}) \quad (3)$$

$$\frac{1}{\Lambda^4} \bar{\chi} \gamma^\mu \chi B_{\mu\nu} H^\dagger D^\nu H \quad (\text{Fermionic DM, dimension-8}) \quad (4)$$

Here χ is the DM particle, which is a gauge singlet under $SU(3)_C \times SU(2)_L \times U(1)_Y$ and may be a scalar or a fermion as specified, $D_\mu(\cdot)$ is the covariant derivative for the full gauge group, and $B_{\mu\nu}$ is the $U(1)_Y$ field strength tensor. The parameters of these models are the DM particle mass m_χ , and the coupling parameter λ or the suppression scale Λ of the heavy mediator that is not directly produced but described by a contact operator in the EFT framework.

A simplified model is also considered which contains a Z' gauge boson and two Higgs fields resulting in five Higgs bosons (often called the two-Higgs-doublet model, 2HDM) [15], where the DM particle is coupled to the heavy pseudoscalar Higgs boson A , as shown in Figure 1(b). In this model (Z' -2HDM), the Z' boson is produced resonantly and decays into h and A in a Type 2 two-Higgs-doublet model [19], where h is the scalar corresponding to the observed Higgs boson, and A has a large branching ratio to DM. The Z' boson can also decay to a Higgs boson and a Z boson, which in turn decays to a pair of neutrinos, thus mimicking the expected signature. While the Ah decay mode is dominant for most of the parameter space probed in this analysis, the Zh decay mode is an important source of signal events at large $\tan\beta$ (the ratio of the vacuum expectation values for the two-Higgs-doublets). Both sources of a Higgs boson plus missing transverse momentum are included for the analysis of this model. The results presented are for the alignment limit, in which the scalar Higgs mixing angle α is related to β by $\alpha = \beta - \pi/2$. Only regions of parameter space consistent with precision electroweak constraints on the ρ_0 parameter [20] and with constraints from direct searches for dijet resonances [21–23] are considered. The Z' boson does not couple to leptons in this model, avoiding potentially stringent constraints from dilepton searches. As the A boson is produced on-shell and decays into DM, the mass of the DM particle does not affect the kinematic properties or cross-section of the signal process when it is below half of the A boson mass. Hence, the Z' -2HDM model is interpreted in the parameter spaces of Z' mass ($m_{Z'}$), A mass (m_A), and $\tan\beta$, with the Z' gauge coupling fixed to its 95% confidence level (CL) upper limit per Z' mass and $\tan\beta$ value from the aforementioned electroweak and dijet search constraints.

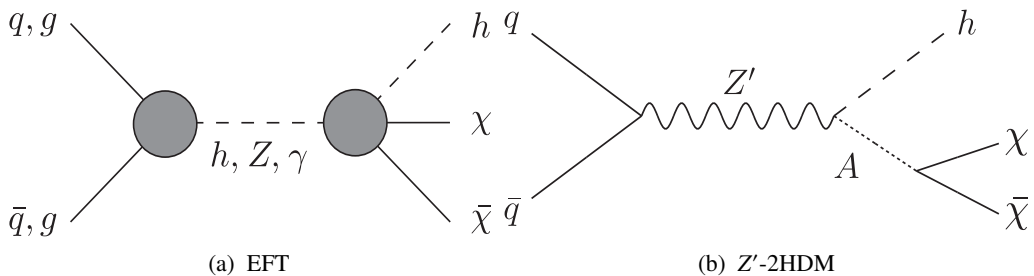


Figure 1: Feynman diagrams for (a) the EFT and (b) the Z' -2HDM models. The χ is the DM particle. The h is the 125 GeV observed Higgs boson. In (a), the left dark circle denotes the coupling from $q\bar{q}$ or gg to an electroweak boson (h, Z, γ) that mediates the DM+ h production, and the right dark circle represents the contact operator in the EFT framework between DM, the Higgs boson, and the mediator. In (b), the A is the heavy pseudoscalar in the two-Higgs-doublet model.

This article describes the search for DM pair production in association with a Higgs boson using the full 2012 ATLAS data set corresponding to 20.3 fb^{-1} of pp collisions with center-of-mass energy $\sqrt{s} = 8 \text{ TeV}$. The final state is a Higgs boson decaying to a pair of bottom quarks and large missing transverse momentum. Two Higgs boson reconstruction techniques are presented that are complementary in their acceptance. The first, “resolved” technique reconstructs Higgs boson candidates from pairs of nearby anti- k_t jets [24] each reconstructed with radius parameter $R = 0.4$ and each identified as having a b -

hadron within the jet using a multivariate b -tagging algorithm [25]. This resolved technique offers good efficiency over a wide kinematic range with the Higgs boson transverse momentum p_T between 150 and 450 GeV. However, for a Higgs boson with $p_T \gtrsim 450$ GeV, the high momentum (“boost”) of the Higgs boson causes the two jet cones containing the b - and \bar{b} -quarks from the Higgs boson decay to significantly overlap, leading to a decrease in the reconstruction efficiency of the two b -tagged anti- k_t jets with $R = 0.4$. This motivates the use of the same “boosted” Higgs boson reconstruction technique in Ref. [26]. The acceptance for these higher- p_T Higgs bosons is maintained through the use of the internal structure of jets, known as “jet substructure” techniques, and the subjet b -tagging algorithms. The Higgs boson candidate is reconstructed as a single anti- k_t $R = 1.0$ jet, trimmed [27] with subjet radius parameter $R_{\text{sub}} = 0.3$ and subjet transverse momentum fraction $p_{T,i}/p_{\text{T}}^{\text{jet}} < 0.05$, where $p_{T,i}$ is the transverse momentum of the i -th subjet and $p_{\text{T}}^{\text{jet}}$ is the p_T of the untrimmed jet [28, 29]. This $R = 1.0$ jet must be associated with two b -tagged anti- k_t $R = 0.3$ jets reconstructed only from charged particle tracks (track-jets) [30]. The use of track-jets with a smaller R parameter allows the decay products of Higgs bosons with higher p_T to be reconstructed.

The interplay between the two sets of models and analysis methods has been studied. In the Z' -2HDM simplified model, the resonant production and decay of the Z' boson leads to clear peaks in the $E_{\text{T}}^{\text{miss}}$ spectra, the positions of which depend on the Z' and A mass values. In most of the parameter space probed with Z' mass between 600 and 1400 GeV, and A mass between 300 and 800 GeV (where kinematically allowed), a higher signal sensitivity is achieved in the resolved channel. On the other hand, the EFT models display very different kinematics with wide tails in high $E_{\text{T}}^{\text{miss}}$ extending beyond 450 GeV, warranting a “boosted” reconstruction of the Higgs boson. Given the clear advantage of one analysis channel over the other for either set of models, and for simplicity, the results for the Z' -2HDM model are given using the resolved analysis, and the EFT models are interpreted using the boosted analysis.

The final signal regions are defined with four increasing thresholds for the missing transverse momentum in the resolved channel, and two thresholds in the boosted channel. To search for the possible presence of non-SM signals, the total numbers of observed events after applying all selection criteria are compared with the total number of expected SM events taking into account their respective uncertainties in both channels. Unlike previous ATLAS searches for resonant production with a similar final state [31, 32], this analysis explores different theoretical models, focuses on the fully hadronic channel with data-driven methods to estimate the main backgrounds, and most importantly, applies selections extending to large $E_{\text{T}}^{\text{miss}}$ utilizing “resolved” as well as “boosted” techniques. The approach for extracting limits in this analysis is also more suited for the models considered here, and reduces the theoretical uncertainty from modeling and fitting of the signal shape.

3 ATLAS detector

ATLAS is a multi-purpose particle physics experiment [33] at the LHC. The detector¹ consists of inner tracking devices surrounded by a superconducting solenoid, electromagnetic and hadronic calorimeters, and a muon spectrometer. The inner tracking system provides charged-particle tracking and vertex reconstruction in the pseudorapidity region $|\eta| < 2.5$. It consists of a silicon pixel detector, a silicon

¹ ATLAS uses a right-handed coordinate system with its origin at the nominal interaction point (IP) in the center of the detector and the z -axis along the beam pipe. The x -axis points from the IP to the center of the LHC ring, and the y -axis points upwards. Cylindrical coordinates (r, ϕ) are used in the transverse plane, ϕ is the azimuthal angle around the beam pipe. The pseudorapidity η is defined in terms of the polar angle θ as $\eta = -\ln[\tan(\theta/2)]$.

microstrip tracker, and a transition radiation tracker. The system is surrounded by a solenoid that produces a 2 T axial magnetic field. The central calorimeter system consists of a liquid-argon electromagnetic sampling calorimeter with high granularity and a steel/scintillator-tile calorimeter providing hadronic energy measurements in the central pseudorapidity range ($|\eta| < 1.7$). The endcap and forward regions are instrumented with liquid-argon calorimeters for electromagnetic and hadronic energy measurements up to $|\eta| = 4.9$. The muon spectrometer is operated in a magnetic field provided by air-core superconducting toroids and includes tracking chambers for precise muon momentum measurements up to $|\eta| = 2.7$ and trigger chambers covering the range of $|\eta| < 2.4$. A three-level trigger system is used to select interesting events [34]. The Level-1 (L1) trigger reduces the event rate to below 75 kHz using hardware-based trigger algorithms acting on a subset of detector information. Two levels of software-based triggers, referred to collectively as the High-Level Trigger (HLT), further reduce the event rate to approximately 400 Hz using information from the entire detector.

4 Data and simulation samples

The data sample used in this analysis, after data quality requirements are applied, corresponds to an integrated luminosity of 20.3 fb^{-1} . The primary data sample is selected using an E_T^{miss} trigger. The L1 E_T^{miss} trigger threshold is 60 GeV, and the HLT E_T^{miss} trigger threshold is 80 GeV. The trigger efficiency is above 98% for events passing the full offline selection across the full E_T^{miss} range considered in this analysis. Muon triggers with transverse momentum thresholds at the HLT of 24 GeV for muons with surrounding inner detector tracking activity below a predefined level, i.e., isolated muons [35], and 36 GeV for muons with no isolation requirement, are used to select the muon data used for the estimation and validation of backgrounds in the control regions. A photon trigger with a transverse momentum threshold of 120 GeV at the HLT is used to select events with a high p_T prompt photon for data-driven $Z(\rightarrow \nu\bar{\nu})+\text{jets}$ background estimation (Section 7.1).

Monte Carlo (MC) simulated event samples are used to model both the signal and backgrounds. Effects of multiple proton–proton interactions (pileup) as a function of the instantaneous luminosity are taken into account by overlaying simulated minimum-bias events generated with Pythia8 [36] onto the hard-scattering process, such that the distribution of the average number of interactions per bunch crossing in the MC simulated samples matches that in the data. The simulated samples are processed either with a full ATLAS detector simulation [37] based on the GEANT4 program [38], or a fast simulation of the response of the electromagnetic and hadronic calorimeters [39]. The results based on fast simulations are validated against fully simulated samples and the difference is found to be negligible. The simulated samples are further processed with a simulation of the trigger system. Both the simulated events and the data are reconstructed and analyzed with the same analysis chain, using the same event selection criteria.

Table 1 summarizes the various event generators and parton distribution function (PDF) sets, as well as parton shower and hadronization software used for the analyses presented in this article.

Signal samples are generated with MADGRAPH [40], interfaced to Pythia8 using the AU2 parameter settings (tune) [41] for parton showering, hadronization, and underlying event simulation. The Higgs boson mass is fixed to 125 GeV. The MSTW2008LO leading-order (LO) PDF set [42] is used for the Z'-2HDM model, while the CTEQ6L1 PDF set [43] is used for the EFT models. For the Z'-2HDM model, samples are produced with Z' mass values between 600 and 1400 GeV, A mass values between 300 and 800 GeV (where kinematically allowed), and DM mass values between 10 and 200 GeV but always less than half the A mass. In addition, $Z' \rightarrow Zh$ samples are produced for Z' mass values between 600 and 1400 GeV.

Table 1: Summary of MC event generators, PDF sets, and parton shower and hadronization models utilized in the analyses for both the signal and background processes.

Model / Process	Generator	PDF	Parton Shower / Hadronization
Z'-2HDM	MADGRAPH v1.5.1	MSTW2008LO	PYTHIA v8.175 with AU2 tune
EFT models	MADGRAPH v1.5.1	CTEQ6L1	PYTHIA v8.175 with AU2 tune
$W/Z/\gamma+$ jets	SHERPA v1.4.3	CT10	SHERPA v1.4.3
$t\bar{t}$	POWHEG-BOX v1.0 r2129	CT10	PYTHIA v6.427 with P2011C tune
Single top (s -ch., Wt)	MC@NLO v3.31	CT10	JIMMY v4.31 with AUET2 tune
Single top (t -ch.)	ACERMC v3.8	CTEQ6L1	PYTHIA v6.426 with AUET2B tune
$WW/WZ/ZZ$ (resolved)	Herwig v6.520	CTEQ6L1	JIMMY v4.31 with AUET2 tune
$WW/WZ/ZZ$ (boosted)	POWHEG r2330.3	CTEQ6L1	PYTHIA v8.175 with AU2 tune
$q\bar{q} \rightarrow Vh$	PYTHIA v8.175	CTEQ6L1	PYTHIA v8.175 with AU2 tune
$gg \rightarrow Zh$	POWHEG r2330.3	CT10	PYTHIA v8.175 with AU2 tune
multipjet	PYTHIA v8.160	CT10	PYTHIA v8.160 with AU2 tune

For the EFT models, samples are produced for scalar and fermionic DM particle masses ranging from 1 to 1000 GeV for both hh and hZ coupling to DM.

A variety of samples are used in the background determination. The dominant $Z(\rightarrow \nu\bar{\nu})$ +jets background is determined from data (Section 7.1), and samples simulated with SHERPA [44] for $Z(\rightarrow \nu\bar{\nu})$ +jets, $Z(\rightarrow \ell\ell)$ +jets, and γ +jets are also used in the calculation process. The $W(\rightarrow \ell\nu)$ +jets processes are generated with SHERPA and are normalized using data as described in Section 7.3. All the SHERPA samples are generated using the CT10 PDF set [45]. The $t\bar{t}$ background is generated with POWHEG-BOX [46] interfaced with PYTHIA6 and the PERUGIA 2011C tune [47]. Single top quark production in the s - and Wt -channels are produced with MC@NLO [48–50] interfaced with JIMMY [51], while the t -channel process is produced with ACERMC [52] interfaced with PYTHIA6. The Diagram Removal scheme [53] is used in the single top quark production in the Wt -channel to remove potential overlap with $t\bar{t}$ production due to interference of the two processes. A top quark mass of 172.5 GeV is used consistently. The cross-sections of the $t\bar{t}$ and single-top-quark processes are determined at next-to-next-to-leading order (NNLO) in QCD including resummation of next-to-next-to-leading logarithmic (NNLL) soft gluon terms with Top++2.0 [54–60]. The normalization and uncertainties are calculated using the PDF4LHC prescription [61] with the MSTW2008 68% CL NNLO [42, 62], CT10 NNLO [45, 63], and NNPDF2.3 [64] PDF sets. Additional kinematic-dependent corrections to the $t\bar{t}$ sample and normalizations determined from data are described in Section 7.3. Diboson (ZZ , WW , and WZ) production is simulated with two different generators, both Herwig [65] interfaced to JIMMY and POWHEG interfaced to PYTHIA8. The differences in event yield and kinematic distributions between the two simulated samples are found to be minimal in the analyses. The diboson samples are normalized to calculations at next-to-leading order (NLO) in QCD performed using MCFM [66]. The multijet background is estimated from data (Section 7.2), with samples simulated with PYTHIA8 used for validation in the control regions. For SM production of Zh and Wh , PYTHIA8 is used with CTEQ6L1 PDFs, and the samples were normalized to total cross-sections calculated at NLO [67], and NNLO [68] in QCD, respectively, with NLO electroweak corrections [69] in both cases.

5 Object reconstruction

This analysis requires the reconstruction of muons, electrons, photons, jets, and missing transverse momentum. Object reconstruction efficiencies in simulated events are corrected to reproduce the performance measured in data, and their systematic uncertainties are detailed in Section 8.

Muon candidates are identified from tracks that are well reconstructed inside both the inner detector and the muon spectrometer [35]. They must fulfill $p_T > 6$ GeV and $|\eta| < 2.5$ requirements. Furthermore, they are required to satisfy the “*tight*” muon identification quality criteria [35]. To reject cosmic-ray muons, muon candidates are required to be consistent with production at the primary vertex, defined as the vertex² with the highest $\Sigma(p_T^{\text{track}})^2$, where p_T^{track} refers to the transverse momentum of each track. In the muon control region or during the overlap removal procedure of the boosted channel, muon candidates are required to be isolated to reduce the multijet background. The scalar sum of the transverse momenta of tracks with $p_T > 1$ GeV within a cone of $\Delta R = \sqrt{(\Delta\eta)^2 + (\Delta\phi)^2} = 0.3$ around the muon track excluding the muon (tracking isolation), as well as the transverse energy measured in the calorimeter in a cone of $\Delta R = 0.3$ (excluding the energy lost by the muon itself) around the muon track (calorimeter isolation), is required to be less than 12% of the muon p_T .

Electron candidates are identified as tracks that are matched to a cluster meeting shower-shape criteria in the electromagnetic calorimeter. Each electron candidate should have $p_T > 7$ GeV and is within $|\eta| < 2.47$. To suppress contamination from multijet background, electron candidates must satisfy the “*medium++*” electron shower shape and track selection criteria, based on Ref. [70] and modified to accommodate the increased pileup in 8 TeV data. Isolated electrons are used in the boosted channel during the overlap removal procedure. These isolated electrons must meet tracking and calorimeter isolation requirements. The scalar sum of the transverse momenta of tracks with $p_T > 1$ GeV within a cone of $\Delta R = 0.3$ around the electron track excluding the electron is required to be less than 16% of the electron p_T . The transverse energy measured in the calorimeter in a cone of $\Delta R = 0.3$ (excluding the energy lost by the electron itself) around the electron track is required to be less than 18% of the electron p_T .

Photon candidates must satisfy the *tight* quality criteria with $p_T > 10$ GeV and $|\eta| < 2.37$ [71]. Additionally, the isolated photons used in the $Z(v\bar{v})+\text{jets}$ background estimation must have $p_T > 125$ GeV, and the sum of the energy deposit in the topological calorimeter clusters within a radius $R = 0.4$ with respect to the photon direction, but excluding the photon, must be less than 5 GeV.

Jets are reconstructed [72] using the anti- k_t jet clustering algorithm from topological clusters of calorimeter cells that are locally calibrated to the hadronic energy scale [73]. Small-radius (small- R ; radius parameter $R = 0.4$) jets as well as large-radius (large- R ; $R = 1.0$) jets are used. The effects of pileup on small- R jet energies are accounted for by a correction based on jet area [74]. The jet trimming algorithm [27] is applied to the reconstruction of large- R jets to minimize the impact of energy depositions due to pileup and the underlying event. This algorithm reconstructs subjets within the large- R jet using the k_t algorithm [75] with radius parameter $R_{\text{sub}} = 0.3$, then removes any subjet with p_T less than 5% of the large- R jet p_T . The energies of all jets and the masses of the large- R jets are then calibrated to their values at particle level using p_T - and η -dependent factors determined from simulation; small- R jets are further calibrated using *in situ* measurements [76]. Small- R jets with $p_T < 50$ GeV and $|\eta| < 2.4$ are required to have at least 50% of the p_T sum of tracks matched to the jet belonging to tracks originating from the primary vertex (jet vertex fraction) to suppress the effects of pileup interactions [77]. Small- R

² Proton–proton collision vertices are reconstructed requiring that at least five tracks with $p_T > 0.4$ GeV are associated with a given vertex.

jets are required to satisfy either $p_T > 25$ GeV and $|\eta| < 2.4$ or $p_T > 30$ GeV and $2.4 < |\eta| < 4.5$, while large- R jets are required to satisfy $p_T > 300$ GeV and $|\eta| < 2.0$.

Track-jets are built from tracks using the anti- k_t algorithm with $R = 0.3$. Tracks are required to satisfy $p_T > 0.5$ GeV and $|\eta| < 2.5$, the transverse and longitudinal impact parameters with respect to the primary vertex below 1.5 mm, and a set of hit criteria to ensure that those tracks are consistent with originating from the primary vertex, thereby reducing the effects of pileup. Track-jets are matched to large- R jets using a process called “ghost association” [74, 78]. Track-jets with $p_T > 20$ GeV and $|\eta| < 2.5$ are kept for further analysis.

Small- R jets and track-jets containing b -hadrons are identified (“ b -tagged”) using the properties of the tracks associated with them, the most important being the impact parameter of each track (defined as the track’s distance of closest approach to the primary vertex in the transverse plane), as well as the presence and properties of displaced vertices. The “MV1” b -tagging algorithm [25] used in this analysis combines the above information using a neural network and is configured to achieve an average efficiency of 60% for tagging small- R jets with b -quarks³, and has misidentification probabilities of $\sim 15\%$ for charm-quark jets and less than 1% for light-flavor jets, as determined in an MC sample of $t\bar{t}$ events. For track-jets, the corresponding numbers are 74% for b -quark jets, 15% for charm-quark jets, and $< 1.5\%$ for light-flavor jets. The b -tagging algorithm is trained on MC simulations and its efficiency is scaled to match data based on studies of candidate $t\bar{t}$ and multijet events [25, 26]. For charm- and light-flavor track-jets, the efficiency calibrations for the small- R jets are used, with additional uncertainties to account for possible differences in b -tagging performance between small- R jets and track-jets. The flavor-tagging efficiency is only calibrated up to p_T of 300 GeV for b - and c -tagged small- R jets, 750 GeV for light-flavor-tagged small- R jets, and 250 GeV for b -tagged track-jets. Beyond the maximum p_T , additional uncertainties on the b -tagging efficiency are extracted from the last calibrated p_T bin with additional uncertainties based on studies of MC-simulated events with high- p_T jets.

Since each type of object reconstruction proceeds independently, the same calorimeter cells or tracks might be used for multiple physics objects. This can lead to double counting of energy and the dual-usage must be resolved. In addition, two separate but close-by objects can also potentially introduce bias in the reconstruction process. To address the problem of duplication while preserving heavy-flavour jets with semi-leptonic decays or the problem where close-by objects bias each other’s position or energy reconstruction, the following sequential overlap removal procedures are implemented separately for the resolved and the boosted channel. In the resolved channel, an object is considered to be an electron (photon) and a small- R jet is discarded if the electron (photon) candidate and the small- R jet that is not b -tagged overlap within $\Delta R < 0.2$. If an electron (photon) candidate and any small- R jet have angular separation in the range of $0.2 < \Delta R < 0.4$, or if an electron (photon) candidate and a b -tagged small- R jet overlap within $\Delta R < 0.2$ of each other, then the electron (photon) is discarded and the object is considered a small- R jet. If a muon candidate and a small- R jet overlap within $\Delta R < 0.4$, then the muon is discarded and the small- R jet is retained. In the boosted channel, an object is considered to be an electron candidate and a small- R jet is removed if the electron that is isolated and the small- R jet overlap within $\Delta R < 0.2$. Electron or muon candidates will be removed if they and any small- R jet overlap within $\Delta R < 0.4$. Furthermore, large- R jets are eliminated if an isolated photon is found within $\Delta R < 1.0$ of the

³ In simulation, a jet is labeled as a b -quark jet if a b -quark (after final-state radiation) with transverse momentum above 5 GeV is identified within a cone of $\Delta R = 0.3$ around the jet axis. If no b -quark is identified, the jet is labeled as a charm-quark jet if a charm-quark is identified with the same criteria. If no charm quark is identified, the jet is labeled as a τ -jet if a τ -lepton is identified with the same criteria. Otherwise the jet is labeled as a light-flavor jet.

large- R jet. Track-jets are discarded if an isolated electron or an isolated muon is found within $\Delta R < 0.1$ of the track-jet.

The missing transverse momentum \vec{E}_T^{miss} is defined as the negative vector sum of the transverse momenta of jets, electrons, photons, and topological calorimeter clusters not assigned to any reconstructed objects [79]. The transverse momenta of reconstructed muons are included, with the energy deposited by these muons in the calorimeters properly removed to avoid double-counting. In addition, a track-based missing transverse momentum vector \vec{p}_T^{miss} is calculated as the negative vector sum of the transverse momenta of tracks with $|\eta| < 2.4$ and the transverse and longitudinal impact parameters with respect to the primary vertex below 1.5 mm.

6 Event selection

A set of common preselection criteria based on objects described in Section 5 is used for events to be considered for the resolved and boosted channels. An initial $E_T^{\text{miss}} + \text{jets}$ sample is obtained by requiring an event to have passed the 80 GeV HLT E_T^{miss} trigger, to have an offline $E_T^{\text{miss}} > 100$ GeV for the resolved channel ($E_T^{\text{miss}} > 200$ GeV for the boosted channel) and to have at least one small- R jet. No electron, muon and photon candidates should be present in the event. Events must have at least one identified pp collision vertex and be produced in stable beam conditions with all relevant subdetectors functioning properly. To suppress contamination from multijet events, the smallest azimuthal angle between \vec{E}_T^{miss} and small- R jets is required to be greater than 1.0.

Table 2: The event selection criteria for signal regions in the resolved and boosted channels. The symbol j represents an anti- k_t jet ($R = 0.4$), j^{trk} a track-jet ($R = 0.3$), J a trimmed anti- k_t jet ($R = 1.0$), b a b -tagged anti- k_t jet ($R = 0.4$), and b^{trk} a b -tagged anti- k_t track-jet ($R = 0.3$). Each b -tagged track-jet is matched by ghost association to the leading- p_T large- R jet. The subscript index i of each jet collection means the i -th jet in descending order of the transverse momentum, of which j_i are inclusive and may or may not be b -tagged. The variable $\Delta\phi_{\min}(\vec{E}_T^{\text{miss}}, j_i)$ refers to the smallest ϕ angular separation between the \vec{E}_T^{miss} and any anti- k_t jet ($R = 0.4$) in the event.

	Resolved	Boosted
$\Delta\phi_{\min}(\vec{E}_T^{\text{miss}}, j_i)$	> 1.0	> 1.0
Jet multiplicity	$2 \leq n_j \leq 3$	$n_J \geq 1$ $n_{j^{\text{trk}}} \geq 2$
b -jet (60% eff.) p_T	$p_T^{b_1} > 100$ GeV	-
b -jet multiplicity	$n_b \geq 2$ (60% eff.)	$n_{b^{\text{trk}}} = 2$ (70% eff.)
Jet p_T	$p_T^{b_2} > 60$ GeV when $n_j = 3$ $p_T^{j_2} > 100$ GeV when $n_j = 3$	$p_T^{J_1} > 350$ GeV
$\Delta\phi(\vec{E}_T^{\text{miss}}, \vec{p}_T^{\text{miss}})$	-	$< \pi/2$
Dijet separation	$\Delta R(j_1, j_2) < 1.5$	-
Invariant mass	$90 \text{ GeV} \leq m_{b_1 b_2} \leq 150 \text{ GeV}$	$90 \text{ GeV} \leq m_{J_1} \leq 150 \text{ GeV}$
E_T^{miss}	$> 150, 200, 300, \text{ or } 400$ GeV	$> 300 \text{ or } 400$ GeV

For the resolved channel, a further set of selection criteria is chosen by optimizing the sensitivity to a simulated Z'-2HDM signal in the presence of the expected background. The selection criteria are summarized in Table 2. If no explicit jet p_T threshold is specified that means only the initial selection

criteria described previously are required. The requirements on the p_T of the subleading b -tagged jet, $p_T^{b_2}$, and that of the subleading jet, $p_T^{j_2}$, for events containing three jets were found to be effective in removing top quark background. The minimum E_T^{miss} value required increases with $m_{Z'}$ to take advantage of the harder E_T^{miss} spectrum for higher Z' mass values. The best signal sensitivity at $\tan\beta = 1$ for the signal samples used in this analysis is achieved by requiring a minimum E_T^{miss} of 200 GeV for $m_{Z'} = 600$ GeV, 300 GeV for $m_{Z'} = 800$ GeV, and 400 GeV for $m_{Z'} = 1000\text{--}1400$ GeV. The product of the detector acceptance and reconstruction efficiency (selection efficiency) of the $Z' \rightarrow h(b\bar{b}) + E_T^{\text{miss}}$ signal after the full set of selection requirements varies from 5% to 10% depending on $m_{Z'}$ and m_A . The number of expected signal events after full selection in the Z' -2HDM model for a few selected values of $m_{Z'}$, m_A and $\tan\beta$ are shown in Table 3 for the $Z' \rightarrow A(\chi\bar{\chi})h(b\bar{b})$ and $Z' \rightarrow Z(v\bar{v})h(b\bar{b})$ processes respectively.

Table 3: The number of expected Z' -2HDM signal events after full selection for selected points in parameter space. Left to right: values of $m_{Z'}$, m_A , and $\tan\beta$, the E_T^{miss} requirement for the given parameter values, the signal yield from the $Z' \rightarrow A(\chi\bar{\chi})h(b\bar{b})$ and $Z' \rightarrow Z(v\bar{v})h(b\bar{b})$ processes respectively.

$m_{Z'}$	m_A	$\tan\beta$	E_T^{miss}	$Z' \rightarrow A(\chi\bar{\chi})h(b\bar{b})$	$Z' \rightarrow Z(v\bar{v})h(b\bar{b})$
600 GeV	300 GeV	0.3	> 150 GeV	10	1.1
600 GeV	300 GeV	1	> 200 GeV	3.5	11.9
800 GeV	300 GeV	1	> 300 GeV	10.4	6.8
1000 GeV	300 GeV	0.3	> 400 GeV	12.2	0.4
1000 GeV	300 GeV	1	> 400 GeV	6.4	2.7
1000 GeV	300 GeV	5	> 400 GeV	0.4	3.9
1200 GeV	400 GeV	1	> 400 GeV	3.3	2.0
1400 GeV	300 GeV	1	> 400 GeV	2.2	0.4

The boosted channel differs from the resolved channel primarily by the requirement of at least one large- R jet designed to contain the decay products of a single $h \rightarrow b\bar{b}$ decay. Table 2 also lists the selection criteria for the boosted channel, designed to achieve high efficiency for the EFT models and good background rejection. The leading large- R jet is required to have $p_T > 350$ GeV. At these high p_T values, the decay products from top quarks are often contained inside a large- R jet, so the requirement on the mass of the leading large- R jet to between 90 GeV and 150 GeV provides good rejection against top quark background. The multijet background is further suppressed by requiring the azimuthal angle between \vec{E}_T^{miss} and \vec{p}_T^{miss} , $\Delta\phi(\vec{E}_T^{\text{miss}}, \vec{p}_T^{\text{miss}})$, to be less than $\pi/2$. Similar to the resolved channel, the final E_T^{miss} requirement in the boosted channel varies as the E_T^{miss} distribution shifts for different EFT models and DM mass. For the models $|\chi|^2|H|^2$, $\bar{\chi}i\gamma_5\chi|H|^2$, and $\chi^\dagger\partial^\mu\chi H^\dagger D_\mu H$, the minimum E_T^{miss} is 300 GeV for $m_\chi = 1$, 65, and 100 GeV, and 400 GeV for $m_\chi = 500$ and 1000 GeV; the selection efficiency for these three EFT models varies from 1% to 8%, with a higher efficiency at larger m_χ . For the $\bar{\chi}\gamma^\mu\chi B_{\mu\nu}H^\dagger D^\nu H$ model, $E_T^{\text{miss}} > 400$ GeV is required for all m_χ values, and the selection efficiency ranges from 10% to 13%, increasing slightly with m_χ .

7 Background estimation

The main source of irreducible background for this search is Z +jets when the Z boson decays into a pair of neutrinos. To reduce the impact of theoretical and experimental uncertainties associated with this process, which are particularly evident in regions with large E_T^{miss} , $Z(\rightarrow v\bar{v})$ +jets background is determined

from data with input from simulation, as described in Section 7.1. Multijet production in which there is large E_T^{miss} is not simulated reliably, so it is also estimated using data, as described in Section 7.2. The $W(\rightarrow \ell\nu)+\text{jets}$ and top quark production processes are estimated using the shape from MC simulation and are normalized to data in 1-lepton control regions, as described in Section 7.3. The other backgrounds are estimated from Monte Carlo simulation, namely $Z(\rightarrow \ell\ell)+\text{jets}$, diboson production, and vector boson associated production with the Standard Model Higgs boson. Section 7.4 shows validations of the background modeling in the zero-lepton validation regions using selections close to those of the signal regions.

7.1 $Z(\rightarrow \nu\bar{\nu})+\text{jets}$ background

The estimation of the $Z(\rightarrow \nu\bar{\nu})+\text{jets}$ background is derived from two data samples. For $E_T^{\text{miss}} < 200$ GeV, the $Z(\rightarrow \mu^+\mu^-)+\text{jets}$ sample is used. The p_T spectrum of produced Z bosons and the kinematic distributions of jets are the same whether the Z boson decays into charged leptons or neutrinos. Thus the $Z(\rightarrow \mu^+\mu^-)+\text{jets}$ data sample provides very good modeling of the $Z(\rightarrow \nu\bar{\nu})+\text{jets}$ background. The $Z(\rightarrow \mu^+\mu^-)+\text{jets}$ events are selected by requesting two isolated muons that pass the 24 GeV muon trigger in the HLT and satisfy the *tight* selection criteria, with opposite charge and p_T above 25 GeV, and the invariant mass of the muon pair be between 70 GeV and 110 GeV. The same selection is applied to both simulated samples and to the data. A transfer function is derived to account for the differences in branching ratio, trigger efficiency, and reconstruction efficiencies between $Z(\rightarrow \nu\bar{\nu})+\text{jets}$ and $Z(\rightarrow \mu^+\mu^-)+\text{jets}$. For higher purity and larger sample size, as well as reduction of systematic uncertainties, SHERPA samples of $Z(\rightarrow \nu\bar{\nu})+\text{jets}$ and $Z(\rightarrow \mu^+\mu^-)+\text{jets}$, which have the same production kinematics, are used to derive the transfer function. The samples are fully reconstructed and the trigger and event selection criteria are applied. The E_T^{miss} in each $Z(\rightarrow \mu^+\mu^-)+\text{jets}$ event is recalculated by adding the two muon transverse momentum vectors to the original E_T^{miss} to create a new variable called $E_T^{\text{miss}+\ell\ell}$. This mimics the E_T^{miss} in $Z(\rightarrow \nu\bar{\nu})+\text{jets}$ events. A transfer function is derived by fitting the ratio of the $Z(\rightarrow \nu\bar{\nu})+\text{jets}$ E_T^{miss} distribution divided by the $Z(\rightarrow \mu^+\mu^-)+\text{jets}$ $E_T^{\text{miss}+\ell\ell}$ distribution. Simulated events from other background processes that passed the aforementioned $Z(\rightarrow \mu^+\mu^-)$ selection are subtracted from the data to obtain a $Z(\rightarrow \mu^+\mu^-)+\text{jets}$ data sample with high purity. The MC-based transfer function is applied to the $Z(\rightarrow \mu^+\mu^-)+\text{jets}$ $E_T^{\text{miss}+\ell\ell}$ distribution in this data sample to estimate the $Z(\rightarrow \nu\bar{\nu})+\text{jets}$ background. As the Z' -2HDM model contains the decay mode $Z' \rightarrow Z h$, the presence of such a signal would have a contribution to the $Z(\rightarrow \mu^+\mu^-)+\text{jets}$ process as well; however, in the $E_T^{\text{miss}} < 200$ GeV region, the expected yield from the $Z' \rightarrow Z(\rightarrow \mu^+\mu^-)h$ process is several orders of magnitude smaller than the Standard Model $Z(\rightarrow \mu^+\mu^-)+\text{jets}$ production, and thus has a negligible impact on the background estimation.

For $E_T^{\text{miss}} > 200$ GeV, the limited size of the $Z(\rightarrow \mu^+\mu^-)+\text{jets}$ data sample reduces its usefulness. In this region the $\gamma+\text{jets}$ data sample is used. For γ (or in this case the modified E_T^{miss} as described below) transverse momenta much greater than the mass of the Z boson, the kinematic properties of $\gamma+\text{jets}$ and $Z+\text{jets}$ events are very similar [80]. A high-purity (above 99% in both the resolved and boosted channels after b -tagging requirements) $\gamma+\text{jets}$ data sample is selected by requiring one high- p_T (≥ 125 GeV), prompt photon that passed the 120 GeV HLT photon trigger. The transfer function is calculated from reconstructed SHERPA samples of $\gamma+\text{jets}$ events that passed the same photon selection, and $Z(\rightarrow \nu\bar{\nu})+\text{jets}$ events. The E_T^{miss} in a $\gamma+\text{jets}$ event is recalculated by using all clustered objects described in Section 5 except the leading photon, and denoted as $E_T^{\text{miss}+\gamma}$. The $Z(\rightarrow \nu\bar{\nu})+\text{jets}$ background for $E_T^{\text{miss}} > 200$ GeV is obtained by multiplying the $\gamma+\text{jets}$ $E_T^{\text{miss}+\gamma}$ distribution in the data by the MC-produced transfer function. Since the photon couples to a quark through its electric charge, while the Z boson coupling depends on

the weak neutral vector and axial-vector couplings, the transfer function varies slightly by $\sim 3\%$ to 10% depending on the number of b -tagged jets in the final state. A MC-based correction factor for each value of b -tagged jet multiplicity is derived and applied to account for the small difference.

To test this procedure over the entire E_T^{miss} distribution above 100 GeV, two control regions are defined in the resolved channel using event selection very similar to that of the signal region except requiring either zero or one b -tagged small- R jet. A similar test is performed in the boosted channel but with E_T^{miss} above 200 GeV where control regions are defined with zero, one or two b -tagged track-jets that are matched by ghost association to the leading large- R jet. Despite the two b -tagged track-jets requirement in the last case, the expected discovery significance of the signal models considered is well below 2σ considering the background estimate. By keeping the yields of the other background processes constant and normalizing the total expected background to the data, a scale factor of 0.9 for the $Z(\rightarrow v\bar{v})+\text{jets}$ estimation is derived from the control regions with no b -tagged jets for both the resolved and boosted channels. The 10% difference from unity is assigned as an additional source of systematic uncertainty on the $Z(\rightarrow v\bar{v})+\text{jets}$ normalization in both channels. After the corrections described above are applied, the data and the estimated background agree well in all five control regions to within 3% to 10% in the resolved channel, and within 1% to 20% in the boosted channel; the differences are larger in regions with higher b -tagged jet multiplicity and hence smaller event sample size. Figure 2 shows the E_T^{miss} distributions in the zero-lepton, zero- b -tagged jet control regions of the resolved and boosted channels. Good agreement is demonstrated between the data and the estimated background.

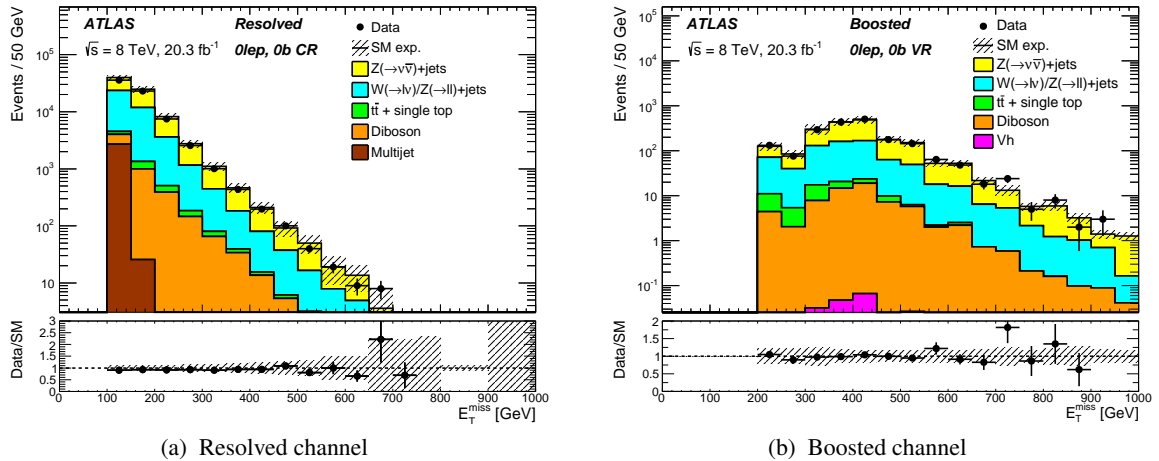


Figure 2: The distribution of the missing transverse momentum with magnitude E_T^{miss} of (a) the resolved channel and (b) the boosted channel in the zero-lepton, zero- b -tagged jet control region (CR) for the estimated backgrounds (solid histograms) and the observed data (points). The hatched areas represent the combined statistical and systematic uncertainties in the total background estimation. The minimum E_T^{miss} requirement in the resolved (boosted) channel is 100 GeV (200 GeV). In the resolved channel, the small contributions from Wh and Zh are included in the W or $Z(\rightarrow v\bar{v})$ plus jets distributions.

7.2 Multijet background

The multijet background in the resolved channel is estimated from data using a “jet smearing” method [81]. A pure multijet sample, used as the “seed” events, is obtained by selecting from the data events contain-

ing multiple jets, no isolated leptons, and E_T^{miss} below 120 GeV, using a set of jet triggers with different requirements on jet p_T threshold and $|\eta|$ coverage. A “smeared” event is generated by multiplying each jet four-momentum in a seed event by a random number drawn from a jet response function. The response function quantifies the probability of fluctuations in the detector response to jets measured in the data. It is determined using data and simulation, and has both Gaussian and non-Gaussian components to account for both the core of the distribution and the tails. After “smearing”, the obtained multijet estimation is compared to the data in a dedicated multijet control region in which $100 < E_T^{\text{miss}} < 120$ GeV, the leading jet has $p_T > 100$ GeV, and $\Delta\phi_{\min}(\vec{E}_T^{\text{miss}}, j_i) < 0.7$. The agreement is good with slight mismodelling likely due to the difference in E_T^{miss} distributions between b -quark jets and light jets. Hence the “smeared” multijet sample is reweighted two-dimensionally with respect to its jet multiplicity and b -tagged jet multiplicity to match the numbers in the data in the multijet control region. The aforementioned small discrepancies in the data and background comparison are removed after reweighting. The multijet background is small in the other control regions in the resolved channel and negligible in the signal region.

The multijet background is estimated in the boosted channel using an “ABCD method” [82], in which the data are divided into four regions based on the $\Delta\phi_{\min}(\vec{E}_T^{\text{miss}}, j_i)$ and $\Delta\phi(\vec{E}_T^{\text{miss}}, \vec{p}_T^{\text{miss}})$ variables, such that three of the regions are dominated by the background. These two variables are found to be weakly correlated in a data sample after the lepton veto, and requiring at least one large- R jet with $p_T^J > 350$ GeV, at least two track-jets matched to the large- R jet, and E_T^{miss} between 100 and 200 GeV. This observation is confirmed in a multijet event sample simulated with PYTHIA8. The signal region (A) is selected with $\Delta\phi_{\min}(\vec{E}_T^{\text{miss}}, j_i) > 1.0$ and $\Delta\phi(\vec{E}_T^{\text{miss}}, \vec{p}_T^{\text{miss}}) < \pi/2$. In region C, the requirement on $\Delta\phi(\vec{E}_T^{\text{miss}}, \vec{p}_T^{\text{miss}})$ is reversed. In regions B and D, $\Delta\phi_{\min}(\vec{E}_T^{\text{miss}}, j_i) < 0.4$ is required, with the same requirement on $\Delta\phi(\vec{E}_T^{\text{miss}}, \vec{p}_T^{\text{miss}})$ as in regions A and C, respectively. The multijet yield in each of the regions B, C, and D is obtained by subtracting from the data the contribution of other backgrounds taken from simulation. The number of multijet events in region A is estimated as a product of the yields in regions D and C divided by the yield in region B. Due to the small number of events, the track-jet b -tagging and the large- R jet mass requirements for the signal region are not applied in regions B, C, and D, and an additional scale factor to estimate the selection efficiencies of these two requirements is applied to the resulting yields. The number of events from multijet background in the signal region is estimated to be consistent with zero within uncertainties, and a 68% CL upper limit of 0.1 events is used as the predicted yield.

7.3 W +jets and top quark backgrounds

In the resolved channel, the W +jets control region is very similar to the signal region, except that the lepton veto is replaced by the requirement of one isolated muon with $p_T > 25$ GeV, and the number of small- R jets must be two. The purity of the W +jets background in this control region is approximately 90% before b -tagging requirements. By keeping the yields of the other background processes constant and normalizing the total expected background to data, a scale factor of 0.92 is derived for the W +jets background. The 8% difference from unity is small compared to the systematic uncertainty on the W +jets normalization as discussed in Section 8. This scale factor is applied to the W +jets background when deriving the normalization for $Z(\rightarrow v\bar{v})$ +jets background in Section 7.1. The top quark control region has the same requirements except that three small- R jets are required. The purity of the top quark background, which includes mostly $t\bar{t}$ but also single-top-quark events, is approximately 78% in the top quark control region after requiring at least one b -tagged small- R jet. Good agreement is observed between the data

and simulation and no additional scale factor is applied to the top quark background. In both control regions, as well as the combined one-lepton validation region where the jet multiplicity requirement is removed, there is good agreement between the data and estimated background in both number of events and modeling of the kinematic variables.

As Monte Carlo simulation predicts a larger fraction of high p_T top quarks in $t\bar{t}$ events than is seen in the data, a correction is applied in the boosted channel at the level of generated top quarks in the $t\bar{t}$ MC sample [83, 84]. For the resolved channel, the correction is not applied since the impact is small, but the effect of it is accounted for as a source of systematic uncertainty, as discussed in Section 8.

The W +jets and top quark ($t\bar{t}$ + single top quark) backgrounds are further studied in the boosted channel in a one-lepton control region selected by requiring one isolated muon with $p_T > 25$ GeV, preselection criteria as described in Section 2 except the lepton veto, and the first two selections in Table 2. Events passing the one-lepton control region selections are categorized as being in the W +jets control region unless at least one b -tagged track-jet is found within $\Delta R = 1.5$ of the muon direction, in which case they are used for a top quark control region. The purity of W +jets background in the W +jets control region is approximately 72%, whereas the purity of the top quark background in the top quark control region is $\sim 90\%$. A pair of linear equations to calculate the normalization factor from background to the data is constructed using the predicted and observed yields of the W +jets and top quark backgrounds. The solution of the equations, 0.82 ± 0.05 and 0.89 ± 0.06 , are applied as scale factors to the W +jets background and top quark background, respectively.

7.4 Zero-lepton validation region

The individual background processes are studied and normalized to the data in the dedicated control regions, as described in the previous sections. To examine the overall modeling of all non-Higgs background processes combined, zero-lepton validation regions are defined for both channels, with selections similar to the signal region, but reversing the requirement on the invariant mass of the $b\bar{b}$ system. In the resolved channel, events are selected with at least one b -tagged small- R jet, and for events with two or more b -tagged jets, the invariant mass of the two leading b -tagged jets is required to be either below 60 GeV or above 150 GeV. In the boosted channel, events are selected with exactly one b -tagged track-jet associated with the leading large- R jet, and the invariant mass of the large- R jet is required to be either below 90 GeV or above 150 GeV. Figure 3(a) and Figure 3(b) show the E_T^{miss} distributions in both channels, and Figure 3(c) and Figure 3(d) show the distribution of the invariant mass of the two leading small- R jets (the invariant mass of the leading large- R jet) in the resolved (boosted) channel. The aforementioned scale factors for the corresponding background processes have been applied. Good agreement between the data and the estimated background is achieved for different kinematic variables, including jet p_T , angular distributions, multiplicity, and number of b -tagged jets, at each selection stage in both channels.

Figure 4 shows the distributions of the invariant mass of the $b\bar{b}$ system in both the resolved and boosted channels with fully hadronic selection very similar to the signal region, but removing the requirement on the invariant mass. The regions with the invariant mass of the $b\bar{b}$ system between 90 GeV and 150 GeV are the signal regions for both channels. The signal regions were blinded in this analysis until all the studies in the aforementioned control regions and validation regions were complete.

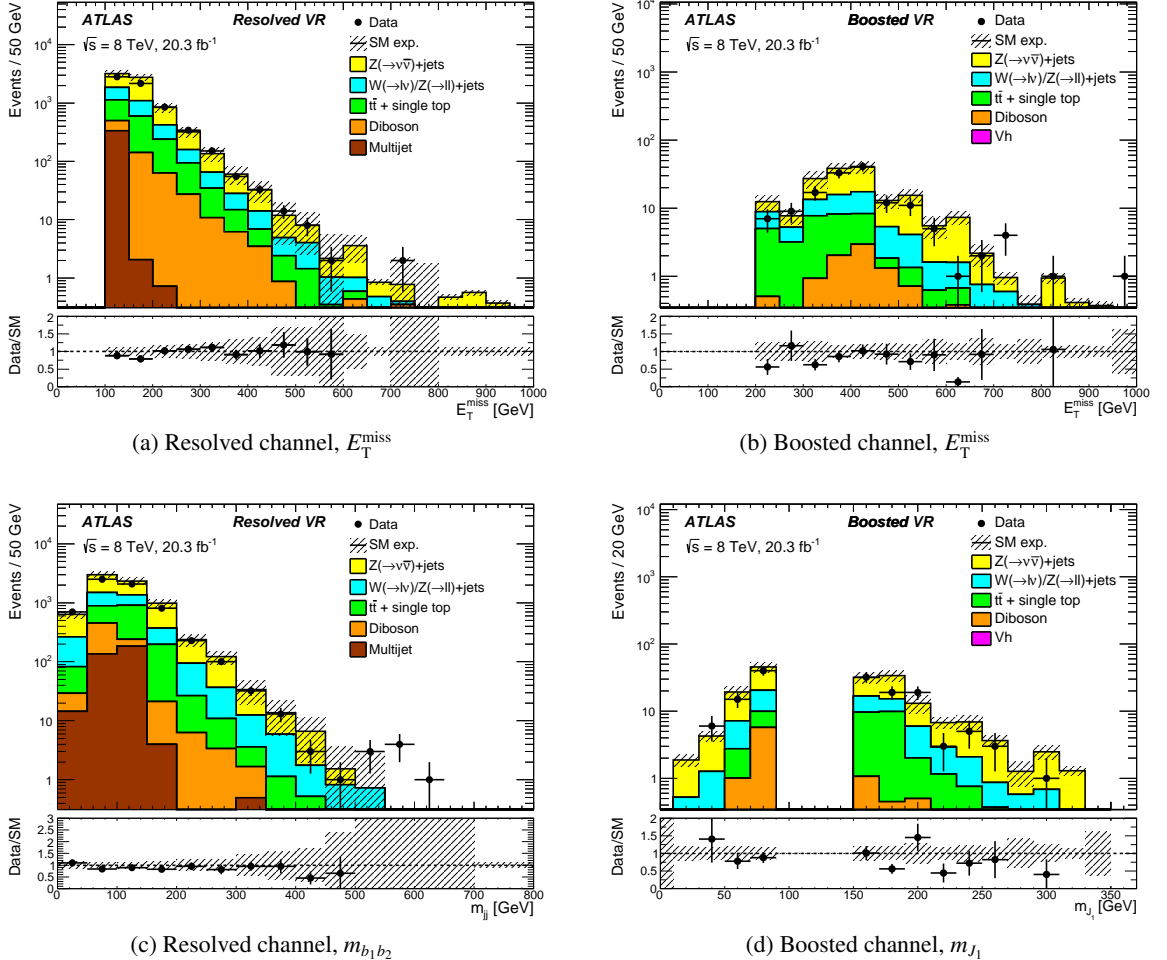


Figure 3: Distributions of the missing transverse momentum with magnitude E_T^{miss} for (a) the resolved channel and (b) the boosted channel and the invariant mass distributions for (c) the two leading small- R jets in the resolved channel and (d) the leading large- R jet in the boosted channel. Events are selected in the zero-lepton validation region (VR) for the estimated backgrounds (solid histograms) and the observed data (points). The hatched areas represent the combined statistical and systematic uncertainties in the total background estimation. At least one (exactly one) b -tagged jet is required in the resolved (boosted) channel. In the resolved channel, the invariant mass of the $b\bar{b}$ system in events with at least two b -tagged jets is required to be either less than 60 GeV or greater than 150 GeV. In the boosted channel, the invariant mass of the large- R jet with exactly one b -tagged track-jet is required to be either less than 90 GeV or greater than 150 GeV. The minimum E_T^{miss} requirement in the resolved (boosted) channel is 100 GeV (200 GeV). In the resolved channel, the small contributions from Wh and Zh are included in the W or $Z(\rightarrow v\bar{v})$ plus jets distributions.

8 Systematic uncertainties

The systematic uncertainty on background estimation and signal processes using Monte Carlo samples comes from several sources, and is evaluated for each of the signal and background processes in both channels. The uncertainty associated with the b -tagging efficiency, which is determined from comparisons between simulation and heavy-flavor-enriched data samples [25], ranges from $\sim 10\%$ to 15% . The

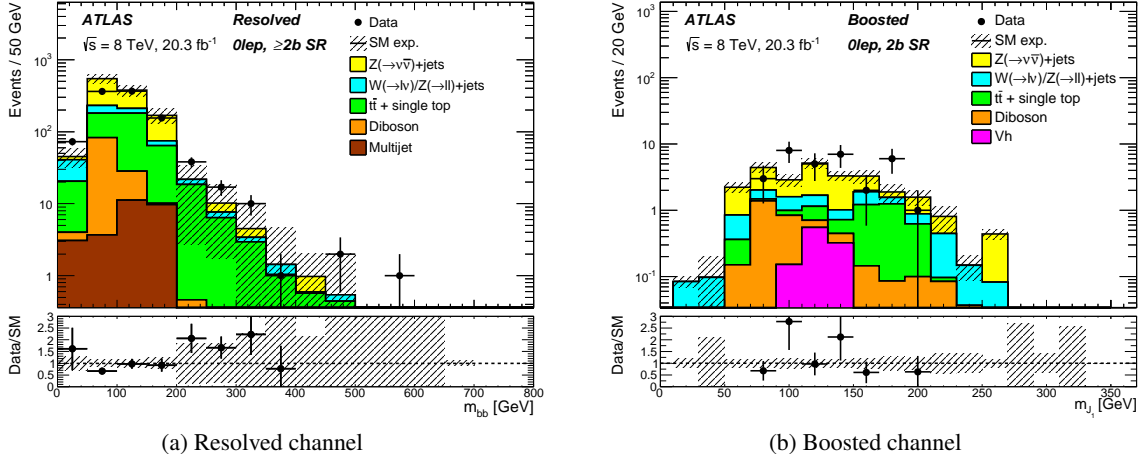


Figure 4: The distributions of the invariant mass of the $b\bar{b}$ system for the estimated backgrounds (solid histograms) and the observed data (points) in (a) the resolved and (b) the boosted channels in the signal region (SR) without the requirement on the invariant mass. The regions with the invariant mass of the $b\bar{b}$ system between 90 GeV and 150 GeV are the signal regions for both channels. The hatched areas represent the combined statistical and systematic uncertainties in the total background estimation. The minimum E_T^{miss} is required to be 100 GeV (200 GeV) in the resolved (boosted) channel. At least (exactly) two b -tagged small- R jets (track-jets) are required in the resolved (boosted) channel. In the resolved channel, the small contributions from Wh and Zh are included in the W or $Z(\rightarrow \nu\bar{\nu})$ plus jets distributions.

uncertainty on the overall background estimate due to light-flavor and charm-quark jets being misidentified as b -quark jets is calculated to be $\sim 1\%$ for small- R jets, and $\sim 2\%$ to 3% for track-jets. The jet energy scale and resolution [73], which directly impact the E_T^{miss} , depend on the kinematic properties of the jet, the distance to its nearest jet neighbor, and the flavor of the initiating parton. The systematic uncertainty associated with the jet energy scale and resolution ranges from $\sim 5\%$ to 15% .

In the boosted channel, the invariant mass of the $b\bar{b}$ system from the Higgs boson decay is selected by requiring the mass of the large- R jet to be between 90 GeV and 150 GeV, leading to additional systematic uncertainties from the jet mass scale and resolution [28]. The uncertainties associated with jet mass are $\sim 1\%$ for the EFT signals and $\sim 3\%$ to 8% for most simulated background processes. While the large- R jet calibration and uncertainty are derived primarily using an inclusive multijet sample, the large- R jet selection in this analysis focuses specifically on identifying jets containing two b -hadrons. As such, there are possible additional sources of uncertainty on the modeling of the jet mass and energy due to the difference in heavy-flavor content between the calibration and analysis selections. However, studies of multijet samples enriched with jets containing two b -hadrons suggest that this uncertainty is small in comparison to the existing uncertainty on jet mass and energy, and thus no additional uncertainty is applied.

The uncertainty on E_T^{miss} originating from the energy scale and resolution of energy clusters not included in jets [79] is small at $\sim 1\%$ or less, as are the uncertainties due to possible mismodeling of the effect of multiple pp collisions (pileup) and the method of removing jets coming from pileup. The uncertainty on the integrated luminosity for the data sample is 2.8%. It is derived using the same methodology as that detailed in Ref. [85].

The cross-section uncertainties for the background processes are as follows. For $t\bar{t}$ production, an uncertainty of 7% is cited from theoretical calculations [86], which is consistent with the ATLAS measurement of top quark pair production [87]. The same uncertainty is used for the small single-top-quark background [88]. For W +jets, a cross-section uncertainty of 20% is taken from the recent ATLAS measurement of W +jets production with b -jets [89]. The uncertainty on the simulated diboson background cross-section increases with the E_T^{miss} threshold from 20% for $E_T^{\text{miss}} > 150 \text{ GeV}$ to 30% for $E_T^{\text{miss}} > 400 \text{ GeV}$ [4]. For vector boson plus Higgs boson production, an uncertainty of 3.1% on the cross-section is estimated from theoretical calculations [90] and is applied here. The signal samples from MC simulation are produced at LO. An estimated value of 10% is used as the uncertainty on the signal cross-section from NLO corrections [91]. The systematic uncertainty on the signal acceptance due to the choice of parton distribution functions (PDFs) is determined by using the uncertainty eigenvectors provided for multiple PDF sets per the PDF4LHC prescription [61]. The uncertainty from this source is given by the maximum difference in detector acceptance of the signal process when using different variations in the MSTW2008 LO [42] and NNPDF2.1 [64] PDF sets, leading to an uncertainty of $\sim 4\%$ to 8% for the Z' -2HDM model, and $\sim 2\%$ to 21% for the different EFT models. For the simulated background processes, the uncertainty due to variations in MSTW2008 NNLO [42, 62], CT10 NNLO [45, 63], and NNPDF2.3 [64] PDF sets and parton shower models is $\sim 5\%$ to 7%.

The systematic uncertainty on the data-driven $Z(\rightarrow v\bar{v})$ +jets background comes from the transfer function and from the simulated backgrounds that are subtracted from the $Z(\rightarrow \mu^+\mu^-)$ +jets data sample (the high- p_T γ +jets sample has a purity of over 99% after b -tagging requirements). For the latter, all of the systematic uncertainties noted above are calculated for simulated samples. Since these backgrounds are subtracted here, the uncertainties are anticorrelated with the variations of the corresponding backgrounds in the signal region. For the transfer function, there are contributions from the functional form used, the stage of event selections from which the transfer function is calculated, the fit range in E_T^{miss} , how well the transfer function describes the shape of the ratio distribution, and the statistical uncertainty on the fit function parameters. In the high- E_T^{miss} region where γ +jets simulation is used to derive the transfer function, there are additional sources of systematic uncertainty on the transfer function from the efficiencies of photon identification, reconstruction, and isolation, and photon energy scale and resolution [71]. A 10% uncertainty on the cross-section is also taken into account from the normalization factor of 0.9 applied to the $Z(\rightarrow v\bar{v})$ +jets background, as described in Section 7.1. The theoretical uncertainty on the Z/γ ratio at high p_T is $\sim 4\%$ [80], which is small in comparison and hence not applied. The total systematic uncertainty on the $Z(\rightarrow v\bar{v})$ +jets background in the resolved channel is 20% in the lower E_T^{miss} region where $Z(\rightarrow \mu^+\mu^-)$ +jets is used and 12% in the higher E_T^{miss} region where γ +jets is used. In the boosted channel, only γ +jets is used to estimate $Z(\rightarrow v\bar{v})$ +jets background and the total systematic uncertainty is approximately 16%.

As explained in Section 7.3, the top quark p_T distribution is reweighted at the Monte Carlo generator level to bring it into agreement with measurements of the data. The size of the correction is found to be 5.5% in shape and normalization combined in the resolved channel, where it is considered as an additional source of systematic uncertainty. The correction has a greater effect in the boosted channel as the original mismodeling in simulation is primarily in high- p_T regions. The systematic uncertainty associated with the top quark p_T reweighting is evaluated to be $\sim 15\%$ and applied to the top quark process in the boosted channel.

Overall, the systematic uncertainty on the estimated background is calculated to be between 10% and 16% in the resolved channel, and between 12% and 14% in the boosted channel, depending on the final E_T^{miss} requirement in the signal region. Table 4 lists the main sources of systematic uncertainty for both the

resolved and boosted channels, and their values for both signals and backgrounds. The values given for the backgrounds are the uncertainties on the total background with the relative weights and correlations of individual background processes taken into account.

Table 4: Summary of systematic uncertainty in percent for all backgrounds combined and signal samples in the resolved and boosted channels. The first column lists the main sources of systematic uncertainty, where the acronym JES refers to the jet energy scale, JER the jet energy resolution, JMS the jet mass scale, JMR the jet mass resolution, and JVF the jet vertex fraction. The uncertainty figures listed for “*b*-tagging” combine the uncertainty from both *b*-tagging efficiency and mistag rates. The uncertainty ranges in “Total Background” reflect the shift in value with increasing E_T^{miss} threshold in the final signal region. The uncertainties for “ $Z(\nu\bar{\nu})$ transfer function” take into account the fractional weight of the $Z(\nu\bar{\nu})$ process in total background, which differs per analysis channel and E_T^{miss} threshold. Most of the systematic uncertainties on the signal models vary little across the parameter space in this analysis, with the exception of signal PDF and α_s , JMS, and pileup uncertainty; hence the ranges of values are shown.

	Resolved (%)		Boosted (%)	
	Z'-2HDM	Total Background	EFT	Total Background
<i>b</i> -tagging	14	6–10	13	5.3
JES(small+large- <i>R</i>)	2.4	1.8–2.8	3.0	2.2–8.5
JER(small+large- <i>R</i>)	0.6	3.5–5.4	1.0	1.5–4.6
JMS(large- <i>R</i>)	-	-	1.0–2.5	1.3
JMR(large- <i>R</i>)	-	-	2.0	1.6
JVF (small- <i>R</i>)	0.7	0.5–0.9	1.1	0.2–0.6
E_T^{miss} resolution/scale	0.0	< 0.2	0.5	0.1–0.8
Pileup	0.3	0.1	0.1–1.7	2.4
Cross-section	10	6.0–11	10	7.6–8.1
PDF and α_s	3.8–7.0	2.9	2.0–21	1.8
$Z(\nu\bar{\nu})$ transfer function	-	1.4–2.7	-	5.4–5.8
Total syst.	18–19	10–16	13–25	13–14

9 Results

Table 5 shows the predicted number of background events in the signal region for each value of the ascending E_T^{miss} thresholds, along with the number of events observed in the data. The numbers of predicted background events and observed events are consistent within 1σ in five out of the six signal regions. For the boosted channel and $E_T^{\text{miss}} > 300$ GeV, 20 events are observed in the data compared to a background expectation of 11.2 ± 2.3 events. The probability that the number of events in the background fluctuates to the value in the data or above corresponds to 2.2σ . Figure 5 shows the E_T^{miss} distributions for the data and the estimated background in the signal regions of the resolved and boosted channels. Also shown in the resolved channel are the E_T^{miss} distributions for two examples of the Z'-2HDM model at different $m_{Z'}$ with $m_A = 300$ GeV and $\tan\beta = 1$. Similarly the E_T^{miss} distributions for two examples of the EFT models with different m_χ are shown in the boosted channel. The 2.2σ upward fluctuation mentioned above is primarily due to events with E_T^{miss} values between 300 GeV and 400 GeV, and mass of the leading large-*R* jet below the Higgs boson mass, while signal events are most likely to have higher E_T^{miss} values and leading large-*R* jet mass close to Higgs boson mass.

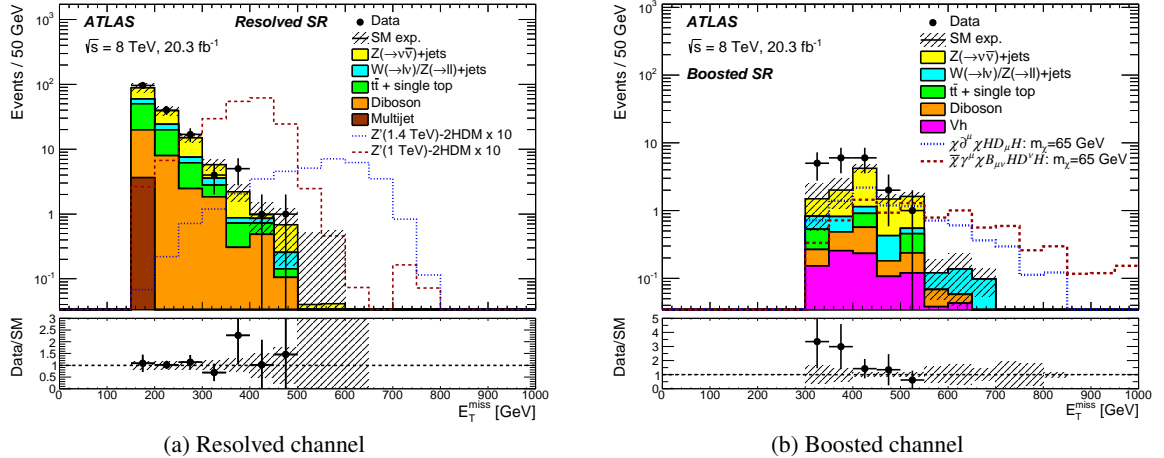


Figure 5: The E_T^{miss} distributions of (a) the resolved channel and (b) the boosted channel in the signal region (SR) for the estimated backgrounds (solid histograms) and the observed data (points). The hatched areas represent the combined statistical and systematic uncertainties in the total background estimation. The E_T^{miss} distributions for a few signal processes are overlayed in dashed lines for shape comparison: the Z' -2HDM signals are scaled by a factor of 10, and the EFT signals are scaled to their corresponding expected cross-section limit. In the resolved channel, the small contributions from Wh and Zh are included in the W or $Z(\rightarrow v\bar{v})$ plus jets distributions.

Table 5: The numbers of predicted background events for each background process, the sum of all background components, and observed data in the signal region (SR) of the resolved and boosted channels for each of the sliding E_T^{miss} requirements. Statistical and systematic uncertainties are combined. The uncertainties on the total background take into account the correlation of systematic uncertainties among different background processes. The large uncertainty on the $Z(\rightarrow v\bar{v})$ -jets process in the $E_T^{\text{miss}} > 150 \text{ GeV}$ SR of the resolved channel is due to limited statistics in the $Z(\rightarrow \mu^+\mu^-)$ -jets data sample used for the estimation of $Z(\rightarrow v\bar{v})$ -jets with $E_T^{\text{miss}} < 200 \text{ GeV}$.

E_T^{miss}	Resolved				Boosted	
	$> 150 \text{ GeV}$	$> 200 \text{ GeV}$	$> 300 \text{ GeV}$	$> 400 \text{ GeV}$	$> 300 \text{ GeV}$	$> 400 \text{ GeV}$
$Z(\rightarrow v\bar{v})$ -jets	48 ± 32	21 ± 5	2.9 ± 1.1	0.3 ± 0.3	7.0 ± 2.0	5.2 ± 1.6
Multijet	3.7 ± 3.1	0.02 ± 0.02	—	—	$< 0.0 \pm 0.1$	$< 0.0 \pm 0.1$
$t\bar{t}$ & single-top	48 ± 10	17 ± 3.8	1.6 ± 0.5	0.3 ± 0.1	0.8 ± 0.5	0.6 ± 0.4
W -jets & Z -jets	15 ± 3.4	6.2 ± 1.5	1.1 ± 0.3	0.3 ± 0.1	1.4 ± 0.7	0.8 ± 0.4
Diboson	29.4 ± 7.5	13.2 ± 3.8	2.8 ± 1.0	0.6 ± 0.3	0.9 ± 0.5	0.6 ± 0.3
Vh (bb)	5.0 ± 0.7	4.2 ± 0.6	1.0 ± 0.2	0.3 ± 0.1	1.0 ± 0.2	0.6 ± 0.1
Total background	148 ± 30	62 ± 7.5	9.4 ± 1.8	1.7 ± 0.5	11.2 ± 2.3	7.7 ± 1.7
Data	164	68	11	2	20	9

A Frequentist approach is used for the statistical interpretation of the results [92]. For this single bin counting experiment, the Poisson probability of the background-only hypothesis, the $p(s=0)$ -value, is calculated for each of the four signal regions with ascending E_T^{miss} threshold in the resolved channel and the two signal regions in the boosted channel. The 95% CL upper limits on the number of non-Standard Model events in each of the signal regions are also obtained using a profile-likelihood-ratio test following the CL_s prescription [93], which can be translated into model-independent 95% CL upper limits on the

visible cross-section, defined as the product of production cross-section, acceptance, and reconstruction efficiency of any signal model. The limits are calculated taking into account the uncertainty on the background estimate, the integrated luminosity of the data sample, and its uncertainty. Table 6 gives the model-independent 95% CL upper limits on the visible cross-section, the observed and expected limits on the number of non-Standard Model events in the signal region, and the $p(s = 0)$ -values.

As a $p(s = 0)$ -value of 0.03 is calculated for $E_T^{\text{miss}} > 300 \text{ GeV}$ in the boosted channel, a calculation of the look-elsewhere effect [94] is performed. Using pseudo-experiments and taking into account correlations between all signal regions in both channels, the probability that there is a deviation in the data from the background expectation at least as significant as the one observed due to a statistical fluctuation in the background is calculated to be approximately 10%.

Table 6: Model-independent upper limits for the resolved and boosted channels. Left to right: signal region (SR) E_T^{miss} requirement, number of observed events, number of expected background events, 95% CL upper limits on the visible cross-section ($\langle \sigma_{\text{vis}} \rangle_{\text{obs}}^{95}$) and the number of non-SM events ($N_{\text{BSM}}_{\text{obs}}^{95}$). The sixth column ($N_{\text{BSM}}_{\text{exp}}^{95}$) shows the expected 95% CL upper limit on the number of non-SM events, given the estimated number and the $\pm 1\sigma$ uncertainty of background events. The last column shows the p -value for the background-only hypothesis ($p(s = 0)$).

	E_T^{miss}	N_{obs}	N_{bkgd}	$\langle \sigma_{\text{vis}} \rangle_{\text{obs}}^{95} [\text{fb}]$	$N_{\text{BSM}}_{\text{obs}}^{95}$	$N_{\text{BSM}}_{\text{exp}}^{95}$	$p(s = 0)$
Resolved	> 150 GeV	164	148	3.6	74	63^{+22}_{-14}	0.31
	> 200 GeV	68	62	1.3	27	$21^{+8.4}_{-3.9}$	0.28
	> 300 GeV	11	9.4	0.49	9.9	$8.2^{+3.4}_{-1.9}$	0.31
	> 400 GeV	2	1.7	0.24	4.8	$4.7^{+1.6}_{-1.0}$	0.39
Boosted	> 300 GeV	20	11.2	0.90	18	$9.9^{+4.2}_{-2.9}$	0.03
	> 400 GeV	9	7.7	0.43	8.8	$7.7^{+3.3}_{-2.0}$	0.37

The numbers of observed events and expected background events, along with each of the signal and background statistical and systematic uncertainties, are used to determine limits for the Z' -2HDM model and EFT models, which are interpreted separately. Limits on the signal yield are set using a similar profile-likelihood-ratio test with the CL_s method as the aforementioned model-independent upper limit calculation. Each of the systematic uncertainties is treated as a nuisance parameter, with the correlations among the sources of systematic uncertainty taken into account.

For the resolved channel, the 95% CL upper limit on the cross-section is derived and used to exclude portions of parameter space of the Z' -2HDM model in both the $m_{Z'} - m_A$ and $m_{Z'} - \tan\beta$ planes. In both cases, the Z' gauge coupling is set to its 95% CL upper limit from precision electroweak constraints and searches for dijet resonances for the corresponding Z' mass and $\tan\beta$ value. Taking the alignment limit of $\alpha = \beta - \pi/2$ evades the constraints in $\tan\beta$ for a Type 2 two-Higgs-doublet model using fits to the observed Higgs boson couplings from the LHC [95]. The exclusion region in the $m_{Z'} - m_A$ plane is shown in Figure 6(a), where $m_A \geq 300 \text{ GeV}$ in accordance with $b \rightarrow s\gamma$ constraints [19]. For $\tan\beta = 1$, $m_{Z'} = 700\text{--}1300 \text{ GeV}$ is excluded for m_A up to 350 GeV, with further exclusion of larger m_A for $m_{Z'}$ around 1200 GeV. Limits in the $m_{Z'} - \tan\beta$ plane are shown in Figure 6(b), where $\tan\beta \geq 0.3$ based on the perturbativity requirement of the Higgs-top Yukawa coupling [96], and is below 10 based on direct searches for the A [97]. For $m_A = 300 \text{ GeV}$, where A decays almost exclusively to a DM pair, $m_{Z'} = 700\text{--}1300 \text{ GeV}$ is excluded for $\tan\beta < 2$, with further exclusion of larger $\tan\beta$ for $m_{Z'}$ between 800 GeV and 1000 GeV due to the inclusion of the $Z' \rightarrow Zh$ contribution in the final state. The limits are stronger in regions with larger $m_{Z'}$ and smaller m_A (or a larger contribution from $Z' \rightarrow Zh$ where the Z boson is

much lighter than A), as the harder E_T^{miss} spectrum in these cases allows a higher E_T^{miss} requirement with better sensitivity, as demonstrated in Table 6. The sensitivity eventually drops at very large $m_{Z'}$ due to the decrease in signal production cross-section.

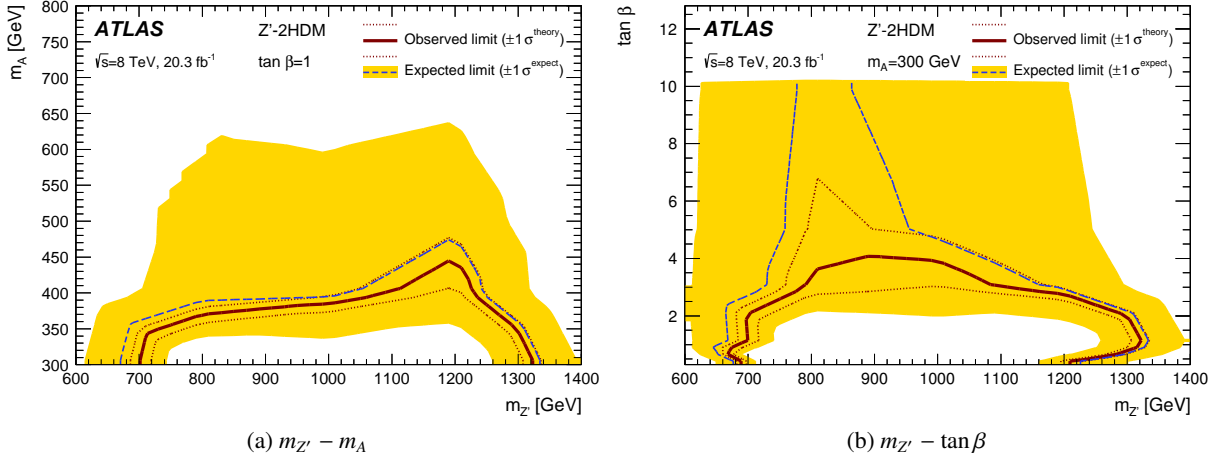


Figure 6: The Z' -2HDM exclusion contour in the (a) $m_{Z'}-m_A$ plane for $\tan \beta = 1$ and (b) $m_{Z'}-\tan \beta$ plane for $m_A = 300$ GeV. The expected limit is given by the dashed blue line, and the yellow bands indicate its $\pm 1\sigma$ uncertainty. The observed limit is given by the solid red line, and the red dotted lines show the variations of the observed limit due to a $\pm 1\sigma$ change in the signal theoretical cross-section. The parameter spaces below the limit contours are excluded at 95% CL.

For the boosted channel, limits on DM production are derived from the cross-section limits at a given DM mass m_χ , and expressed as 95% CL limits on the suppression scale Λ or coupling parameter λ for the effective field theory operators described by Equations 1 to 4. As mentioned earlier, the effective field theory model becomes a poor approximation of an ultraviolet-complete model containing a heavy mediator V when the momentum transferred in the interaction, Q_{tr} , is comparable to the mass of the intermediate state $m_V = \Lambda \sqrt{g_q g_\chi}$ [98, 99], where g_q and g_χ represent the coupling of V to SM and DM particles, respectively. To give an indication of the impact of the unknown ultraviolet details of the theory, a truncation method is adopted [100], and limits are computed in which only simulated events with $Q_{\text{tr}} = m_{\chi\chi} < m_V$ are retained. These limits are calculated for both values of $g = \sqrt{g_q g_\chi} = 1$ and 4π , the latter being the maximum possible value for the interaction to remain perturbative. The limits are derived assuming that the kinematic properties of the events in the signal processes are independent of $\Lambda(\lambda)$. The assumption is not valid in certain regions of parameter space already excluded by invisible Higgs boson [95, 101] or Z boson [102] decays or near the perturbativity boundary. The limits for operators $|\chi|^2 |H|^2$ and $\bar{\chi} i \gamma_5 \chi |H|^2$ are calculated to be in such regions where the aforementioned kinematic assumption is not valid, hence only limits for the $\chi^\dagger \partial^\mu \chi H^\dagger D_\mu H$ and $\bar{\chi} \gamma^\mu \chi B_{\mu\nu} H^\dagger D^\nu H$ operators are shown in Figure 7 for regions of parameter space where the kinematic assumption holds.

For both operators shown in Figure 7 corresponding to either fermionic or scalar DM candidates, the limits achieved by this analysis are a few times stronger than the prior ATLAS search for DM production in association with a Higgs boson where the Higgs boson decays to a pair of photons [16]. For the $\chi^\dagger \partial^\mu \chi H^\dagger D_\mu H$ operator, the Z coupling between DM and nucleon leads to a sizable cross-section for direct detection, and results from the LUX Collaboration [103] exclude larger regions of parameter space than this search. However, the LUX limits are not applicable if the DM is inelastic leading to insufficient

energy transition for direct detection. The upper limit on the branching ratio of the Z boson decaying invisibly places stronger constraints for this model for DM with mass values below half of the Z boson mass. For the lowest m_χ region not excluded by results from searches for invisible Higgs boson decays or invisible Z boson decays near $m_\chi = m_H/2$, with the kinematic assumption, values of Λ up to 24, 91, and 270 GeV are excluded for the $\bar{\chi} i\gamma_5 \chi |H|^2$, $\chi^\dagger \partial^\mu \chi H^\dagger D_\mu H$, and $\bar{\chi} \gamma^\mu \chi B_{\mu\nu} H^\dagger D^\nu H$ operators respectively; values of λ above 6.7 are excluded for the $|\chi|^2 |H|^2$ operator.

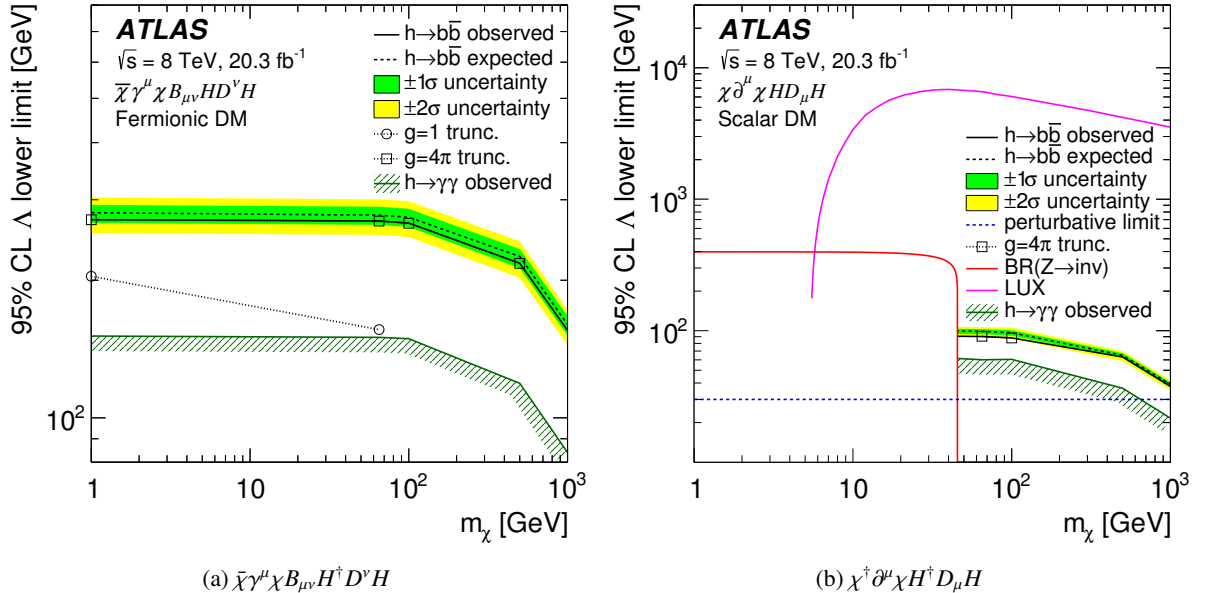


Figure 7: Limits at 95% CL on the suppression scale Λ as a function of the DM mass (m_χ) for EFT operators (a) $\bar{\chi} \gamma^\mu \chi B_{\mu\nu} H^\dagger D^\nu H$ and (b) $\chi^\dagger \partial^\mu \chi H^\dagger D_\mu H$. Solid black lines are due to $h(\rightarrow b\bar{b}) + E_T^{\text{miss}}$ (this article); regions below the lines are excluded. Results where EFT truncation is applied are also shown, assuming coupling values $g = \sqrt{g_q g_\chi} = 1$ (line with circles), 4π (line with squares). The $g = 4\pi$ case overlaps with the no-truncation result. The solid green line with hash marks indicates regions excluded by collider searches for $h(\rightarrow \gamma\gamma) + E_T^{\text{miss}}$ [16]. In the right figure, the region below the dashed blue line fails the perturbativity requirement, the red line indicates regions excluded by upper limits on the invisible branching ratio (BR) of the Z boson [102], and the magenta line indicates regions excluded by the LUX Collaboration [103].

10 Conclusion

A search has been carried out for dark matter pair production in association with a Higgs boson that decays into two b -quarks, using 20.3 fb^{-1} of pp collisions collected at $\sqrt{s} = 8 \text{ TeV}$ by the ATLAS detector at the LHC. Two techniques have been employed, one in which the two b -quark jets from the Higgs boson decay are reconstructed separately (resolved), and the other in which they are found inside a single large-radius jet using boosted jet techniques (boosted). A set of increasing E_T^{miss} thresholds defines the final signal regions for each channel, optimized for individual signals in the parameter space probed.

The numbers of observed events have been found to be consistent with Standard Model predictions. Results from the resolved channel are used to set constraints in regions of parameter space for a Z' -two-

Higgs-doublet simplified model. For $m_A = 300$ GeV, $m_{Z'} = 700\text{--}1300$ GeV is excluded for $\tan\beta < 2$, with further exclusion of larger m_A when $\tan\beta = 1$. The boosted channel results have been interpreted in the framework of different effective field theory operators that describe the interaction between dark matter particles and the Higgs boson. In addition, model-independent upper limits have been placed in both channels on the visible cross-section of events with large missing transverse momentum and a Higgs boson decaying to two b -quarks for each of the ascending E_T^{miss} thresholds up to $E_T^{\text{miss}} > 400$ GeV.

Acknowledgements

We thank CERN for the very successful operation of the LHC, as well as the support staff from our institutions without whom ATLAS could not be operated efficiently.

We acknowledge the support of ANPCyT, Argentina; YerPhI, Armenia; ARC, Australia; BMWFW and FWF, Austria; ANAS, Azerbaijan; SSTC, Belarus; CNPq and FAPESP, Brazil; NSERC, NRC and CFI, Canada; CERN; CONICYT, Chile; CAS, MOST and NSFC, China; COLCIENCIAS, Colombia; MSMT CR, MPO CR and VSC CR, Czech Republic; DNRF, DNSRC and Lundbeck Foundation, Denmark; IN2P3-CNRS, CEA-DSM/IRFU, France; GNSF, Georgia; BMBF, HGF, and MPG, Germany; GSRT, Greece; RGC, Hong Kong SAR, China; ISF, I-CORE and Benoziyo Center, Israel; INFN, Italy; MEXT and JSPS, Japan; CNRST, Morocco; FOM and NWO, Netherlands; RCN, Norway; MNiSW and NCN, Poland; FCT, Portugal; MNE/IFA, Romania; MES of Russia and NRC KI, Russian Federation; JINR; MESTD, Serbia; MSSR, Slovakia; ARRS and MIZŠ, Slovenia; DST/NRF, South Africa; MINECO, Spain; SRC and Wallenberg Foundation, Sweden; SERI, SNSF and Cantons of Bern and Geneva, Switzerland; MOST, Taiwan; TAEK, Turkey; STFC, United Kingdom; DOE and NSF, United States of America. In addition, individual groups and members have received support from BCKDF, the Canada Council, CANARIE, CRC, Compute Canada, FQRNT, and the Ontario Innovation Trust, Canada; EPLANET, ERC, FP7, Horizon 2020 and Marie Skłodowska-Curie Actions, European Union; Investissements d’Avenir Labex and Idex, ANR, Region Auvergne and Fondation Partager le Savoir, France; DFG and AvH Foundation, Germany; Herakleitos, Thales and Aristeia programmes co-financed by EU-ESF and the Greek NSRF; BSF, GIF and Minerva, Israel; BRF, Norway; the Royal Society and Leverhulme Trust, United Kingdom.

The crucial computing support from all WLCG partners is acknowledged gratefully, in particular from CERN and the ATLAS Tier-1 facilities at TRIUMF (Canada), NDGF (Denmark, Norway, Sweden), CC-IN2P3 (France), KIT/GridKA (Germany), INFN-CNAF (Italy), NL-T1 (Netherlands), PIC (Spain), ASGC (Taiwan), RAL (UK) and BNL (USA) and in the Tier-2 facilities worldwide.

References

- [1] G. Bertone, D. Hooper and J. Silk, *Particle dark matter: Evidence, candidates and constraints*, *Phys. Rept.* **405** (2005) 279–390, arXiv:[hep-ph/0404175 \[hep-ph\]](#).
- [2] D. Bauer et al.,
Dark matter in the coming decade: Complementary paths to discovery and beyond,
Phys. Dark Univ. **7-8** (2015) 16–23, arXiv:[1305.1605 \[hep-ph\]](#).

- [3] G. Steigman and M. S. Turner, *Cosmological constraints on the properties of weakly interacting massive particles*, Nucl. Phys. **B253** (1985) 375.
- [4] ATLAS Collaboration, *Search for new phenomena in final states with an energetic jet and large missing transverse momentum in pp collisions at $\sqrt{s} = 8$ TeV with the ATLAS detector*, Eur. Phys. J. **C75** (2015) 299, arXiv:[1502.01518 \[hep-ex\]](#).
- [5] CMS Collaboration, *Search for dark matter, extra dimensions, and unparticles in monojet events in proton–proton collisions at $\sqrt{s} = 8$ TeV*, Eur. Phys. J. **C75** (2015) 235, arXiv:[1408.3583 \[hep-ex\]](#).
- [6] ATLAS Collaboration, *Search for dark matter in events with heavy quarks and missing transverse momentum in pp collisions with the ATLAS detector*, Eur. Phys. J. **C75** (2015) 92, arXiv:[1410.4031 \[hep-ex\]](#).
- [7] CMS Collaboration, *Search for Monotop Signatures in Proton-Proton Collisions at $\sqrt{s} = 8$ TeV*, Phys. Rev. Lett. **114** (2015) 101801, arXiv:[1410.1149 \[hep-ex\]](#).
- [8] ATLAS Collaboration, *Search for new phenomena in events with a photon and missing transverse momentum in pp collisions at $\sqrt{s} = 8$ TeV with the ATLAS detector*, Phys. Rev. **D91** (2015) 012008, arXiv:[1411.1559 \[hep-ex\]](#).
- [9] CMS Collaboration, *Search for Dark Matter and Large Extra Dimensions in pp Collisions Yielding a Photon and Missing Transverse Energy*, Phys. Rev. Lett. **108** (2012) 261803, arXiv:[1204.0821 \[hep-ex\]](#).
- [10] ATLAS Collaboration, *Search for dark matter in events with a Z boson and missing transverse momentum in pp collisions at $\sqrt{s}=8$ TeV with the ATLAS detector*, Phys. Rev. **D90** (2014) 012004, arXiv:[1404.0051 \[hep-ex\]](#).
- [11] ATLAS Collaboration, *Search for dark matter in events with a hadronically decaying W or Z boson and missing transverse momentum in pp collisions at $\sqrt{s}=8$ TeV with the ATLAS detector*, Phys. Rev. Lett. **112** (2014) 041802, arXiv:[1309.4017 \[hep-ex\]](#).
- [12] ATLAS Collaboration, *Observation of a new particle in the search for the Standard Model Higgs boson with the ATLAS detector at the LHC*, Phys. Lett. **B716** (2012) 1–29, arXiv:[1207.7214 \[hep-ex\]](#).
- [13] CMS Collaboration, *Observation of a new boson at a mass of 125 GeV with the CMS experiment at the LHC*, Phys. Lett. **B716** (2012) 30–61, arXiv:[1207.7235 \[hep-ex\]](#).
- [14] L. Carpenter et al., *Mono-Higgs-boson: A new collider probe of dark matter*, Phys. Rev. **D89** (2014) 075017, arXiv:[1312.2592 \[hep-ph\]](#).
- [15] A. Berlin, T. Lin and L.-T. Wang, *Mono-Higgs detection of dark matter at the LHC*, JHEP **06** (2014) 078, arXiv:[1402.7074 \[hep-ph\]](#).
- [16] ATLAS Collaboration, *Search for Dark Matter in Events with Missing Transverse Momentum and a Higgs Boson Decaying to Two Photons in pp Collisions at $\sqrt{s} = 8$ TeV with the ATLAS Detector*, Phys. Rev. Lett. **115** (2015) 131801, arXiv:[1506.01081 \[hep-ex\]](#).
- [17] D. Abercrombie et al., *Dark Matter Benchmark Models for Early LHC Run-2 Searches: Report of the ATLAS/CMS Dark Matter Forum* (2015), arXiv:[1507.00966 \[hep-ex\]](#).

- [18] J. Abdallah et al., *Simplified Models for Dark Matter Searches at the LHC*, *Phys. Dark Univ.* **9-10** (2015) 8–23, arXiv:[1506.03116 \[hep-ph\]](#).
- [19] G. C. Branco et al., *Theory and phenomenology of two-Higgs-doublet models*, *Phys. Rept.* **516** (2012) 1–102, arXiv:[1106.0034 \[hep-ph\]](#).
- [20] J. Beringer et al., *Review of particle physics (RPP)*, Section 10.7, *Phys. Rev. D* **86** (2012) 010001.
- [21] CDF Collaboration, T. Aaltonen et al., *Search for new particles decaying into dijets in proton-antiproton collisions at $\sqrt{s} = 1.96$ TeV*, *Phys. Rev. D* **79** (2009) 112002, arXiv:[0812.4036 \[hep-ex\]](#).
- [22] CMS Collaboration, *Search for narrow resonances and quantum black holes in inclusive and b-tagged dijet mass spectra from pp collisions at $\sqrt{s} = 7$ TeV*, *JHEP* **01** (2013) 013, arXiv:[1210.2387 \[hep-ex\]](#).
- [23] CMS Collaboration, *Search for resonances and quantum black holes using dijet mass spectra in proton-proton collisions at $\sqrt{s} = 8$ TeV*, *Phys. Rev. D* **91** (2015) 052009, arXiv:[1501.04198 \[hep-ex\]](#).
- [24] M. Cacciari, G. P. Salam and G. Soyez, *The anti- k_t jet clustering algorithm*, *JHEP* **04** (2008) 063, arXiv:[0802.1189 \[hep-ph\]](#).
- [25] ATLAS Collaboration, *Performance of b-Jet Identification in the ATLAS Experiment*, submitted to *JINST* (2015), arXiv:[1512.01094 \[hep-ex\]](#).
- [26] ATLAS Collaboration, *Search for Higgs boson pair production in the $b\bar{b}b\bar{b}$ final state from pp collisions at $\sqrt{s} = 8$ TeV with the ATLAS detector*, *Eur. Phys. J. C* **75** (2015) 412, arXiv:[1506.00285 \[hep-ex\]](#).
- [27] D. Krohn, J. Thaler and L.-T. Wang, *Jet trimming*, *JHEP* **02** (2010) 084, arXiv:[0912.1342 \[hep-ph\]](#).
- [28] ATLAS Collaboration, *Performance of jet substructure techniques for large-R jets in proton-proton collisions at $\sqrt{s} = 7$ TeV using the ATLAS detector*, *JHEP* **09** (2013) 076, arXiv:[1306.4945 \[hep-ex\]](#).
- [29] G. Aad et al., *Identification of boosted, hadronically decaying W bosons and comparisons with ATLAS data taken at $\sqrt{s} = 8$ TeV*, *Eur. Phys. J. C* **76** (2016) 154, arXiv:[1510.05821 \[hep-ex\]](#).
- [30] ATLAS Collaboration, *Flavor Tagging with Track Jets in Boosted Topologies with the ATLAS Detector* (2014), URL: <https://cds.cern.ch/record/1750681>.
- [31] ATLAS Collaboration, *Search for a new resonance decaying to a W or Z boson and a Higgs boson in the $\ell\ell/\ell\nu/vv + b\bar{b}$ final states with the ATLAS detector*, *Eur. Phys. J. C* **75** (2015) 263, arXiv:[1503.08089 \[hep-ex\]](#).
- [32] ATLAS Collaboration, *Search for a CP-odd Higgs boson decaying to Zh in pp collisions at $\sqrt{s} = 8$ TeV with the ATLAS detector*, *Phys. Lett. B* **744** (2015) 163–183, arXiv:[1502.04478 \[hep-ex\]](#).
- [33] ATLAS Collaboration, *The ATLAS Experiment at the CERN Large Hadron Collider*, *JINST* **3** (2008) S08003.
- [34] ATLAS Collaboration, *Performance of the ATLAS trigger system in 2010*, *Eur. Phys. J. C* **72** (2012) 1849, arXiv:[1110.1530 \[hep-ex\]](#).

- [35] ATLAS Collaboration, *Measurement of the muon reconstruction performance of the ATLAS detector using 2011 and 2012 LHC proton–proton collision data*, *Eur. Phys. J.* **C74** (2014) 3130, arXiv:1407.3935 [hep-ex].
- [36] T. Sjöstrand, S. Mrenna and P. Z. Skands, *A brief introduction to PYTHIA 8.1*, *Comput. Phys. Commun.* **178** (2008) 852–867, arXiv:0710.3820 [hep-ph].
- [37] ATLAS Collaboration, *The ATLAS Simulation Infrastructure*, *Eur. Phys. J.* **C70** (2010) 823–874, arXiv:1005.4568 [physics.ins-det].
- [38] S. Agostinelli et al., *GEANT4: A Simulation toolkit*, *Nucl. Instrum. Meth.* **A506** (2003) 250–303.
- [39] ATLAS Collaboration, *The simulation principle and performance of the ATLAS fast calorimeter simulation FastCaloSim* (2010), URL: <https://cds.cern.ch/record/1300517>.
- [40] J. Alwall et al., *MadGraph 5 : going beyond*, *JHEP* **06** (2011) 128, arXiv:1106.0522 [hep-ph].
- [41] ATLAS Collaboration, *Summary of ATLAS Pythia 8 tunes* (2012), URL: <http://cds.cern.ch/record/1474107>.
- [42] A. D. Martin et al., *Parton distributions for the LHC*, *Eur. Phys. J.* **C63** (2009) 189–285, arXiv:0901.0002 [hep-ph].
- [43] P. M. Nadolsky et al., *Implications of CTEQ global analysis for collider observables*, *Phys. Rev.* **D78** (2008) 013004, arXiv:0802.0007 [hep-ph].
- [44] T. Gleisberg et al., *Event generation with SHERPA 1.1*, *JHEP* **02** (2009) 007, arXiv:0811.4622 [hep-ph].
- [45] H.-L. Lai et al., *New parton distributions for collider physics*, *Phys. Rev.* **D82** (2010) 074024, arXiv:1007.2241 [hep-ph].
- [46] S. Alioli et al., *A general framework for implementing NLO calculations in shower Monte Carlo programs: the POWHEG BOX*, *JHEP* **06** (2010) 043, arXiv:1002.2581 [hep-ph].
- [47] P. Z. Skands, *Tuning Monte Carlo generators: the Perugia tunes*, *Phys. Rev.* **D82** (2010) 074018, arXiv:1005.3457 [hep-ph].
- [48] S. Frixione and B. R. Webber, *The MC@NLO 3.3 Event Generator* (2006), arXiv:hep-ph/0612272 [hep-ph].
- [49] S. Frixione and B. R. Webber, *Matching NLO QCD computations and parton shower simulations*, *JHEP* **06** (2002) 029, arXiv:hep-ph/0204244 [hep-ph].
- [50] S. Frixione et al., *Single-top production in MC@NLO*, *JHEP* **03** (2006) 092, arXiv:hep-ph/0512250 [hep-ph].
- [51] J. M. Butterworth, J. R. Forshaw and M. H. Seymour, *Multiparton interactions in photoproduction at HERA*, *Z. Phys.* **C72** (1996) 637–646, arXiv:hep-ph/9601371 [hep-ph].
- [52] B. P. Kersevan et al., *The Monte Carlo event generator AcerMC versions 2.0 to 3.8 with interfaces to PYTHIA 6.4, HERWIG 6.5 and ARIADNE 4.1*, *Comput. Phys. Commun.* **184** (2013) 919–985, arXiv:hep-ph/0405247 [hep-ph].
- [53] S. Frixione et al., *Single-top hadroproduction in association with a W boson*, *JHEP* **07** (2008) 029, arXiv:0805.3067 [hep-ph].

- [54] M. Cacciari et al., *Top-pair production at hadron colliders with next-to-next-to-leading logarithmic soft-gluon resummation*, *Phys. Lett.* **B710** (2012) 612–622, arXiv:1111.5869 [hep-ph].
- [55] M. Beneke et al., *Hadronic top-quark pair production with NNLL threshold resummation*, *Nucl. Phys.* **B855** (2012) 695–741, arXiv:1109.1536 [hep-ph].
- [56] P. Bärnreuther, M. Czakon and A. Mitov, *Percent level precision physics at the Tevatron: First genuine NNLO QCD corrections to $q\bar{q} \rightarrow t\bar{t} + X$* , *Phys. Rev. Lett.* **109** (2012) 132001, arXiv:1204.5201 [hep-ph].
- [57] M. Czakon and A. Mitov, *NNLO corrections to top pair production at hadron colliders: the quark-gluon reaction*, *JHEP* **01** (2013) 080, arXiv:1210.6832 [hep-ph].
- [58] M. Czakon and A. Mitov, *NNLO corrections to top-pair production at hadron colliders: the all-fermionic scattering channels*, *JHEP* **12** (2012) 054, arXiv:1207.0236 [hep-ph].
- [59] M. Czakon, P. Fiedler and A. Mitov, *Total Top-Quark Pair-Production Cross Section at Hadron Colliders Through $O(\alpha_S^4)$* , *Phys. Rev. Lett.* **110** (2013) 252004, arXiv:1303.6254 [hep-ph].
- [60] M. Czakon and A. Mitov, *Top++: A Program for the Calculation of the Top-Pair Cross-Section at Hadron Colliders*, *Comput. Phys. Commun.* **185** (2014) 2930, arXiv:1112.5675 [hep-ph].
- [61] M. Botje et al., *The PDF4LHC Working Group Interim Recommendations* (2011), arXiv:1101.0538 [hep-ph].
- [62] A. D. Martin et al., *Uncertainties on alpha(S) in global PDF analyses and implications for predicted hadronic cross sections*, *Eur. Phys. J.* **C64** (2009) 653–680, arXiv:0905.3531 [hep-ph].
- [63] J. Gao et al., *CT10 next-to-next-to-leading order global analysis of QCD*, *Phys. Rev.* **D89** (2014) 033009, arXiv:1302.6246 [hep-ph].
- [64] R. D. Ball et al., *Parton distributions with LHC data*, *Nucl. Phys.* **B867** (2013) 244–289, arXiv:1207.1303 [hep-ph].
- [65] G. Corcella et al., *HERWIG 6: An Event generator for hadron emission reactions with interfering gluons (including supersymmetric processes)*, *JHEP* **01** (2001) 010, arXiv:hep-ph/0011363 [hep-ph].
- [66] J. M. Campbell and R. K. Ellis, *MCFM for the Tevatron and the LHC*, *Nucl. Phys. Proc. Suppl.* **205-206** (2010) 10–15, arXiv:1007.3492 [hep-ph].
- [67] T. Han and S. Willenbrock, *QCD correction to the $p p \rightarrow W H$ and $Z H$ total cross-sections*, *Phys. Lett.* **B273** (1991) 167–172.
- [68] O. Brein, A. Djouadi and R. Harlander, *NNLO QCD corrections to the Higgs-strahlung processes at hadron colliders*, *Phys. Lett.* **B579** (2004) 149–156, arXiv:hep-ph/0307206 [hep-ph].
- [69] M. L. Ciccolini, S. Dittmaier and M. Kramer, *Electroweak radiative corrections to associated WH and ZH production at hadron colliders*, *Phys. Rev.* **D68** (2003) 073003, arXiv:hep-ph/0306234 [hep-ph].

- [70] ATLAS Collaboration, *Electron reconstruction and identification efficiency measurements with the ATLAS detector using the 2011 LHC proton-proton collision data*, *Eur. Phys. J.* **C74** (2014) 2941, arXiv:[1404.2240 \[hep-ex\]](#).
- [71] ATLAS Collaboration, *Electron and photon energy calibration with the ATLAS detector using LHC Run 1 data*, *Eur. Phys. J.* **C74** (2014) 3071, arXiv:[1407.5063 \[hep-ex\]](#).
- [72] M. Cacciari, G. P. Salam and G. Soyez, *FastJet user manual*, *Eur. Phys. J.* **C72** (2012) 1896, arXiv:[1111.6097 \[hep-ph\]](#).
- [73] ATLAS Collaboration, *Jet energy measurement and its systematic uncertainty in proton-proton collisions at $\sqrt{s} = 7$ TeV with the ATLAS detector*, *Eur. Phys. J.* **C75** (2015) 17, arXiv:[1406.0076 \[hep-ex\]](#).
- [74] M. Cacciari, G. P. Salam and G. Soyez, *The Catchment Area of Jets*, *JHEP* **04** (2008) 005, arXiv:[0802.1188 \[hep-ph\]](#).
- [75] S. Catani et al., *Longitudinally invariant K_\perp clustering algorithms for hadron hadron collisions*, *Nucl. Phys.* **B406** (1993) 187–224.
- [76] ATLAS Collaboration, *Jet energy measurement with the ATLAS detector in proton-proton collisions at $\sqrt{s} = 7$ TeV*, *Eur. Phys. J.* **C73** (2013) 2304, arXiv:[1112.6426 \[hep-ex\]](#).
- [77] ATLAS Collaboration, *Pile-up subtraction and suppression for jets in ATLAS* (2013), URL: <http://cds.cern.ch/record/1570994>.
- [78] M. Cacciari and G. P. Salam, *Pileup subtraction using jet areas*, *Phys. Lett.* **B659** (2008) 119–126, arXiv:[0707.1378 \[hep-ph\]](#).
- [79] ATLAS Collaboration, *Performance of Missing Transverse Momentum Reconstruction in Proton-Proton Collisions at 7 TeV with ATLAS*, *Eur. Phys. J.* **C72** (2012) 1844, arXiv:[1108.5602 \[hep-ex\]](#).
- [80] S. Ask et al., *Using γ +jets Production to Calibrate the Standard Model $Z(vv)+\text{jets}$ Background to New Physics Processes at the LHC*, *JHEP* **10** (2011) 058, arXiv:[1107.2803 \[hep-ph\]](#).
- [81] ATLAS Collaboration, *Search for squarks and gluinos with the ATLAS detector in final states with jets and missing transverse momentum using 4.7 fb^{-1} of $\sqrt{s} = 7$ TeV proton-proton collision data*, *Phys. Rev.* **D87** (2013) 012008, arXiv:[1208.0949 \[hep-ex\]](#).
- [82] ATLAS Collaboration, *Search for the direct production of charginos, neutralinos and staus in final states with at least two hadronically decaying taus and missing transverse momentum in pp collisions at $\sqrt{s} = 8$ TeV with the ATLAS detector*, *JHEP* **10** (2014) 96, arXiv:[1407.0350 \[hep-ex\]](#).
- [83] ATLAS Collaboration, *Measurements of normalized differential cross sections for $t\bar{t}$ production in pp collisions at $\sqrt{s} = 7$ TeV using the ATLAS detector*, *Phys. Rev.* **D90** (2014) 072004, arXiv:[1407.0371 \[hep-ex\]](#).
- [84] ATLAS Collaboration, *Search for the Standard Model Higgs boson produced in association with top quarks and decaying into $b\bar{b}$ in pp collisions at $\sqrt{s} = 8$ TeV with the ATLAS detector*, *Eur. Phys. J.* **C75** (2015) 349, arXiv:[1503.05066 \[hep-ex\]](#).

- [85] ATLAS Collaboration, *Improved luminosity determination in pp collisions at $\sqrt{s} = 7$ TeV using the ATLAS detector at the LHC*, *Eur. Phys. J.* **C73** (2013) 2518, arXiv:1302.4393 [hep-ex].
- [86] S. Moch and P. Uwer, *Heavy-quark pair production at two loops in QCD*, *Nucl. Phys. Proc. Suppl.* **183** (2008) 75–80, arXiv:0807.2794 [hep-ph].
- [87] ATLAS Collaboration, *Measurement of the top pair production cross section in 8 TeV proton-proton collisions using kinematic information in the lepton+jets final state with ATLAS*, *Phys. Rev.* **D91** (2015) 112013, arXiv:1504.04251 [hep-ex].
- [88] N. Kidonakis, *Two-loop soft anomalous dimensions for single top quark associated production with a W^- or H^-* , *Phys. Rev.* **D82** (2010) 054018, arXiv:1005.4451 [hep-ph].
- [89] ATLAS Collaboration, *Measurement of the cross-section for W boson production in association with b -jets in pp collisions at $\sqrt{s} = 7$ TeV with the ATLAS detector*, *JHEP* **06** (2013) 084, arXiv:1302.2929 [hep-ex].
- [90] LHC Higgs Cross Section Working Group, *Handbook of LHC Higgs Cross Sections: 3. Higgs Properties* (2013), arXiv:1307.1347 [hep-ph].
- [91] U. Haisch, F. Kahlhoefer and E. Re, *QCD effects in mono-jet searches for dark matter*, *JHEP* **12** (2013) 007, arXiv:1310.4491 [hep-ph].
- [92] M. Baak et al., *HistFitter software framework for statistical data analysis*, *Eur. Phys. J.* **C75** (2015) 153, arXiv:1410.1280 [hep-ex].
- [93] A. L. Read, *Presentation of search results: the CL s technique*, *Journal of Physics G: Nuclear and Particle Physics* **28** (2002) 2693, URL: <http://stacks.iop.org/0954-3899/28/i=10/a=313>.
- [94] E. Gross and O. Vitells, *Trial factors for the look elsewhere effect in high energy physics*, *Eur. Phys. J. C* **70** (Nov. 2010) 525–530, arXiv:1005.1891 [physics.data-an].
- [95] G. Aad et al., *Constraints on new phenomena via Higgs boson couplings and invisible decays with the ATLAS detector*, *JHEP* **11** (2015) 206, arXiv:1509.00672 [hep-ex].
- [96] A. Azatov et al., *Higgs fits preference for suppressed down-type couplings: Implications for supersymmetry*, *Phys. Rev.* **D86** (2012) 075033, arXiv:1206.1058 [hep-ph].
- [97] ATLAS Collaboration, *Search for neutral Higgs bosons of the minimal supersymmetric standard model in pp collisions at $\sqrt{s} = 8$ TeV with the ATLAS detector*, *JHEP* **11** (2014) 056, arXiv:1409.6064 [hep-ex].
- [98] J. Goodman et al., *Constraints on dark matter from colliders*, *Phys. Rev.* **D82** (2010) 116010, arXiv:1008.1783 [hep-ph].
- [99] G. Busoni et al., *On the validity of the effective field theory for dark matter searches at the LHC*, *Phys. Lett.* **B728** (2014) 412–421, arXiv:1307.2253 [hep-ph].
- [100] G. Busoni et al., *On the validity of the effective field theory for dark matter searches at the LHC, part II: complete analysis for the s -channel*, *JCAP* **1406** (2014) 060, arXiv:1402.1275 [hep-ph].
- [101] G. Belanger et al., *Global fit to Higgs signal strengths and couplings and implications for extended Higgs sectors*, *Phys. Rev.* **D88** (2013) 075008, arXiv:1306.2941 [hep-ph].

- [102] S. Schael et al., *Precision electroweak measurements on the Z resonance*, Phys. Rept. **427** (2006) 257–454, arXiv:[hep-ex/0509008](#) [hep-ex].
- [103] D. S. Akerib et al., *First results from the LUX dark matter experiment at the Sanford Underground Research Facility*, Phys. Rev. Lett. **112** (2014) 091303, arXiv:[1310.8214](#) [astro-ph.CO].

The ATLAS Collaboration

G. Aad⁸⁵, B. Abbott¹¹³, J. Abdallah¹⁵¹, O. Abdinov¹¹, R. Aben¹⁰⁷, M. Abolins⁹⁰, O.S. AbouZeid¹⁵⁸, H. Abramowicz¹⁵³, H. Abreu¹⁵², R. Abreu¹¹⁶, Y. Abulaiti^{146a,146b}, B.S. Acharya^{164a,164b,^a}, L. Adamczyk^{38a}, D.L. Adams²⁵, J. Adelman¹⁰⁸, S. Adomeit¹⁰⁰, T. Adye¹³¹, A.A. Affolder⁷⁴, T. Agatonovic-Jovin¹³, J. Agricola⁵⁴, J.A. Aguilar-Saavedra^{126a,126f}, S.P. Ahlen²², F. Ahmadov^{65,b}, G. Aielli^{133a,133b}, H. Akerstedt^{146a,146b}, T.P.A. Åkesson⁸¹, A.V. Akimov⁹⁶, G.L. Alberghi^{20a,20b}, J. Albert¹⁶⁹, S. Albrand⁵⁵, M.J. Alconada Verzini⁷¹, M. Alekса³⁰, I.N. Aleksandrov⁶⁵, C. Alexa^{26b}, G. Alexander¹⁵³, T. Alexopoulos¹⁰, M. Alhroob¹¹³, G. Alimonti^{91a}, L. Alio⁸⁵, J. Alison³¹, S.P. Alkire³⁵, B.M.M. Allbrooke¹⁴⁹, P.P. Allport¹⁸, A. Aloisio^{104a,104b}, A. Alonso³⁶, F. Alonso⁷¹, C. Alpigiani¹³⁸, A. Altheimer³⁵, B. Alvarez Gonzalez³⁰, D. Álvarez Piqueras¹⁶⁷, M.G. Alvaggi^{104a,104b}, B.T. Amadio¹⁵, K. Amako⁶⁶, Y. Amaral Coutinho^{24a}, C. Amelung²³, D. Amidei⁸⁹, S.P. Amor Dos Santos^{126a,126c}, A. Amorim^{126a,126b}, S. Amoroso⁴⁸, N. Amram¹⁵³, G. Amundsen²³, C. Anastopoulos¹³⁹, L.S. Ancu⁴⁹, N. Andari¹⁰⁸, T. Andeen³⁵, C.F. Anders^{58b}, G. Anders³⁰, J.K. Anders⁷⁴, K.J. Anderson³¹, A. Andreazza^{91a,91b}, V. Andrei^{58a}, S. Angelidakis⁹, I. Angelozzi¹⁰⁷, P. Anger⁴⁴, A. Angerami³⁵, F. Anghinolfi³⁰, A.V. Anisenkov^{109,c}, N. Anjos¹², A. Annovi^{124a,124b}, M. Antonelli⁴⁷, A. Antonov⁹⁸, J. Antos^{144b}, F. Anulli^{132a}, M. Aoki⁶⁶, L. Aperio Bella¹⁸, G. Arabidze⁹⁰, Y. Arai⁶⁶, J.P. Araque^{126a}, A.T.H. Arce⁴⁵, F.A. Arduh⁷¹, J.-F. Arguin⁹⁵, S. Argyropoulos⁶³, M. Arik^{19a}, A.J. Armbruster³⁰, O. Arnaez³⁰, H. Arnold⁴⁸, M. Arratia²⁸, O. Arslan²¹, A. Artamonov⁹⁷, G. Artoni²³, S. Artz⁸³, S. Asai¹⁵⁵, N. Asbah⁴², A. Ashkenazi¹⁵³, B. Åsman^{146a,146b}, L. Asquith¹⁴⁹, K. Assamagan²⁵, R. Astalos^{144a}, M. Atkinson¹⁶⁵, N.B. Atlay¹⁴¹, K. Augsten¹²⁸, M. Aurousseau^{145b}, G. Avolio³⁰, B. Axen¹⁵, M.K. Ayoub¹¹⁷, G. Azuelos^{95,d}, M.A. Baak³⁰, A.E. Baas^{58a}, M.J. Baca¹⁸, C. Bacci^{134a,134b}, H. Bachacou¹³⁶, K. Bachas¹⁵⁴, M. Backes³⁰, M. Backhaus³⁰, P. Bagiacchi^{132a,132b}, P. Bagnaia^{132a,132b}, Y. Bai^{33a}, T. Bain³⁵, J.T. Baines¹³¹, O.K. Baker¹⁷⁶, E.M. Baldin^{109,c}, P. Balek¹²⁹, T. Balestri¹⁴⁸, F. Balli⁸⁴, W.K. Balunas¹²², E. Banas³⁹, Sw. Banerjee^{173,e}, A.A.E. Bannoura¹⁷⁵, L. Barak³⁰, E.L. Barberio⁸⁸, D. Barberis^{50a,50b}, M. Barbero⁸⁵, T. Barillari¹⁰¹, M. Barisonzi^{164a,164b}, T. Barklow¹⁴³, N. Barlow²⁸, S.L. Barnes⁸⁴, B.M. Barnett¹³¹, R.M. Barnett¹⁵, Z. Barnovska⁵, A. Baroncelli^{134a}, G. Barone²³, A.J. Barr¹²⁰, F. Barreiro⁸², J. Barreiro Guimarães da Costa^{33a}, R. Bartoldus¹⁴³, A.E. Barton⁷², P. Bartos^{144a}, A. Basalaev¹²³, A. Bassalat¹¹⁷, A. Basye¹⁶⁵, R.L. Bates⁵³, S.J. Batista¹⁵⁸, J.R. Batley²⁸, M. Battaglia¹³⁷, M. Bauce^{132a,132b}, F. Bauer¹³⁶, H.S. Bawa^{143,f}, J.B. Beacham¹¹¹, M.D. Beattie⁷², T. Beau⁸⁰, P.H. Beauchemin¹⁶¹, R. Beccherle^{124a,124b}, P. Bechtle²¹, H.P. Beck^{17,g}, K. Becker¹²⁰, M. Becker⁸³, M. Beckingham¹⁷⁰, C. Becot¹¹⁷, A.J. Beddall^{19b}, A. Beddall^{19b}, V.A. Bednyakov⁶⁵, C.P. Bee¹⁴⁸, L.J. Beemster¹⁰⁷, T.A. Beermann³⁰, M. Begel²⁵, J.K. Behr¹²⁰, C. Belanger-Champagne⁸⁷, W.H. Bell⁴⁹, G. Bella¹⁵³, L. Bellagamba^{20a}, A. Bellerive²⁹, M. Bellomo⁸⁶, K. Belotskiy⁹⁸, O. Beltramello³⁰, O. Benary¹⁵³, D. Benchekroun^{135a}, M. Bender¹⁰⁰, K. Bendtz^{146a,146b}, N. Benekos¹⁰, Y. Benhammou¹⁵³, E. Benhar Noccioli⁴⁹, J.A. Benitez Garcia^{159b}, D.P. Benjamin⁴⁵, J.R. Bensinger²³, S. Bentvelsen¹⁰⁷, L. Beresford¹²⁰, M. Beretta⁴⁷, D. Berge¹⁰⁷, E. Bergeaas Kuutmann¹⁶⁶, N. Berger⁵, F. Berghaus¹⁶⁹, J. Beringer¹⁵, C. Bernard²², N.R. Bernard⁸⁶, C. Bernius¹¹⁰, F.U. Bernlochner²¹, T. Berry⁷⁷, P. Berta¹²⁹, C. Bertella⁸³, G. Bertoli^{146a,146b}, F. Bertolucci^{124a,124b}, C. Bertsche¹¹³, D. Bertsche¹¹³, M.I. Besana^{91a}, G.J. Besjes³⁶, O. Bessidskaia Bylund^{146a,146b}, M. Bessner⁴², N. Besson¹³⁶, C. Betancourt⁴⁸, S. Bethke¹⁰¹, A.J. Bevan⁷⁶, W. Bhimji¹⁵, R.M. Bianchi¹²⁵, L. Bianchini²³, M. Bianco³⁰, O. Biebel¹⁰⁰, D. Biedermann¹⁶, N.V. Biesuz^{124a,124b}, M. Biglietti^{134a}, J. Bilbao De Mendizabal⁴⁹, H. Bilokon⁴⁷, M. Bindi⁵⁴, S. Binet¹¹⁷, A. Bingul^{19b}, C. Bini^{132a,132b}, S. Biondi^{20a,20b}, D.M. Bjergaard⁴⁵, C.W. Black¹⁵⁰, J.E. Black¹⁴³, K.M. Black²², D. Blackburn¹³⁸, R.E. Blair⁶, J.-B. Blanchard¹³⁶, J.E. Blanco⁷⁷, T. Blazek^{144a}, I. Bloch⁴², C. Blocker²³, W. Blum^{83,*}, U. Blumenschein⁵⁴, S. Blunier^{32a},

G.J. Bobbink¹⁰⁷, V.S. Bobrovnikov^{109,c}, S.S. Bocchetta⁸¹, A. Bocci⁴⁵, C. Bock¹⁰⁰, M. Boehler⁴⁸,
 J.A. Bogaerts³⁰, D. Bogavac¹³, A.G. Bogdanchikov¹⁰⁹, C. Bohm^{146a}, V. Boisvert⁷⁷, T. Bold^{38a},
 V. Boldea^{26b}, A.S. Boldyrev⁹⁹, M. Bomben⁸⁰, M. Bona⁷⁶, M. Boonekamp¹³⁶, A. Borisov¹³⁰,
 G. Borissov⁷², S. Borroni⁴², J. Bortfeldt¹⁰⁰, V. Bortolotto^{60a,60b,60c}, K. Bos¹⁰⁷, D. Boscherini^{20a},
 M. Bosman¹², J. Boudreau¹²⁵, J. Bouffard², E.V. Bouhova-Thacker⁷², D. Boumediene³⁴,
 C. Bourdarios¹¹⁷, N. Bousson¹¹⁴, S.K. Boute⁵³, A. Boveia³⁰, J. Boyd³⁰, I.R. Boyko⁶⁵, I. Bozic¹³,
 J. Bracinik¹⁸, A. Brandt⁸, G. Brandt⁵⁴, O. Brandt^{58a}, U. Bratzler¹⁵⁶, B. Brau⁸⁶, J.E. Brau¹¹⁶,
 H.M. Braun^{175,*}, W.D. Breaden Madden⁵³, K. Brendlinger¹²², A.J. Brennan⁸⁸, L. Brenner¹⁰⁷,
 R. Brenner¹⁶⁶, S. Bressler¹⁷², T.M. Bristow⁴⁶, D. Britton⁵³, D. Britzger⁴², F.M. Brochu²⁸, I. Brock²¹,
 R. Brock⁹⁰, J. Bronner¹⁰¹, G. Brooijmans³⁵, T. Brooks⁷⁷, W.K. Brooks^{32b}, J. Brosamer¹⁵, E. Brost¹¹⁶,
 P.A. Bruckman de Renstrom³⁹, D. Bruncko^{144b}, R. Bruneliere⁴⁸, A. Bruni^{20a}, G. Bruni^{20a},
 M. Bruschi^{20a}, N. Bruscino²¹, L. Bryngemark⁸¹, T. Buanes¹⁴, Q. Buat¹⁴², P. Buchholz¹⁴¹,
 A.G. Buckley⁵³, I.A. Budagov⁶⁵, F. Buehrer⁴⁸, L. Bugge¹¹⁹, M.K. Bugge¹¹⁹, O. Bulekov⁹⁸, D. Bullock⁸,
 H. Burckhart³⁰, S. Burdin⁷⁴, C.D. Burgard⁴⁸, B. Burghgrave¹⁰⁸, S. Burke¹³¹, I. Burmeister⁴³,
 E. Busato³⁴, D. Büscher⁴⁸, V. Büscher⁸³, P. Bussey⁵³, J.M. Butler²², A.I. Butt³, C.M. Buttar⁵³,
 J.M. Butterworth⁷⁸, P. Butti¹⁰⁷, W. Buttinger²⁵, A. Buzatu⁵³, A.R. Buzykaev^{109,c}, S. Cabrera Urbán¹⁶⁷,
 D. Caforio¹²⁸, V.M. Cairo^{37a,37b}, O. Cakir^{4a}, N. Calace⁴⁹, P. Calafiura¹⁵, A. Calandri¹³⁶, G. Calderini⁸⁰,
 P. Calfayan¹⁰⁰, L.P. Caloba^{24a}, D. Calvet³⁴, S. Calvet³⁴, R. Camacho Toro³¹, S. Camarda⁴²,
 P. Camarri^{133a,133b}, D. Cameron¹¹⁹, R. Caminal Armadans¹⁶⁵, S. Campana³⁰, M. Campanelli⁷⁸,
 A. Campoverde¹⁴⁸, V. Canale^{104a,104b}, A. Canepa^{159a}, M. Cano Bret^{33e}, J. Cantero⁸², R. Cantrill^{126a},
 T. Cao⁴⁰, M.D.M. Capeans Garrido³⁰, I. Caprini^{26b}, M. Caprini^{26b}, M. Capua^{37a,37b}, R. Caputo⁸³,
 R.M. Carbone³⁵, R. Cardarelli^{133a}, F. Cardillo⁴⁸, T. Carli³⁰, G. Carlino^{104a}, L. Carminati^{91a,91b},
 S. Caron¹⁰⁶, E. Carquin^{32a}, G.D. Carrillo-Montoya³⁰, J.R. Carter²⁸, J. Carvalho^{126a,126c}, D. Casadei⁷⁸,
 M.P. Casado¹², M. Casolino¹², D.W. Casper¹⁶³, E. Castaneda-Miranda^{145a}, A. Castelli¹⁰⁷,
 V. Castillo Gimenez¹⁶⁷, N.F. Castro^{126a,h}, P. Catastini⁵⁷, A. Catinaccio³⁰, J.R. Catmore¹¹⁹, A. Cattai³⁰,
 J. Caudron⁸³, V. Cavaliere¹⁶⁵, D. Cavalli^{91a}, M. Cavalli-Sforza¹², V. Cavasinni^{124a,124b},
 F. Ceradini^{134a,134b}, L. Cerdá Alberich¹⁶⁷, B.C. Cerio⁴⁵, K. Cerny¹²⁹, A.S. Cerqueira^{24b}, A. Cerri¹⁴⁹,
 L. Cerrito⁷⁶, F. Cerutti¹⁵, M. Cerv³⁰, A. Cervelli¹⁷, S.A. Cetin^{19c}, A. Chafaq^{135a}, D. Chakraborty¹⁰⁸,
 I. Chalupkova¹²⁹, Y.L. Chan^{60a}, P. Chang¹⁶⁵, J.D. Chapman²⁸, D.G. Charlton¹⁸, C.C. Chau¹⁵⁸,
 C.A. Chavez Barajas¹⁴⁹, S. Che¹¹¹, S. Cheatham¹⁵², A. Chegwidden⁹⁰, S. Chekanov⁶,
 S.V. Chekulaev^{159a}, G.A. Chelkov^{65,i}, M.A. Chelstowska⁸⁹, C. Chen⁶⁴, H. Chen²⁵, K. Chen¹⁴⁸,
 L. Chen^{33d,j}, S. Chen^{33c}, S. Chen¹⁵⁵, X. Chen^{33f}, Y. Chen⁶⁷, H.C. Cheng⁸⁹, Y. Cheng³¹, A. Cheplakov⁶⁵,
 E. Cheremushkina¹³⁰, R. Cherkaoui El Moursli^{135e}, V. Chernyatin^{25,*}, E. Cheu⁷, L. Chevalier¹³⁶,
 V. Chiarella⁴⁷, G. Chiarelli^{124a,124b}, G. Chiodini^{73a}, A.S. Chisholm¹⁸, R.T. Chislett⁷⁸, A. Chitan^{26b},
 M.V. Chizhov⁶⁵, K. Choi⁶¹, S. Chouridou⁹, B.K.B. Chow¹⁰⁰, V. Christodoulou⁷⁸,
 D. Chromek-Burckhart³⁰, J. Chudoba¹²⁷, A.J. Chuinard⁸⁷, J.J. Chwastowski³⁹, L. Chytka¹¹⁵,
 G. Ciapetti^{132a,132b}, A.K. Ciftci^{4a}, D. Cinca⁵³, V. Cindro⁷⁵, I.A. Cioara²¹, A. Ciocio¹⁵, F. Cirotto^{104a,104b},
 Z.H. Citron¹⁷², M. Ciubancan^{26b}, A. Clark⁴⁹, B.L. Clark⁵⁷, P.J. Clark⁴⁶, R.N. Clarke¹⁵,
 C. Clement^{146a,146b}, Y. Coadou⁸⁵, M. Cobal^{164a,164c}, A. Coccaro⁴⁹, J. Cochran⁶⁴, L. Coffey²³,
 L. Colasurdo¹⁰⁶, B. Cole³⁵, S. Cole¹⁰⁸, A.P. Colijn¹⁰⁷, J. Collot⁵⁵, T. Colombo^{58c}, G. Compostella¹⁰¹,
 P. Conde Muiño^{126a,126b}, E. Coniavitis⁴⁸, S.H. Connell^{145b}, I.A. Connolly⁷⁷, V. Consorti⁴⁸,
 S. Constantinescu^{26b}, C. Conta^{121a,121b}, G. Conti³⁰, F. Conventi^{104a,k}, M. Cooke¹⁵, B.D. Cooper⁷⁸,
 A.M. Cooper-Sarkar¹²⁰, T. Cornelissen¹⁷⁵, M. Corradi^{132a,132b}, F. Corriveau^{87,l}, A. Corso-Radu¹⁶³,
 A. Cortes-Gonzalez¹², G. Cortiana¹⁰¹, G. Costa^{91a}, M.J. Costa¹⁶⁷, D. Costanzo¹³⁹, D. Côté⁸, G. Cottin²⁸,
 G. Cowan⁷⁷, B.E. Cox⁸⁴, K. Cranmer¹¹⁰, G. Cree²⁹, S. Crépé-Renaudin⁵⁵, F. Crescioli⁸⁰,
 W.A. Cribbs^{146a,146b}, M. Crispin Ortizar¹²⁰, M. Cristinziani²¹, V. Croft¹⁰⁶, G. Crosetti^{37a,37b},
 T. Cuhadar Donszelmann¹³⁹, J. Cummings¹⁷⁶, M. Curatolo⁴⁷, J. Cúth⁸³, C. Cuthbert¹⁵⁰, H. Czirr¹⁴¹,

P. Czodrowski³, S. D'Auria⁵³, M. D'Onofrio⁷⁴, M.J. Da Cunha Sargedas De Sousa^{126a,126b}, C. Da Via⁸⁴, W. Dabrowski^{38a}, A. Dafinca¹²⁰, T. Dai⁸⁹, O. Dale¹⁴, F. Dallaire⁹⁵, C. Dallapiccola⁸⁶, M. Dam³⁶, J.R. Dandoy³¹, N.P. Dang⁴⁸, A.C. Daniells¹⁸, M. Danninger¹⁶⁸, M. Dano Hoffmann¹³⁶, V. Dao⁴⁸, G. Darbo^{50a}, S. Darmora⁸, J. Dassoulas³, A. Dattagupta⁶¹, W. Davey²¹, C. David¹⁶⁹, T. Davidek¹²⁹, E. Davies^{120,m}, M. Davies¹⁵³, P. Davison⁷⁸, Y. Davygora^{58a}, E. Dawe⁸⁸, I. Dawson¹³⁹, R.K. Daya-Ishmukhametova⁸⁶, K. De⁸, R. de Asmundis^{104a}, A. De Benedetti¹¹³, S. De Castro^{20a,20b}, S. De Cecco⁸⁰, N. De Groot¹⁰⁶, P. de Jong¹⁰⁷, H. De la Torre⁸², F. De Lorenzi⁶⁴, D. De Pedis^{132a}, A. De Salvo^{132a}, U. De Sanctis¹⁴⁹, A. De Santo¹⁴⁹, J.B. De Vivie De Regie¹¹⁷, W.J. Dearnaley⁷², R. Debbe²⁵, C. Debenedetti¹³⁷, D.V. Dedovich⁶⁵, I. Deigaard¹⁰⁷, J. Del Peso⁸², T. Del Prete^{124a,124b}, D. Delgove¹¹⁷, F. Deliot¹³⁶, C.M. Delitzsch⁴⁹, M. Deliyergiyev⁷⁵, A. Dell'Acqua³⁰, L. Dell'Asta²², M. Dell'Orso^{124a,124b}, M. Della Pietra^{104a,k}, D. della Volpe⁴⁹, M. Delmastro⁵, P.A. Delsart⁵⁵, C. Deluca¹⁰⁷, D.A. DeMarco¹⁵⁸, S. Demers¹⁷⁶, M. Demichev⁶⁵, A. Demilly⁸⁰, S.P. Denisov¹³⁰, D. Derendarz³⁹, J.E. Derkaoui^{135d}, F. Derue⁸⁰, P. Dervan⁷⁴, K. Desch²¹, C. Deterre⁴², K. Dette⁴³, P.O. Deviveiros³⁰, A. Dewhurst¹³¹, S. Dhaliwal²³, A. Di Ciaccio^{133a,133b}, L. Di Ciaccio⁵, A. Di Domenico^{132a,132b}, C. Di Donato^{132a,132b}, A. Di Girolamo³⁰, B. Di Girolamo³⁰, A. Di Mattia¹⁵², B. Di Micco^{134a,134b}, R. Di Nardo⁴⁷, A. Di Simone⁴⁸, R. Di Sipio¹⁵⁸, D. Di Valentino²⁹, C. Diaconu⁸⁵, M. Diamond¹⁵⁸, F.A. Dias⁴⁶, M.A. Diaz^{32a}, E.B. Diehl⁸⁹, J. Dietrich¹⁶, S. Diglio⁸⁵, A. Dimitrievska¹³, J. Dingfelder²¹, P. Dita^{26b}, S. Dita^{26b}, F. Dittus³⁰, F. Djama⁸⁵, T. Djobava^{51b}, J.I. Djuvsland^{58a}, M.A.B. do Vale^{24c}, D. Dobos³⁰, M. Dobre^{26b}, C. Doglioni⁸¹, T. Dohmae¹⁵⁵, J. Dolejsi¹²⁹, Z. Dolezal¹²⁹, B.A. Dolgoshein^{98,*}, M. Donadelli^{24d}, S. Donati^{124a,124b}, P. Dondero^{121a,121b}, J. Donini³⁴, J. Dopke¹³¹, A. Doria^{104a}, M.T. Dova⁷¹, A.T. Doyle⁵³, E. Drechsler⁵⁴, M. Dris¹⁰, Y. Du^{33d}, E. Dubreuil³⁴, E. Duchovni¹⁷², G. Duckeck¹⁰⁰, O.A. Ducu^{26b,85}, D. Duda¹⁰⁷, A. Dudarev³⁰, L. Duflot¹¹⁷, L. Duguid⁷⁷, M. Dührssen³⁰, M. Dunford^{58a}, H. Duran Yildiz^{4a}, M. Düren⁵², A. Durglishvili^{51b}, D. Duschinger⁴⁴, B. Dutta⁴², M. Dyndal^{38a}, C. Eckardt⁴², K.M. Ecker¹⁰¹, R.C. Edgar⁸⁹, W. Edson², N.C. Edwards⁴⁶, W. Ehrenfeld²¹, T. Eifert³⁰, G. Eigen¹⁴, K. Einsweiler¹⁵, T. Ekelof¹⁶⁶, M. El Kacimi^{135c}, M. Ellert¹⁶⁶, S. Elles⁵, F. Ellinghaus¹⁷⁵, A.A. Elliot¹⁶⁹, N. Ellis³⁰, J. Elmsheuser¹⁰⁰, M. Elsing³⁰, D. Emeliyanov¹³¹, Y. Enari¹⁵⁵, O.C. Endner⁸³, M. Endo¹¹⁸, J. Erdmann⁴³, A. Ereditato¹⁷, G. Ernis¹⁷⁵, J. Ernst², M. Ernst²⁵, S. Errede¹⁶⁵, E. Ertel⁸³, M. Escalier¹¹⁷, H. Esch⁴³, C. Escobar¹²⁵, B. Esposito⁴⁷, A.I. Etienne¹³⁶, E. Etzion¹⁵³, H. Evans⁶¹, A. Ezhilov¹²³, L. Fabbri^{20a,20b}, G. Facini³¹, R.M. Fakhrutdinov¹³⁰, S. Falciano^{132a}, R.J. Falla⁷⁸, J. Faltova¹²⁹, Y. Fang^{33a}, M. Fanti^{91a,91b}, A. Farbin⁸, A. Farilla^{134a}, T. Farooque¹², S. Farrell¹⁵, S.M. Farrington¹⁷⁰, P. Farthouat³⁰, F. Fassi^{135e}, P. Fassnacht³⁰, D. Fassouliotis⁹, M. Faucci Giannelli⁷⁷, A. Favaretto^{50a,50b}, L. Fayard¹¹⁷, O.L. Fedin^{123,n}, W. Fedorko¹⁶⁸, S. Feigl³⁰, L. Feligioni⁸⁵, C. Feng^{33d}, E.J. Feng³⁰, H. Feng⁸⁹, A.B. Fenyuk¹³⁰, L. Feremenga⁸, P. Fernandez Martinez¹⁶⁷, S. Fernandez Perez³⁰, J. Ferrando⁵³, A. Ferrari¹⁶⁶, P. Ferrari¹⁰⁷, R. Ferrari^{121a}, D.E. Ferreira de Lima⁵³, A. Ferrer¹⁶⁷, D. Ferrere⁴⁹, C. Ferretti⁸⁹, A. Ferretto Parodi^{50a,50b}, M. Fiascaris³¹, F. Fiedler⁸³, A. Filipčič⁷⁵, M. Filipuzzi⁴², F. Filthaut¹⁰⁶, M. Fincke-Keeler¹⁶⁹, K.D. Finelli¹⁵⁰, M.C.N. Fiolhais^{126a,126c}, L. Fiorini¹⁶⁷, A. Firan⁴⁰, A. Fischer², C. Fischer¹², J. Fischer¹⁷⁵, W.C. Fisher⁹⁰, N. Flaschel⁴², I. Fleck¹⁴¹, P. Fleischmann⁸⁹, G.T. Fletcher¹³⁹, G. Fletcher⁷⁶, R.R.M. Fletcher¹²², T. Flick¹⁷⁵, A. Floderus⁸¹, L.R. Flores Castillo^{60a}, M.J. Flowerdew¹⁰¹, G.T. Forcolin⁸⁴, A. Formica¹³⁶, A. Forti⁸⁴, D. Fournier¹¹⁷, H. Fox⁷², S. Fracchia¹², P. Francavilla⁸⁰, M. Franchini^{20a,20b}, D. Francis³⁰, L. Franconi¹¹⁹, M. Franklin⁵⁷, M. Frate¹⁶³, M. Fraternali^{121a,121b}, D. Freeborn⁷⁸, S.T. French²⁸, S.M. Fressard-Batraneanu³⁰, F. Friedrich⁴⁴, D. Froidevaux³⁰, J.A. Frost¹²⁰, C. Fukunaga¹⁵⁶, E. Fullana Torregrosa⁸³, B.G. Fulsom¹⁴³, T. Fusayasu¹⁰², J. Fuster¹⁶⁷, C. Gabaldon⁵⁵, O. Gabizon¹⁷⁵, A. Gabrielli^{20a,20b}, A. Gabrielli¹⁵, G.P. Gach¹⁸, S. Gadatsch³⁰, S. Gadomski⁴⁹, G. Gagliardi^{50a,50b}, P. Gagnon⁶¹, C. Galea¹⁰⁶, B. Galhardo^{126a,126c}, E.J. Gallas¹²⁰, B.J. Gallop¹³¹, P. Gallus¹²⁸, G. Galster³⁶, K.K. Gan¹¹¹, J. Gao^{33b,85}, Y. Gao⁴⁶, Y.S. Gao^{143,f}, F.M. Garay Walls⁴⁶, F. Garberson¹⁷⁶, C. García¹⁶⁷, J.E. García Navarro¹⁶⁷, M. Garcia-Sciveres¹⁵, R.W. Gardner³¹,

N. Garelli¹⁴³, V. Garonne¹¹⁹, C. Gatti⁴⁷, A. Gaudiello^{50a,50b}, G. Gaudio^{121a}, B. Gaur¹⁴¹, L. Gauthier⁹⁵,
 P. Gauzzi^{132a,132b}, I.L. Gavrilenko⁹⁶, C. Gay¹⁶⁸, G. Gaycken²¹, E.N. Gazis¹⁰, P. Ge^{33d}, Z. Gecse¹⁶⁸,
 C.N.P. Gee¹³¹, Ch. Geich-Gimbel²¹, M.P. Geisler^{58a}, C. Gemme^{50a}, M.H. Genest⁵⁵, C. Geng^{33b,o},
 S. Gentile^{132a,132b}, S. George⁷⁷, D. Gerbaudo¹⁶³, A. Gershon¹⁵³, S. Ghasemi¹⁴¹, H. Ghazlane^{135b},
 B. Giacobbe^{20a}, S. Giagu^{132a,132b}, V. Giangiobbe¹², P. Giannetti^{124a,124b}, B. Gibbard²⁵, S.M. Gibson⁷⁷,
 M. Gignac¹⁶⁸, M. Gilchriese¹⁵, T.P.S. Gillam²⁸, D. Gillberg³⁰, G. Gilles³⁴, D.M. Gingrich^{3,d},
 N. Giokaris⁹, M.P. Giordani^{164a,164c}, F.M. Giorgi^{20a}, F.M. Giorgi¹⁶, P.F. Giraud¹³⁶, P. Giromini⁴⁷,
 D. Giugni^{91a}, C. Giuliani¹⁰¹, M. Giulini^{58b}, B.K. Gjelsten¹¹⁹, S. Gkaitatzis¹⁵⁴, I. Gkialas¹⁵⁴,
 E.L. Gkougkousis¹¹⁷, L.K. Gladilin⁹⁹, C. Glasman⁸², J. Glatzer³⁰, P.C.F. Glaysher⁴⁶, A. Glazov⁴²,
 M. Goblirsch-Kolb¹⁰¹, J.R. Goddard⁷⁶, J. Godlewski³⁹, S. Goldfarb⁸⁹, T. Golling⁴⁹, D. Golubkov¹³⁰,
 A. Gomes^{126a,126b,126d}, R. Gonçalo^{126a}, J. Goncalves Pinto Firmino Da Costa¹³⁶, L. Gonella²¹,
 S. González de la Hoz¹⁶⁷, G. Gonzalez Parra¹², S. Gonzalez-Sevilla⁴⁹, L. Goossens³⁰, P.A. Gorbounov⁹⁷,
 H.A. Gordon²⁵, I. Gorelov¹⁰⁵, B. Gorini³⁰, E. Gorini^{73a,73b}, A. Gorišek⁷⁵, E. Gornicki³⁹, A.T. Goshaw⁴⁵,
 C. Gössling⁴³, M.I. Gostkin⁶⁵, D. Goujdami^{135c}, A.G. Goussiou¹³⁸, N. Govender^{145b}, E. Gozani¹⁵²,
 L. Graber⁵⁴, I. Grabowska-Bold^{38a}, P.O.J. Gradin¹⁶⁶, P. Grafström^{20a,20b}, J. Gramling⁴⁹, E. Gramstad¹¹⁹,
 S. Grancagnolo¹⁶, V. Gratchev¹²³, H.M. Gray³⁰, E. Graziani^{134a}, Z.D. Greenwood^{79,p}, C. Grefe²¹,
 K. Gregersen⁷⁸, I.M. Gregor⁴², P. Grenier¹⁴³, J. Griffiths⁸, A.A. Grillo¹³⁷, K. Grimm⁷², S. Grinstein^{12,q},
 Ph. Gris³⁴, J.-F. Grivaz¹¹⁷, S. Groh⁸³, J.P. Grohs⁴⁴, A. Grohsjean⁴², E. Gross¹⁷², J. Grosse-Knetter⁵⁴,
 G.C. Grossi⁷⁹, Z.J. Grout¹⁴⁹, L. Guan⁸⁹, J. Guenther¹²⁸, F. Guescini⁴⁹, D. Guest¹⁶³, O. Gueta¹⁵³,
 E. Guido^{50a,50b}, T. Guillemin¹¹⁷, S. Guindon², U. Gul⁵³, C. Gumpert³⁰, J. Guo^{33e}, Y. Guo^{33b,o},
 S. Gupta¹²⁰, G. Gustavino^{132a,132b}, P. Gutierrez¹¹³, N.G. Gutierrez Ortiz⁷⁸, C. Gutschow⁴⁴, C. Guyot¹³⁶,
 C. Gwenlan¹²⁰, C.B. Gwilliam⁷⁴, A. Haas¹¹⁰, C. Haber¹⁵, H.K. Hadavand⁸, N. Haddad^{135e}, P. Haefner²¹,
 S. Hageböck²¹, Z. Hajduk³⁹, H. Hakobyan¹⁷⁷, M. Haleem⁴², J. Haley¹¹⁴, D. Hall¹²⁰, G. Halladjian⁹⁰,
 G.D. Hallewell⁸⁵, K. Hamacher¹⁷⁵, P. Hamal¹¹⁵, K. Hamano¹⁶⁹, A. Hamilton^{145a}, G.N. Hamity¹³⁹,
 P.G. Hamnett⁴², L. Han^{33b}, K. Hanagaki^{66,r}, K. Hanawa¹⁵⁵, M. Hance¹³⁷, B. Haney¹²², P. Hanke^{58a},
 R. Hanna¹³⁶, J.B. Hansen³⁶, J.D. Hansen³⁶, M.C. Hansen²¹, P.H. Hansen³⁶, K. Hara¹⁶⁰, A.S. Hard¹⁷³,
 T. Harenberg¹⁷⁵, F. Hariri¹¹⁷, S. Harkusha⁹², R.D. Harrington⁴⁶, P.F. Harrison¹⁷⁰, F. Hartjes¹⁰⁷,
 M. Hasegawa⁶⁷, Y. Hasegawa¹⁴⁰, A. Hasib¹¹³, S. Hassani¹³⁶, S. Haug¹⁷, R. Hauser⁹⁰, L. Hauswald⁴⁴,
 M. Havranek¹²⁷, C.M. Hawkes¹⁸, R.J. Hawkings³⁰, A.D. Hawkins⁸¹, T. Hayashi¹⁶⁰, D. Hayden⁹⁰,
 C.P. Hays¹²⁰, J.M. Hays⁷⁶, H.S. Hayward⁷⁴, S.J. Haywood¹³¹, S.J. Head¹⁸, T. Heck⁸³, V. Hedberg⁸¹,
 L. Heelan⁸, S. Heim¹²², T. Heim¹⁷⁵, B. Heinemann¹⁵, L. Heinrich¹¹⁰, J. Hejbal¹²⁷, L. Helary²²,
 S. Hellman^{146a,146b}, C. Helsens³⁰, J. Henderson¹²⁰, R.C.W. Henderson⁷², Y. Heng¹⁷³, C. Hengl⁴²,
 S. Henkelmann¹⁶⁸, A. Henrichs¹⁷⁶, A.M. Henriques Correia³⁰, S. Henrot-Versille¹¹⁷, G.H. Herbert¹⁶,
 Y. Hernández Jiménez¹⁶⁷, G. Herten⁴⁸, R. Hertenberger¹⁰⁰, L. Hervas³⁰, G.G. Hesketh⁷⁸,
 N.P. Hessey¹⁰⁷, J.W. Hetherly⁴⁰, R. Hickling⁷⁶, E. Higón-Rodriguez¹⁶⁷, E. Hill¹⁶⁹, J.C. Hill²⁸,
 K.H. Hiller⁴², S.J. Hillier¹⁸, I. Hincliffe¹⁵, E. Hines¹²², R.R. Hinman¹⁵, M. Hirose¹⁵⁷,
 D. Hirschbuehl¹⁷⁵, J. Hobbs¹⁴⁸, N. Hod¹⁰⁷, M.C. Hodgkinson¹³⁹, P. Hodgson¹³⁹, A. Hoecker³⁰,
 M.R. Hoeferkamp¹⁰⁵, F. Hoenig¹⁰⁰, M. Hohlfeld⁸³, D. Hohn²¹, T.R. Holmes¹⁵, M. Homann⁴³,
 T.M. Hong¹²⁵, B.H. Hooberman¹⁶⁵, W.H. Hopkins¹¹⁶, Y. Horii¹⁰³, A.J. Horton¹⁴², J-Y. Hostachy⁵⁵,
 S. Hou¹⁵¹, A. Hoummada^{135a}, J. Howard¹²⁰, J. Howarth⁴², M. Hrabovsky¹¹⁵, I. Hristova¹⁶,
 J. Hrvnac¹¹⁷, T. Hrynn'ova⁵, A. Hrynevich⁹³, C. Hsu^{145c}, P.J. Hsu^{151,s}, S.-C. Hsu¹³⁸, D. Hu³⁵, Q. Hu^{33b},
 X. Hu⁸⁹, Y. Huang⁴², Z. Hubacek¹²⁸, F. Hubaut⁸⁵, F. Huegging²¹, T.B. Huffman¹²⁰, E.W. Hughes³⁵,
 G. Hughes⁷², M. Huhtinen³⁰, T.A. Hülsing⁸³, N. Huseynov^{65,b}, J. Huston⁹⁰, J. Huth⁵⁷, G. Iacobucci⁴⁹,
 G. Iakovidis²⁵, I. Ibragimov¹⁴¹, L. Iconomidou-Fayard¹¹⁷, E. Ideal¹⁷⁶, Z. Idrissi^{135e}, P. Iengo³⁰,
 O. Igonkina¹⁰⁷, T. Iizawa¹⁷¹, Y. Ikegami⁶⁶, M. Ikeno⁶⁶, Y. Ilchenko^{31,t}, D. Iliadis¹⁵⁴, N. Ilic¹⁴³,
 T. Ince¹⁰¹, G. Introzzi^{121a,121b}, P. Ioannou⁹, M. Iodice^{134a}, K. Iordanidou³⁵, V. Ippolito⁵⁷,
 A. Irles Quiles¹⁶⁷, C. Isaksson¹⁶⁶, M. Ishino⁶⁸, M. Ishitsuka¹⁵⁷, R. Ishmukhametov¹¹¹, C. Issever¹²⁰,

S. Istin^{19a}, J.M. Iturbe Ponce⁸⁴, R. Iuppa^{133a,133b}, J. Ivarsson⁸¹, W. Iwanski³⁹, H. Iwasaki⁶⁶, J.M. Izen⁴¹, V. Izzo^{104a}, S. Jabbar³, B. Jackson¹²², M. Jackson⁷⁴, P. Jackson¹, M.R. Jaekel³⁰, V. Jain², K.B. Jakobi⁸³, K. Jakobs⁴⁸, S. Jakobsen³⁰, T. Jakoubek¹²⁷, J. Jakubek¹²⁸, D.O. Jamin¹¹⁴, D.K. Jana⁷⁹, E. Jansen⁷⁸, R. Jansky⁶², J. Janssen²¹, M. Janus⁵⁴, G. Jarlskog⁸¹, N. Javadov^{65,b}, T. Javůrek⁴⁸, L. Jeanty¹⁵, J. Jejelava^{51a,u}, G.-Y. Jeng¹⁵⁰, D. Jennens⁸⁸, P. Jenni^{48,v}, J. Jentzsch⁴³, C. Jeske¹⁷⁰, S. Jézéquel⁵, H. Ji¹⁷³, J. Jia¹⁴⁸, H. Jiang⁶⁴, Y. Jiang^{33b}, S. Jiggins⁷⁸, J. Jimenez Pena¹⁶⁷, S. Jin^{33a}, A. Jinaru^{26b}, O. Jinnouchi¹⁵⁷, M.D. Joergensen³⁶, P. Johansson¹³⁹, K.A. Johns⁷, W.J. Johnson¹³⁸, K. Jon-And^{146a,146b}, G. Jones¹⁷⁰, R.W.L. Jones⁷², T.J. Jones⁷⁴, J. Jongmanns^{58a}, P.M. Jorge^{126a,126b}, K.D. Joshi⁸⁴, J. Jovicevic^{159a}, X. Ju¹⁷³, A. Juste Rozas^{12,q}, M. Kaci¹⁶⁷, A. Kaczmarska³⁹, M. Kado¹¹⁷, H. Kagan¹¹¹, M. Kagan¹⁴³, S.J. Kahn⁸⁵, E. Kajomovitz⁴⁵, C.W. Kalderon¹²⁰, A. Kaluza⁸³, S. Kama⁴⁰, A. Kamenshchikov¹³⁰, N. Kanaya¹⁵⁵, S. Kaneti²⁸, V.A. Kantserov⁹⁸, J. Kanzaki⁶⁶, B. Kaplan¹¹⁰, L.S. Kaplan¹⁷³, A. Kapliy³¹, D. Kar^{145c}, K. Karakostas¹⁰, A. Karamaoun³, N. Karastathis^{10,107}, M.J. Kareem⁵⁴, E. Karentzos¹⁰, M. Karnevskiy⁸³, S.N. Karpov⁶⁵, Z.M. Karpova⁶⁵, K. Karthik¹¹⁰, V. Kartvelishvili⁷², A.N. Karyukhin¹³⁰, K. Kasahara¹⁶⁰, L. Kashif¹⁷³, R.D. Kass¹¹¹, A. Kastanas¹⁴, Y. Kataoka¹⁵⁵, C. Kato¹⁵⁵, A. Katre⁴⁹, J. Katzy⁴², K. Kawade¹⁰³, K. Kawagoe⁷⁰, T. Kawamoto¹⁵⁵, G. Kawamura⁵⁴, S. Kazama¹⁵⁵, V.F. Kazanin^{109,c}, R. Keeler¹⁶⁹, R. Kehoe⁴⁰, J.S. Keller⁴², J.J. Kempster⁷⁷, H. Keoshkerian⁸⁴, O. Kepka¹²⁷, B.P. Kerševan⁷⁵, S. Kersten¹⁷⁵, R.A. Keyes⁸⁷, F. Khalil-zada¹¹, H. Khandanyan^{146a,146b}, A. Khanov¹¹⁴, A.G. Kharlamov^{109,c}, T.J. Khoo²⁸, V. Khovanskiy⁹⁷, E. Khramov⁶⁵, J. Khubua^{51b,w}, S. Kido⁶⁷, H.Y. Kim⁸, S.H. Kim¹⁶⁰, Y.K. Kim³¹, N. Kimura¹⁵⁴, O.M. Kind¹⁶, B.T. King⁷⁴, M. King¹⁶⁷, S.B. King¹⁶⁸, J. Kirk¹³¹, A.E. Kiryunin¹⁰¹, T. Kishimoto⁶⁷, D. Kisielewska^{38a}, F. Kiss⁴⁸, K. Kiuchi¹⁶⁰, O. Kivernyk¹³⁶, E. Kladiva^{144b}, M.H. Klein³⁵, M. Klein⁷⁴, U. Klein⁷⁴, K. Kleinknecht⁸³, P. Klimek^{146a,146b}, A. Klimentov²⁵, R. Klingenberg⁴³, J.A. Klinger¹³⁹, T. Klioutchnikova³⁰, E.-E. Kluge^{58a}, P. Kluit¹⁰⁷, S. Kluth¹⁰¹, J. Knapik³⁹, E. Kneringer⁶², E.B.F.G. Knoops⁸⁵, A. Knue⁵³, A. Kobayashi¹⁵⁵, D. Kobayashi¹⁵⁷, T. Kobayashi¹⁵⁵, M. Kobel⁴⁴, M. Kocian¹⁴³, P. Kodys¹²⁹, T. Koffas²⁹, E. Koffeman¹⁰⁷, L.A. Kogan¹²⁰, S. Kohlmann¹⁷⁵, Z. Kohout¹²⁸, T. Kohriki⁶⁶, T. Koi¹⁴³, H. Kolanoski¹⁶, M. Kolb^{58b}, I. Koletsou⁵, A.A. Komar^{96,*}, Y. Komori¹⁵⁵, T. Kondo⁶⁶, N. Kondrashova⁴², K. Köneke⁴⁸, A.C. König¹⁰⁶, T. Kono^{66,x}, R. Konoplich^{110,y}, N. Konstantinidis⁷⁸, R. Kopeliansky¹⁵², S. Koperny^{38a}, L. Köpke⁸³, A.K. Kopp⁴⁸, K. Korcyl³⁹, K. Kordas¹⁵⁴, A. Korn⁷⁸, A.A. Korol^{109,c}, I. Korolkov¹², E.V. Korolkova¹³⁹, O. Kortner¹⁰¹, S. Kortner¹⁰¹, T. Kosek¹²⁹, V.V. Kostyukhin²¹, V.M. Kotov⁶⁵, A. Kotwal⁴⁵, A. Kourkoumeli-Charalampidi¹⁵⁴, C. Kourkoumelis⁹, V. Kouskoura²⁵, A. Koutsman^{159a}, R. Kowalewski¹⁶⁹, T.Z. Kowalski^{38a}, W. Kozanecki¹³⁶, A.S. Kozhin¹³⁰, V.A. Kramarenko⁹⁹, G. Kramberger⁷⁵, D. Krasnopalovtsev⁹⁸, M.W. Krasny⁸⁰, A. Krasznahorkay³⁰, J.K. Kraus²¹, A. Kravchenko²⁵, S. Kreiss¹¹⁰, M. Kretz^{58c}, J. Kretzschmar⁷⁴, K. Kreutzfeldt⁵², P. Krieger¹⁵⁸, K. Krizka³¹, K. Kroeninger⁴³, H. Kroha¹⁰¹, J. Kroll¹²², J. Kroseberg²¹, J. Krstic¹³, U. Kruchonak⁶⁵, H. Krüger²¹, N. Krumnack⁶⁴, A. Kruse¹⁷³, M.C. Kruse⁴⁵, M. Kruskal²², T. Kubota⁸⁸, H. Kucuk⁷⁸, S. Kuday^{4b}, S. Kuehn⁴⁸, A. Kugel^{58c}, F. Kuger¹⁷⁴, A. Kuhl¹³⁷, T. Kuhl⁴², V. Kukhtin⁶⁵, R. Kukla¹³⁶, Y. Kulchitsky⁹², S. Kuleshov^{32b}, M. Kuna^{132a,132b}, T. Kunigo⁶⁸, A. Kupco¹²⁷, H. Kurashige⁶⁷, Y.A. Kurochkin⁹², V. Kus¹²⁷, E.S. Kuwertz¹⁶⁹, M. Kuze¹⁵⁷, J. Kvita¹¹⁵, T. Kwan¹⁶⁹, D. Kyriazopoulos¹³⁹, A. La Rosa¹³⁷, J.L. La Rosa Navarro^{24d}, L. La Rotonda^{37a,37b}, C. Lacasta¹⁶⁷, F. Lacava^{132a,132b}, J. Lacey²⁹, H. Lacker¹⁶, D. Lacour⁸⁰, V.R. Lacuesta¹⁶⁷, E. Ladygin⁶⁵, R. Lafaye⁵, B. Laforge⁸⁰, T. Lagouri¹⁷⁶, S. Lai⁵⁴, L. Lambourne⁷⁸, S. Lammers⁶¹, C.L. Lampen⁷, W. Lampl⁷, E. Lançon¹³⁶, U. Landgraf⁴⁸, M.P.J. Landon⁷⁶, V.S. Lang^{58a}, J.C. Lange¹², A.J. Lankford¹⁶³, F. Lanni²⁵, K. Lantzsch²¹, A. Lanza^{121a}, S. Laplace⁸⁰, C. Lapoire³⁰, J.F. Laporte¹³⁶, T. Lari^{91a}, F. Lasagni Manghi^{20a,20b}, M. Lassnig³⁰, P. Laurelli⁴⁷, W. Lavrijssen¹⁵, A.T. Law¹³⁷, P. Laycock⁷⁴, T. Lazovich⁵⁷, O. Le Dortz⁸⁰, E. Le Guirriec⁸⁵, E. Le Menedeu¹², M. LeBlanc¹⁶⁹, T. LeCompte⁶, F. Ledroit-Guillon⁵⁵, C.A. Lee^{145a}, S.C. Lee¹⁵¹, L. Lee¹, G. Lefebvre⁸⁰, M. Lefebvre¹⁶⁹, F. Legger¹⁰⁰, C. Leggett¹⁵, A. Lehan⁷⁴, G. Lehmann Miotto³⁰, X. Lei⁷, W.A. Leight²⁹, A. Leisos^{154,z}, A.G. Leister¹⁷⁶,

M.A.L. Leite^{24d}, R. Leitner¹²⁹, D. Lellouch¹⁷², B. Lemmer⁵⁴, K.J.C. Leney⁷⁸, T. Lenz²¹, B. Lenzi³⁰,
 R. Leone⁷, S. Leone^{124a,124b}, C. Leonidopoulos⁴⁶, S. Leontsinis¹⁰, C. Leroy⁹⁵, C.G. Lester²⁸,
 M. Levchenko¹²³, J. Levêque⁵, D. Levin⁸⁹, L.J. Levinson¹⁷², M. Levy¹⁸, A. Lewis¹²⁰, A.M. Leyko²¹,
 M. Leyton⁴¹, B. Li^{33b,aa}, H. Li¹⁴⁸, H.L. Li³¹, L. Li⁴⁵, L. Li^{33e}, S. Li⁴⁵, X. Li⁸⁴, Y. Li^{33c,ab}, Z. Liang¹³⁷,
 H. Liao³⁴, B. Liberti^{133a}, A. Liblong¹⁵⁸, P. Lichard³⁰, K. Lie¹⁶⁵, J. Liebal²¹, W. Liebig¹⁴, C. Limbach²¹,
 A. Limosani¹⁵⁰, S.C. Lin^{151,ac}, T.H. Lin⁸³, F. Linde¹⁰⁷, B.E. Lindquist¹⁴⁸, J.T. Linnemann⁹⁰,
 E. Lipeles¹²², A. Lipniacka¹⁴, M. Lisovyi^{58b}, T.M. Liss¹⁶⁵, D. Lissauer²⁵, A. Lister¹⁶⁸, A.M. Litke¹³⁷,
 B. Liu^{151,ad}, D. Liu¹⁵¹, H. Liu⁸⁹, J. Liu⁸⁵, J.B. Liu^{33b}, K. Liu⁸⁵, L. Liu¹⁶⁵, M. Liu⁴⁵, M. Liu^{33b}, Y. Liu^{33b},
 M. Livan^{121a,121b}, A. Lleres⁵⁵, J. Llorente Merino⁸², S.L. Lloyd⁷⁶, F. Lo Sterzo¹⁵¹, E. Lobodzinska⁴²,
 P. Loch⁷, W.S. Lockman¹³⁷, F.K. Loebinger⁸⁴, A.E. Loevschall-Jensen³⁶, K.M. Loew²³, A. Loginov¹⁷⁶,
 T. Lohse¹⁶, K. Lohwasser⁴², M. Lokajicek¹²⁷, B.A. Long²², J.D. Long¹⁶⁵, R.E. Long⁷², K.A.Looper¹¹¹,
 L. Lopes^{126a}, D. Lopez Mateos⁵⁷, B. Lopez Paredes¹³⁹, I. Lopez Paz¹², J. Lorenz¹⁰⁰,
 N. Lorenzo Martinez⁶¹, M. Losada¹⁶², P.J. Lösel¹⁰⁰, X. Lou^{33a}, A. Lounis¹¹⁷, J. Love⁶, P.A. Love⁷²,
 H. Lu^{60a}, N. Lu⁸⁹, H.J. Lubatti¹³⁸, C. Luci^{132a,132b}, A. Lucotte⁵⁵, C. Luedtke⁴⁸, F. Luehring⁶¹,
 W. Lukas⁶², L. Luminari^{132a}, O. Lundberg^{146a,146b}, B. Lund-Jensen¹⁴⁷, D. Lynn²⁵, R. Lysak¹²⁷,
 E. Lytken⁸¹, H. Ma²⁵, L.L. Ma^{33d}, G. Maccarrone⁴⁷, A. Macchiolo¹⁰¹, C.M. Macdonald¹³⁹, B. Maček⁷⁵,
 J. Machado Miguens^{122,126b}, D. Macina³⁰, D. Madaffari⁸⁵, R. Madar³⁴, H.J. Maddocks⁷², W.F. Mader⁴⁴,
 A. Madsen⁴², J. Maeda⁶⁷, S. Maeland¹⁴, T. Maeno²⁵, A. Maevskiy⁹⁹, E. Magradze⁵⁴, K. Mahboubi⁴⁸,
 J. Mahlstedt¹⁰⁷, C. Maiani¹³⁶, C. Maidantchik^{24a}, A.A. Maier¹⁰¹, T. Maier¹⁰⁰, A. Maio^{126a,126b,126d},
 S. Majewski¹¹⁶, Y. Makida⁶⁶, N. Makovec¹¹⁷, B. Malaescu⁸⁰, Pa. Malecki³⁹, V.P. Maleev¹²³, F. Malek⁵⁵,
 U. Mallik⁶³, D. Malon⁶, C. Malone¹⁴³, S. Maltezos¹⁰, V.M. Malyshев¹⁰⁹, S. Malyukov³⁰, J. Mamuzic⁴²,
 G. Mancini⁴⁷, B. Mandelli³⁰, L. Mandelli^{91a}, I. Mandić⁷⁵, R. Mandrysch⁶³, J. Maneira^{126a,126b},
 L. Manhaes de Andrade Filho^{24b}, J. Manjarres Ramos^{159b}, A. Mann¹⁰⁰, A. Manousakis-Katsikakis⁹,
 B. Mansouline¹³⁶, R. Mantifel⁸⁷, M. Mantoani⁵⁴, L. Mapelli³⁰, L. March^{145c}, G. Marchiori⁸⁰,
 M. Marcisovsky¹²⁷, C.P. Marino¹⁶⁹, M. Marjanovic¹³, D.E. Marley⁸⁹, F. Marroquim^{24a}, S.P. Marsden⁸⁴,
 Z. Marshall¹⁵, L.F. Marti¹⁷, S. Marti-Garcia¹⁶⁷, B. Martin⁹⁰, T.A. Martin¹⁷⁰, V.J. Martin⁴⁶,
 B. Martin dit Latour¹⁴, M. Martinez^{12,q}, S. Martin-Haugh¹³¹, V.S. Martoiu^{26b}, A.C. Martyniuk⁷⁸,
 M. Marx¹³⁸, F. Marzano^{132a}, A. Marzin³⁰, L. Masetti⁸³, T. Mashimo¹⁵⁵, R. Mashinistov⁹⁶, J. Masić⁸⁴,
 A.L. Maslennikov^{109,c}, I. Massa^{20a,20b}, L. Massa^{20a,20b}, P. Mastrandrea⁵, A. Mastroberardino^{37a,37b},
 T. Masubuchi¹⁵⁵, P. Mättig¹⁷⁵, J. Mattmann⁸³, J. Maurer^{26b}, S.J. Maxfield⁷⁴, D.A. Maximov^{109,c},
 R. Mazini¹⁵¹, S.M. Mazza^{91a,91b}, G. Mc Goldrick¹⁵⁸, S.P. Mc Kee⁸⁹, A. McCarn⁸⁹, R.L. McCarthy¹⁴⁸,
 T.G. McCarthy²⁹, N.A. McCubbin¹³¹, K.W. McFarlane^{56,*}, J.A. McFayden⁷⁸, G. Mchedlidze⁵⁴,
 S.J. McMahon¹³¹, R.A. McPherson^{169,l}, M. Medinnis⁴², S. Meehan¹³⁸, S. Mehlhase¹⁰⁰, A. Mehta⁷⁴,
 K. Meier^{58a}, C. Meineck¹⁰⁰, B. Meirose⁴¹, B.R. Mellado Garcia^{145c}, F. Meloni¹⁷, A. Mengarelli^{20a,20b},
 S. Menke¹⁰¹, E. Meoni¹⁶¹, K.M. Mercurio⁵⁷, S. Mergelmeyer²¹, P. Mermod⁴⁹, L. Merola^{104a,104b},
 C. Meroni^{91a}, F.S. Merritt³¹, A. Messina^{132a,132b}, J. Metcalfe⁶, A.S. Mete¹⁶³, C. Meyer⁸³, C. Meyer¹²²,
 J-P. Meyer¹³⁶, J. Meyer¹⁰⁷, H. Meyer Zu Theenhausen^{58a}, R.P. Middleton¹³¹, S. Miglioranzi^{164a,164c},
 L. Mijovic²¹, G. Mikenberg¹⁷², M. Mikestikova¹²⁷, M. Mikuž⁷⁵, M. Milesi⁸⁸, A. Milic³⁰, D.W. Miller³¹,
 C. Mills⁴⁶, A. Milov¹⁷², D.A. Milstead^{146a,146b}, A.A. Minaenko¹³⁰, Y. Minami¹⁵⁵, I.A. Minashvili⁶⁵,
 A.I. Mincer¹¹⁰, B. Mindur^{38a}, M. Mineev⁶⁵, Y. Ming¹⁷³, L.M. Mir¹², K.P. Mistry¹²², T. Mitani¹⁷¹,
 J. Mitrevski¹⁰⁰, V.A. Mitsou¹⁶⁷, A. Miucci⁴⁹, P.S. Miyagawa¹³⁹, J.U. Mjörnmark⁸¹, T. Moa^{146a,146b},
 K. Mochizuki⁸⁵, S. Mohapatra³⁵, W. Mohr⁴⁸, S. Molander^{146a,146b}, R. Moles-Valls²¹, R. Monden⁶⁸,
 M.C. Mondragon⁹⁰, K. Mönig⁴², C. Monini⁵⁵, J. Monk³⁶, E. Monnier⁸⁵, A. Montalbano¹⁴⁸,
 J. Montejo Berlingen³⁰, F. Monticelli⁷¹, S. Monzani^{132a,132b}, R.W. Moore³, N. Morange¹¹⁷,
 D. Moreno¹⁶², M. Moreno Llácer⁵⁴, P. Morettini^{50a}, D. Mori¹⁴², T. Mori¹⁵⁵, M. Morii⁵⁷,
 M. Morinaga¹⁵⁵, V. Morisbak¹¹⁹, S. Moritz⁸³, A.K. Morley¹⁵⁰, G. Mornacchi³⁰, J.D. Morris⁷⁶,
 S.S. Mortensen³⁶, A. Morton⁵³, L. Morvaj¹⁰³, M. Mosidze^{51b}, J. Moss¹⁴³, K. Motohashi¹⁵⁷,

R. Mount¹⁴³, E. Mountricha²⁵, S.V. Mouraviev^{96,*}, E.J.W. Moyse⁸⁶, S. Muanza⁸⁵, R.D. Mudd¹⁸,
 F. Mueller¹⁰¹, J. Mueller¹²⁵, R.S.P. Mueller¹⁰⁰, T. Mueller²⁸, D. Muenstermann⁴⁹, P. Mullen⁵³,
 G.A. Mullier¹⁷, F.J. Munoz Sanchez⁸⁴, J.A. Murillo Quijada¹⁸, W.J. Murray^{170,131}, H. Musheghyan⁵⁴,
 E. Musto¹⁵², A.G. Myagkov^{130,ae}, M. Myska¹²⁸, B.P. Nachman¹⁴³, O. Nackenhorst⁴⁹, J. Nadal⁵⁴,
 K. Nagai¹²⁰, R. Nagai¹⁵⁷, Y. Nagai⁸⁵, K. Nagano⁶⁶, A. Nagarkar¹¹¹, Y. Nagasaka⁵⁹, K. Nagata¹⁶⁰,
 M. Nagel¹⁰¹, E. Nagy⁸⁵, A.M. Nairz³⁰, Y. Nakahama³⁰, K. Nakamura⁶⁶, T. Nakamura¹⁵⁵, I. Nakano¹¹²,
 H. Namasivayam⁴¹, R.F. Naranjo Garcia⁴², R. Narayan³¹, D.I. Narrias Villar^{58a}, T. Naumann⁴²,
 G. Navarro¹⁶², R. Nayyar⁷, H.A. Neal⁸⁹, P.Yu. Nechaeva⁹⁶, T.J. Neep⁸⁴, P.D. Nef¹⁴³, A. Negri^{121a,121b},
 M. Negrini^{20a}, S. Nektarijevic¹⁰⁶, C. Nellist¹¹⁷, A. Nelson¹⁶³, S. Nemecek¹²⁷, P. Nemethy¹¹⁰,
 A.A. Nepomuceno^{24a}, M. Nessi^{30,af}, M.S. Neubauer¹⁶⁵, M. Neumann¹⁷⁵, R.M. Neves¹¹⁰, P. Nevski²⁵,
 P.R. Newman¹⁸, D.H. Nguyen⁶, R.B. Nickerson¹²⁰, R. Nicolaïdou¹³⁶, B. Nicquevert³⁰, J. Nielsen¹³⁷,
 N. Nikiforou³⁵, A. Nikiforov¹⁶, V. Nikolaenko^{130,ae}, I. Nikolic-Audit⁸⁰, K. Nikolopoulos¹⁸,
 J.K. Nilsen¹¹⁹, P. Nilsson²⁵, Y. Ninomiya¹⁵⁵, A. Nisati^{132a}, R. Nisius¹⁰¹, T. Nobe¹⁵⁵, L. Nodulman⁶,
 M. Nomachi¹¹⁸, I. Nomidis²⁹, T. Nooney⁷⁶, S. Norberg¹¹³, M. Nordberg³⁰, O. Novgorodova⁴⁴,
 S. Nowak¹⁰¹, M. Nozaki⁶⁶, L. Nozka¹¹⁵, K. Ntekas¹⁰, G. Nunes Hanninger⁸⁸, T. Nunnemann¹⁰⁰,
 E. Nurse⁷⁸, F. Nuti⁸⁸, F. O'grady⁷, D.C. O'Neil¹⁴², V. O'Shea⁵³, F.G. Oakham^{29,d}, H. Oberlack¹⁰¹,
 T. Obermann²¹, J. Ocariz⁸⁰, A. Ochi⁶⁷, I. Ochoa³⁵, J.P. Ochoa-Ricoux^{32a}, S. Oda⁷⁰, S. Odaka⁶⁶,
 H. Ogren⁶¹, A. Oh⁸⁴, S.H. Oh⁴⁵, C.C. Ohm¹⁵, H. Ohman¹⁶⁶, H. Oide³⁰, W. Okamura¹¹⁸, H. Okawa¹⁶⁰,
 Y. Okumura³¹, T. Okuyama⁶⁶, A. Olariu^{26b}, S.A. Olivares Pino⁴⁶, D. Oliveira Damazio²⁵,
 A. Olszewski³⁹, J. Olszowska³⁹, A. Onofre^{126a,126e}, K. Onogi¹⁰³, P.U.E. Onyisi^{31,t}, C.J. Oram^{159a},
 M.J. Oreglia³¹, Y. Oren¹⁵³, D. Orestano^{134a,134b}, N. Orlando¹⁵⁴, C. Oropeza Barrera⁵³, R.S. Orr¹⁵⁸,
 B. Osculati^{50a,50b}, R. Ospanov⁸⁴, G. Otero y Garzon²⁷, H. Otono⁷⁰, M. Ouchrif^{135d}, F. Ould-Saada¹¹⁹,
 A. Ouraou¹³⁶, K.P. Oussoren¹⁰⁷, Q. Ouyang^{33a}, A. Ovcharova¹⁵, M. Owen⁵³, R.E. Owen¹⁸,
 V.E. Ozcan^{19a}, N. Ozturk⁸, K. Pachal¹⁴², A. Pacheco Pages¹², C. Padilla Aranda¹², M. Pagáčová⁴⁸,
 S. Pagan Griso¹⁵, E. Paganis¹³⁹, F. Paige²⁵, P. Pais⁸⁶, K. Pajchel¹¹⁹, G. Palacino^{159b}, S. Palestini³⁰,
 M. Palka^{38b}, D. Pallin³⁴, A. Palma^{126a,126b}, Y.B. Pan¹⁷³, E.St. Panagiotopoulou¹⁰, C.E. Pandini⁸⁰,
 J.G. Panduro Vazquez⁷⁷, P. Pani^{146a,146b}, S. Panitkin²⁵, D. Pantea^{26b}, L. Paolozzi⁴⁹,
 Th.D. Papadopoulou¹⁰, K. Papageorgiou¹⁵⁴, A. Paramonov⁶, D. Paredes Hernandez¹⁷⁶, M.A. Parker²⁸,
 K.A. Parker¹³⁹, F. Parodi^{50a,50b}, J.A. Parsons³⁵, U. Parzefall⁴⁸, E. Pasqualucci^{132a}, S. Passaggio^{50a},
 F. Pastore^{134a,134b,*}, Fr. Pastore⁷⁷, G. Pásztor²⁹, S. Pataraia¹⁷⁵, N.D. Patel¹⁵⁰, J.R. Pater⁸⁴, T. Pauly³⁰,
 J. Pearce¹⁶⁹, B. Pearson¹¹³, L.E. Pedersen³⁶, M. Pedersen¹¹⁹, S. Pedraza Lopez¹⁶⁷, R. Pedro^{126a,126b},
 S.V. Peleganchuk^{109,c}, D. Pelikan¹⁶⁶, O. Penc¹²⁷, C. Peng^{33a}, H. Peng^{33b}, B. Penning³¹, J. Penwell⁶¹,
 D.V. Perepelitsa²⁵, E. Perez Codina^{159a}, M.T. Pérez García-Estañ¹⁶⁷, L. Perini^{91a,91b}, H. Pernegger³⁰,
 S. Perrella^{104a,104b}, R. Peschke⁴², V.D. Peshekhanov⁶⁵, K. Peters³⁰, R.F.Y. Peters⁸⁴, B.A. Petersen³⁰,
 T.C. Petersen³⁶, E. Petit⁴², A. Petridis¹, C. Petridou¹⁵⁴, P. Petroff¹¹⁷, E. Petrolo^{132a}, F. Petrucci^{134a,134b},
 N.E. Pettersson¹⁵⁷, R. Pezoa^{32b}, P.W. Phillips¹³¹, G. Piacquadio¹⁴³, E. Pianori¹⁷⁰, A. Picazio⁴⁹,
 E. Piccaro⁷⁶, M. Piccinini^{20a,20b}, M.A. Pickering¹²⁰, R. Piegaia²⁷, D.T. Pignotti¹¹¹, J.E. Pilcher³¹,
 A.D. Pilkington⁸⁴, A.W.J. Pin⁸⁴, J. Pina^{126a,126b,126d}, M. Pinamonti^{164a,164c,ag}, J.L. Pinfold³, A. Pingel³⁶,
 S. Pires⁸⁰, H. Pirumov⁴², M. Pitt¹⁷², C. Pizio^{91a,91b}, L. Plazak^{144a}, M.-A. Pleier²⁵, V. Pleskot¹²⁹,
 E. Plotnikova⁶⁵, P. Plucinski^{146a,146b}, D. Pluth⁶⁴, R. Poettgen^{146a,146b}, L. Poggioli¹¹⁷, D. Pohl²¹,
 G. Polesello^{121a}, A. Poley⁴², A. Pollicchio^{37a,37b}, R. Polifka¹⁵⁸, A. Polini^{20a}, C.S. Pollard⁵³,
 V. Polychronakos²⁵, K. Pommès³⁰, L. Pontecorvo^{132a}, B.G. Pope⁹⁰, G.A. Popeneciu^{26c}, D.S. Popovic¹³,
 A. Poppleton³⁰, S. Pospisil¹²⁸, K. Potamianos¹⁵, I.N. Potrap⁶⁵, C.J. Potter¹⁴⁹, C.T. Potter¹¹⁶,
 G. Poulard³⁰, J. Poveda³⁰, V. Pozdnyakov⁶⁵, M.E. Pozo Astigarraga³⁰, P. Pralavorio⁸⁵, A. Pranko¹⁵,
 S. Prasad³⁰, S. Prell⁶⁴, D. Price⁸⁴, L.E. Price⁶, M. Primavera^{73a}, S. Prince⁸⁷, M. Proissl⁴⁶,
 K. Prokofiev^{60c}, F. Prokoshin^{32b}, E. Protopapadaki¹³⁶, S. Protopopescu²⁵, J. Proudfoot⁶,
 M. Przybycien^{38a}, E. Ptacek¹¹⁶, D. Puddu^{134a,134b}, E. Pueschel⁸⁶, D. Puldon¹⁴⁸, M. Purohit^{25,ah},

P. Puzo¹¹⁷, J. Qian⁸⁹, G. Qin⁵³, Y. Qin⁸⁴, A. Quadt⁵⁴, D.R. Quarrie¹⁵, W.B. Quayle^{164a,164b},
 M. Queitsch-Maitland⁸⁴, D. Quilty⁵³, S. Raddum¹¹⁹, V. Radeka²⁵, V. Radescu⁴², S.K. Radhakrishnan¹⁴⁸,
 P. Radloff¹¹⁶, P. Rados⁸⁸, F. Ragusa^{91a,91b}, G. Rahal¹⁷⁸, S. Rajagopalan²⁵, M. Rammensee³⁰,
 C. Rangel-Smith¹⁶⁶, F. Rauscher¹⁰⁰, S. Rave⁸³, T. Ravenscroft⁵³, M. Raymond³⁰, A.L. Read¹¹⁹,
 N.P. Readioff⁷⁴, D.M. Rebuzzi^{121a,121b}, A. Redelbach¹⁷⁴, G. Redlinger²⁵, R. Reece¹³⁷, K. Reeves⁴¹,
 L. Rehnisch¹⁶, J. Reichert¹²², H. Reisin²⁷, C. Rembser³⁰, H. Ren^{33a}, A. Renaud¹¹⁷, M. Rescigno^{132a},
 S. Resconi^{91a}, O.L. Rezanova^{109,c}, P. Reznicek¹²⁹, R. Rezvani⁹⁵, R. Richter¹⁰¹, S. Richter⁷⁸,
 E. Richter-Was^{38b}, O. Ricken²¹, M. Ridel⁸⁰, P. Rieck¹⁶, C.J. Riegel¹⁷⁵, J. Rieger⁵⁴, O. Rifki¹¹³,
 M. Rijssenbeek¹⁴⁸, A. Rimoldi^{121a,121b}, L. Rinaldi^{20a}, B. Ristić⁴⁹, E. Ritsch³⁰, I. Riu¹²,
 F. Rizatdinova¹¹⁴, E. Rizvi⁷⁶, S.H. Robertson^{87,l}, A. Robichaud-Veronneau⁸⁷, D. Robinson²⁸,
 J.E.M. Robinson⁴², A. Robson⁵³, C. Roda^{124a,124b}, S. Roe³⁰, O. Røhne¹¹⁹, A. Romaniouk⁹⁸,
 M. Romano^{20a,20b}, S.M. Romano Saez³⁴, E. Romero Adam¹⁶⁷, N. Rompotis¹³⁸, M. Ronzani⁴⁸,
 L. Roos⁸⁰, E. Ros¹⁶⁷, S. Rosati^{132a}, K. Rosbach⁴⁸, P. Rose¹³⁷, O. Rosenthal¹⁴¹, V. Rossetti^{146a,146b},
 E. Rossi^{104a,104b}, L.P. Rossi^{50a}, J.H.N. Rosten²⁸, R. Rosten¹³⁸, M. Rotaru^{26b}, I. Roth¹⁷², J. Rothberg¹³⁸,
 D. Rousseau¹¹⁷, C.R. Royon¹³⁶, A. Rozanov⁸⁵, Y. Rozen¹⁵², X. Ruan^{145c}, F. Rubbo¹⁴³, I. Rubinskiy⁴²,
 V.I. Rud⁹⁹, C. Rudolph⁴⁴, M.S. Rudolph¹⁵⁸, F. Rühr⁴⁸, A. Ruiz-Martinez³⁰, Z. Rurikova⁴⁸,
 N.A. Rusakovich⁶⁵, A. Ruschke¹⁰⁰, H.L. Russell¹³⁸, J.P. Rutherford⁷, N. Ruthmann³⁰, Y.F. Ryabov¹²³,
 M. Rybar¹⁶⁵, G. Rybkin¹¹⁷, N.C. Ryder¹²⁰, A. Ryzhov¹³⁰, A.F. Saavedra¹⁵⁰, G. Sabato¹⁰⁷,
 S. Sacerdoti²⁷, A. Saddique³, H.F-W. Sadrozinski¹³⁷, R. Sadykov⁶⁵, F. Safai Tehrani^{132a}, P. Saha¹⁰⁸,
 M. Sahinsoy^{58a}, M. Saimpert¹³⁶, T. Saito¹⁵⁵, H. Sakamoto¹⁵⁵, Y. Sakurai¹⁷¹, G. Salamanna^{134a,134b},
 A. Salamon^{133a}, J.E. Salazar Loyola^{32b}, M. Saleem¹¹³, D. Salek¹⁰⁷, P.H. Sales De Bruin¹³⁸,
 D. Salihagic¹⁰¹, A. Salnikov¹⁴³, J. Salt¹⁶⁷, D. Salvatore^{37a,37b}, F. Salvatore¹⁴⁹, A. Salvucci^{60a},
 A. Salzburger³⁰, D. Sammel⁴⁸, D. Sampsonidis¹⁵⁴, A. Sanchez^{104a,104b}, J. Sánchez¹⁶⁷,
 V. Sanchez Martinez¹⁶⁷, H. Sandaker¹¹⁹, R.L. Sandbach⁷⁶, H.G. Sander⁸³, M.P. Sanders¹⁰⁰,
 M. Sandhoff¹⁷⁵, C. Sandoval¹⁶², R. Sandstroem¹⁰¹, D.P.C. Sankey¹³¹, M. Sannino^{50a,50b}, A. Sansoni⁴⁷,
 C. Santoni³⁴, R. Santonacci^{133a,133b}, H. Santos^{126a}, I. Santoyo Castillo¹⁴⁹, K. Sapp¹²⁵, A. Sapronov⁶⁵,
 J.G. Saraiva^{126a,126d}, B. Sarrazin²¹, O. Sasaki⁶⁶, Y. Sasaki¹⁵⁵, K. Sato¹⁶⁰, G. Sauvage^{5,*}, E. Sauvan⁵,
 G. Savage⁷⁷, P. Savard^{158,d}, C. Sawyer¹³¹, L. Sawyer^{79,p}, J. Saxon³¹, C. Sbarra^{20a}, A. Sbrizzi^{20a,20b},
 T. Scanlon⁷⁸, D.A. Scannicchio¹⁶³, M. Scarcella¹⁵⁰, V. Scarfone^{37a,37b}, J. Schaarschmidt¹⁷²,
 P. Schacht¹⁰¹, D. Schaefer³⁰, R. Schaefer⁴², J. Schaeffer⁸³, S. Schaepe²¹, S. Schaetzl^{58b}, U. Schäfer⁸³,
 A.C. Schaffer¹¹⁷, D. Schaile¹⁰⁰, R.D. Schamberger¹⁴⁸, V. Scharf^{58a}, V.A. Schegelsky¹²³, D. Scheirich¹²⁹,
 M. Schernau¹⁶³, C. Schiavi^{50a,50b}, C. Schillo⁴⁸, M. Schioppa^{37a,37b}, S. Schlenker³⁰, K. Schmieden³⁰,
 C. Schmitt⁸³, S. Schmitt^{58b}, S. Schmitt⁴², S. Schmitz⁸³, B. Schneider^{159a}, Y.J. Schnellbach⁷⁴,
 U. Schnoor⁴⁴, L. Schoeffel¹³⁶, A. Schoening^{58b}, B.D. Schoenrock⁹⁰, E. Schopf²¹,
 A.L.S. Schorlemmer⁵⁴, M. Schott⁸³, D. Schouten^{159a}, J. Schovancova⁸, S. Schramm⁴⁹, M. Schreyer¹⁷⁴,
 N. Schuh⁸³, M.J. Schultens²¹, H.-C. Schultz-Coulon^{58a}, H. Schulz¹⁶, M. Schumacher⁴⁸,
 B.A. Schumm¹³⁷, Ph. Schune¹³⁶, C. Schwanenberger⁸⁴, A. Schwartzman¹⁴³, T.A. Schwarz⁸⁹,
 Ph. Schwegler¹⁰¹, H. Schweiger⁸⁴, Ph. Schwemling¹³⁶, R. Schwienhorst⁹⁰, J. Schwindling¹³⁶,
 T. Schwindt²¹, E. Scifo¹¹⁷, G. Sciolla²³, F. Scuri^{124a,124b}, F. Scutti⁸⁸, J. Searcy⁸⁹, G. Sedov⁴²,
 E. Sedykh¹²³, P. Seema²¹, S.C. Seidel¹⁰⁵, A. Seiden¹³⁷, F. Seifert¹²⁸, J.M. Seixas^{24a}, G. Sekhniaidze^{104a},
 K. Sekhon⁸⁹, S.J. Sekula⁴⁰, D.M. Seliverstov^{123,*}, N. Semprini-Cesari^{20a,20b}, C. Serfon³⁰, L. Serin¹¹⁷,
 L. Serkin^{164a,164b}, T. Serre⁸⁵, M. Sessa^{134a,134b}, R. Seuster^{159a}, H. Severini¹¹³, T. Sfiligoj⁷⁵, F. Sforza³⁰,
 A. Sfyrla³⁰, E. Shabalina⁵⁴, M. Shamim¹¹⁶, L.Y. Shan^{33a}, R. Shang¹⁶⁵, J.T. Shank²², M. Shapiro¹⁵,
 P.B. Shatalov⁹⁷, K. Shaw^{164a,164b}, S.M. Shaw⁸⁴, A. Shcherbakova^{146a,146b}, C.Y. Shehu¹⁴⁹, P. Sherwood⁷⁸,
 L. Shi^{151,ai}, S. Shimizu⁶⁷, C.O. Shimmin¹⁶³, M. Shimojima¹⁰², M. Shiyakova⁶⁵, A. Shmeleva⁹⁶,
 D. Shoaleh Saadi⁹⁵, M.J. Shochet³¹, S. Shojaii^{91a,91b}, S. Shrestha¹¹¹, E. Shulg⁹⁸, M.A. Shupe⁷,
 P. Sicho¹²⁷, P.E. Sidebo¹⁴⁷, O. Sidiropoulou¹⁷⁴, D. Sidorov¹¹⁴, A. Sidoti^{20a,20b}, F. Siegert⁴⁴,

Dj. Sijacki¹³, J. Silva^{126a,126d}, Y. Silver¹⁵³, S.B. Silverstein^{146a}, V. Simak¹²⁸, O. Simard⁵, Lj. Simic¹³, S. Simion¹¹⁷, E. Simioni⁸³, B. Simmons⁷⁸, D. Simon³⁴, M. Simon⁸³, P. Sinervo¹⁵⁸, N.B. Sinev¹¹⁶, M. Sioli^{20a,20b}, G. Siragusa¹⁷⁴, A.N. Sisakyan^{65,*}, S.Yu. Sivoklokov⁹⁹, J. Sjölin^{146a,146b}, T.B. Sjursen¹⁴, M.B. Skinner⁷², H.P. Skottowe⁵⁷, P. Skubic¹¹³, M. Slater¹⁸, T. Slavicek¹²⁸, M. Slawinska¹⁰⁷, K. Sliwa¹⁶¹, V. Smakhtin¹⁷², B.H. Smart⁴⁶, L. Smestad¹⁴, S.Yu. Smirnov⁹⁸, Y. Smirnov⁹⁸, L.N. Smirnova^{99,aj}, O. Smirnova⁸¹, M.N.K. Smith³⁵, R.W. Smith³⁵, M. Smizanska⁷², K. Smolek¹²⁸, A.A. Snesarev⁹⁶, G. Snidero⁷⁶, S. Snyder²⁵, R. Sobie^{169,l}, F. Socher⁴⁴, A. Soffer¹⁵³, D.A. Soh^{151,ai}, G. Sokhrannyi⁷⁵, C.A. Solans³⁰, M. Solar¹²⁸, J. Solc¹²⁸, E.Yu. Soldatov⁹⁸, U. Soldevila¹⁶⁷, A.A. Solodkov¹³⁰, A. Soloshenko⁶⁵, O.V. Solovyanov¹³⁰, V. Solovyev¹²³, P. Sommer⁴⁸, H.Y. Song^{33b,aa}, N. Soni¹, A. Sood¹⁵, A. Sopczak¹²⁸, B. Sopko¹²⁸, V. Sopko¹²⁸, V. Sorin¹², D. Sosa^{58b}, M. Sosebee⁸, C.L. Sotiropoulou^{124a,124b}, R. Soualah^{164a,164c}, A.M. Soukharev^{109,c}, D. South⁴², B.C. Sowden⁷⁷, S. Spagnolo^{73a,73b}, M. Spalla^{124a,124b}, M. Spangenberg¹⁷⁰, F. Spanò⁷⁷, W.R. Spearman⁵⁷, D. Sperlich¹⁶, F. Spettel¹⁰¹, R. Spighi^{20a}, G. Spigo³⁰, L.A. Spiller⁸⁸, M. Spousta¹²⁹, R.D. St. Denis^{53,*}, A. Stabile^{91a}, S. Staerz³⁰, J. Stahlman¹²², R. Stamen^{58a}, S. Stamm¹⁶, E. Stanecka³⁹, R.W. Stanek⁶, C. Stanescu^{134a}, M. Stanescu-Bellu⁴², M.M. Stanitzki⁴², S. Stapnes¹¹⁹, E.A. Starchenko¹³⁰, J. Stark⁵⁵, P. Staroba¹²⁷, P. Starovoitov^{58a}, R. Staszewski³⁹, P. Steinberg²⁵, B. Stelzer¹⁴², H.J. Stelzer³⁰, O. Stelzer-Chilton^{159a}, H. Stenzel⁵², G.A. Stewart⁵³, J.A. Stillings²¹, M.C. Stockton⁸⁷, M. Stoebe⁸⁷, G. Stoica^{26b}, P. Stolte⁵⁴, S. Stonjek¹⁰¹, A.R. Stradling⁸, A. Straessner⁴⁴, M.E. Stramaglia¹⁷, J. Strandberg¹⁴⁷, S. Strandberg^{146a,146b}, A. Strandlie¹¹⁹, E. Strauss¹⁴³, M. Strauss¹¹³, P. Strizenec^{144b}, R. Ströhmer¹⁷⁴, D.M. Strom¹¹⁶, R. Stroynowski⁴⁰, A. Strubig¹⁰⁶, S.A. Stucci¹⁷, B. Stugu¹⁴, N.A. Styles⁴², D. Su¹⁴³, J. Su¹²⁵, R. Subramaniam⁷⁹, A. Succurro¹², S. Suchek^{58a}, Y. Sugaya¹¹⁸, M. Suk¹²⁸, V.V. Sulin⁹⁶, S. Sultansoy^{4c}, T. Sumida⁶⁸, S. Sun⁵⁷, X. Sun^{33a}, J.E. Sundermann⁴⁸, K. Suruliz¹⁴⁹, G. Susinno^{37a,37b}, M.R. Sutton¹⁴⁹, S. Suzuki⁶⁶, M. Svatos¹²⁷, M. Swiatlowski³¹, I. Sykora^{144a}, T. Sykora¹²⁹, D. Ta⁴⁸, C. Taccini^{134a,134b}, K. Tackmann⁴², J. Taenzer¹⁵⁸, A. Taffard¹⁶³, R. Tafirout^{159a}, N. Taiblum¹⁵³, H. Takai²⁵, R. Takashima⁶⁹, H. Takeda⁶⁷, T. Takeshita¹⁴⁰, Y. Takubo⁶⁶, M. Talby⁸⁵, A.A. Talyshев^{109,c}, J.Y.C. Tam¹⁷⁴, K.G. Tan⁸⁸, J. Tanaka¹⁵⁵, R. Tanaka¹¹⁷, S. Tanaka⁶⁶, B.B. Tannenwald¹¹¹, S. Tapia Araya^{32b}, S. Tapprogge⁸³, S. Tarem¹⁵², F. Tarrade²⁹, G.F. Tartarelli^{91a}, P. Tas¹²⁹, M. Tasevsky¹²⁷, T. Tashiro⁶⁸, E. Tassi^{37a,37b}, A. Tavares Delgado^{126a,126b}, Y. Tayalati^{135d}, A.C. Taylor¹⁰⁵, F.E. Taylor⁹⁴, G.N. Taylor⁸⁸, P.T.E. Taylor⁸⁸, W. Taylor^{159b}, F.A. Teischinger³⁰, P. Teixeira-Dias⁷⁷, K.K. Temming⁴⁸, D. Temple¹⁴², H. Ten Kate³⁰, P.K. Teng¹⁵¹, J.J. Teoh¹¹⁸, F. Tepel¹⁷⁵, S. Terada⁶⁶, K. Terashi¹⁵⁵, J. Terron⁸², S. Terzo¹⁰¹, M. Testa⁴⁷, R.J. Teuscher^{158,l}, T. Theveneaux-Pelzer³⁴, J.P. Thomas¹⁸, J. Thomas-Wilsker⁷⁷, E.N. Thompson³⁵, P.D. Thompson¹⁸, R.J. Thompson⁸⁴, A.S. Thompson⁵³, L.A. Thomsen¹⁷⁶, E. Thomson¹²², M. Thomson²⁸, R.P. Thun^{89,*}, M.J. Tibbetts¹⁵, R.E. Ticse Torres⁸⁵, V.O. Tikhomirov^{96,ak}, Yu.A. Tikhonov^{109,c}, S. Timoshenko⁹⁸, E. Tiouchichine⁸⁵, P. Tipton¹⁷⁶, S. Tisserant⁸⁵, K. Todome¹⁵⁷, T. Todorov^{5,*}, S. Todorova-Nova¹²⁹, J. Tojo⁷⁰, S. Tokár^{144a}, K. Tokushuku⁶⁶, K. Tollefson⁹⁰, E. Tolley⁵⁷, L. Tomlinson⁸⁴, M. Tomoto¹⁰³, L. Tompkins^{143,al}, K. Toms¹⁰⁵, E. Torrence¹¹⁶, H. Torres¹⁴², E. Torró Pastor¹³⁸, J. Toth^{85,am}, F. Touchard⁸⁵, D.R. Tovey¹³⁹, T. Trefzger¹⁷⁴, L. Tremblet³⁰, A. Tricoli³⁰, I.M. Trigger^{159a}, S. Trincaz-Duvold⁸⁰, M.F. Tripiana¹², W. Trischuk¹⁵⁸, B. Trocmé⁵⁵, C. Troncon^{91a}, M. Trottier-McDonald¹⁵, M. Trovatelli¹⁶⁹, L. Truong^{164a,164c}, M. Trzebinski³⁹, A. Trzupek³⁹, C. Tsarouchas³⁰, J.C-L. Tseng¹²⁰, P.V. Tsiareshka⁹², D. Tsionou¹⁵⁴, G. Tsipolitis¹⁰, N. Tsirintanis⁹, S. Tsiskaridze¹², V. Tsiskaridze⁴⁸, E.G. Tskhadadze^{51a}, K.M. Tsui^{60a}, I.I. Tsukerman⁹⁷, V. Tsulaia¹⁵, S. Tsuno⁶⁶, D. Tsybychev¹⁴⁸, A. Tudorache^{26b}, V. Tudorache^{26b}, A.N. Tuna⁵⁷, S.A. Tupputi^{20a,20b}, S. Turchikhin^{99,aj}, D. Turecek¹²⁸, R. Turra^{91a,91b}, A.J. Turvey⁴⁰, P.M. Tuts³⁵, A. Tykhonov⁴⁹, M. Tylmad^{146a,146b}, M. Tyndel¹³¹, I. Ueda¹⁵⁵, R. Ueno²⁹, M. Ughetto^{146a,146b}, F. Ukegawa¹⁶⁰, G. Unal³⁰, A. Undrus²⁵, G. Unel¹⁶³, F.C. Ungaro⁸⁸, Y. Unno⁶⁶, C. Unverdorben¹⁰⁰, J. Urban^{144b}, P. Urquijo⁸⁸, P. Urrejola⁸³, G. Usai⁸, A. Usanova⁶², L. Vacavant⁸⁵, V. Vacek¹²⁸, B. Vachon⁸⁷, C. Valderanis⁸³, N. Valencic¹⁰⁷, S. Valentinetto^{20a,20b}, A. Valero¹⁶⁷,

L. Valery¹², S. Valkar¹²⁹, S. Vallecorsa⁴⁹, J.A. Valls Ferrer¹⁶⁷, W. Van Den Wollenberg¹⁰⁷,
 P.C. Van Der Deijl¹⁰⁷, R. van der Geer¹⁰⁷, H. van der Graaf¹⁰⁷, N. van Eldik¹⁵², P. van Gemmeren⁶,
 J. Van Nieuwkoop¹⁴², I. van Vulpen¹⁰⁷, M.C. van Woerden³⁰, M. Vanadia^{132a,132b}, W. Vandelli³⁰,
 R. Vanguri¹²², A. Vaniachine⁶, F. Vannucci⁸⁰, G. Vardanyan¹⁷⁷, R. Vari^{132a}, E.W. Varnes⁷, T. Varol⁴⁰,
 D. Varouchas⁸⁰, A. Vartapetian⁸, K.E. Varvell¹⁵⁰, F. Vazeille³⁴, T. Vazquez Schroeder⁸⁷, J. Veatch⁷,
 L.M. Veloce¹⁵⁸, F. Veloso^{126a,126c}, T. Velz²¹, S. Veneziano^{132a}, A. Ventura^{73a,73b}, D. Ventura⁸⁶,
 M. Venturi¹⁶⁹, N. Venturi¹⁵⁸, A. Venturini²³, V. Vercesi^{121a}, M. Verducci^{132a,132b}, W. Verkerke¹⁰⁷,
 J.C. Vermeulen¹⁰⁷, A. Vest⁴⁴, M.C. Vetterli^{142,d}, O. Viazlo⁸¹, I. Vichou¹⁶⁵, T. Vickey¹³⁹,
 O.E. Vickey Boeriu¹³⁹, G.H.A. Viehhauser¹²⁰, S. Viel¹⁵, R. Vigne⁶², M. Villa^{20a,20b},
 M. Villaplana Perez^{91a,91b}, E. Vilucchi⁴⁷, M.G. Vinchter²⁹, V.B. Vinogradov⁶⁵, I. Vivarelli¹⁴⁹,
 S. Vlachos¹⁰, D. Vladoiu¹⁰⁰, M. Vlasak¹²⁸, M. Vogel^{32a}, P. Vokac¹²⁸, G. Volpi^{124a,124b}, M. Volpi⁸⁸,
 H. von der Schmitt¹⁰¹, H. von Radziewski⁴⁸, E. von Toerne²¹, V. Vorobel¹²⁹, K. Vorobev⁹⁸, M. Vos¹⁶⁷,
 R. Voss³⁰, J.H. Vossebeld⁷⁴, N. Vranjes¹³, M. Vranjes Milosavljevic¹³, V. Vrba¹²⁷, M. Vreeswijk¹⁰⁷,
 R. Vuillermet³⁰, I. Vukotic³¹, Z. Vykydal¹²⁸, P. Wagner²¹, W. Wagner¹⁷⁵, H. Wahlberg⁷¹,
 S. Wahrmund⁴⁴, J. Wakabayashi¹⁰³, J. Walder⁷², R. Walker¹⁰⁰, W. Walkowiak¹⁴¹, C. Wang¹⁵¹,
 F. Wang¹⁷³, H. Wang¹⁵, H. Wang⁴⁰, J. Wang⁴², J. Wang¹⁵⁰, K. Wang⁸⁷, R. Wang⁶, S.M. Wang¹⁵¹,
 T. Wang²¹, T. Wang³⁵, X. Wang¹⁷⁶, C. Wanotayaroj¹¹⁶, A. Warburton⁸⁷, C.P. Ward²⁸, D.R. Wardrope⁷⁸,
 A. Washbrook⁴⁶, C. Wasicki⁴², P.M. Watkins¹⁸, A.T. Watson¹⁸, I.J. Watson¹⁵⁰, M.F. Watson¹⁸,
 G. Watts¹³⁸, S. Watts⁸⁴, B.M. Waugh⁷⁸, S. Webb⁸⁴, M.S. Weber¹⁷, S.W. Weber¹⁷⁴, J.S. Webster⁶,
 A.R. Weidberg¹²⁰, B. Weinert⁶¹, J. Weingarten⁵⁴, C. Weiser⁴⁸, H. Weits¹⁰⁷, P.S. Wells³⁰, T. Wenaus²⁵,
 T. Wengler³⁰, S. Wenig³⁰, N. Wermes²¹, M. Werner⁴⁸, P. Werner³⁰, M. Wessels^{58a}, J. Wetter¹⁶¹,
 K. Whalen¹¹⁶, N.L. Whallon¹³⁸, A.M. Wharton⁷², A. White⁸, M.J. White¹, R. White^{32b},
 S. White^{124a,124b}, D. Whiteson¹⁶³, F.J. Wickens¹³¹, W. Wiedenmann¹⁷³, M. Wielers¹³¹, P. Wienemann²¹,
 C. Wiglesworth³⁶, L.A.M. Wiik-Fuchs²¹, A. Wildauer¹⁰¹, H.G. Wilkens³⁰, H.H. Williams¹²²,
 S. Williams¹⁰⁷, C. Willis⁹⁰, S. Willocq⁸⁶, A. Wilson⁸⁹, J.A. Wilson¹⁸, I. Wingerter-Seez⁵,
 F. Winklmeier¹¹⁶, B.T. Winter²¹, M. Wittgen¹⁴³, J. Wittkowski¹⁰⁰, S.J. Wollstadt⁸³, M.W. Wolter³⁹,
 H. Wolters^{126a,126c}, B.K. Wosiek³⁹, J. Wotschack³⁰, M.J. Woudstra⁸⁴, K.W. Wozniak³⁹, M. Wu⁵⁵,
 M. Wu³¹, S.L. Wu¹⁷³, X. Wu⁴⁹, Y. Wu⁸⁹, T.R. Wyatt⁸⁴, B.M. Wynne⁴⁶, S. Xella³⁶, D. Xu^{33a}, L. Xu²⁵,
 B. Yabsley¹⁵⁰, S. Yacoob^{145a}, R. Yakabe⁶⁷, M. Yamada⁶⁶, D. Yamaguchi¹⁵⁷, Y. Yamaguchi¹¹⁸,
 A. Yamamoto⁶⁶, S. Yamamoto¹⁵⁵, T. Yamanaka¹⁵⁵, K. Yamauchi¹⁰³, Y. Yamazaki⁶⁷, Z. Yan²²,
 H. Yang^{33e}, H. Yang¹⁷³, Y. Yang¹⁵¹, W.-M. Yao¹⁵, Y.C. Yap⁸⁰, Y. Yasu⁶⁶, E. Yatsenko⁵,
 K.H. Yau Wong²¹, J. Ye⁴⁰, S. Ye²⁵, I. Yeletskikh⁶⁵, A.L. Yen⁵⁷, E. Yildirim⁴², K. Yorita¹⁷¹, R. Yoshida⁶,
 K. Yoshihara¹²², C. Young¹⁴³, C.J.S. Young³⁰, S. Youssef²², D.R. Yu¹⁵, J. Yu⁸, J.M. Yu⁸⁹, J. Yu¹¹⁴,
 L. Yuan⁶⁷, S.P.Y. Yuen²¹, A. Yurkewicz¹⁰⁸, I. Yusuff^{28,an}, B. Zabinski³⁹, R. Zaidan⁶³, A.M. Zaitsev^{130,ae},
 J. Zalieckas¹⁴, A. Zaman¹⁴⁸, S. Zambito⁵⁷, L. Zanello^{132a,132b}, D. Zanzi⁸⁸, C. Zeitnitz¹⁷⁵, M. Zeman¹²⁸,
 A. Zemla^{38a}, J.C. Zeng¹⁶⁵, Q. Zeng¹⁴³, K. Zengel²³, O. Zenin¹³⁰, T. Ženiš^{144a}, D. Zerwas¹¹⁷,
 D. Zhang⁸⁹, F. Zhang¹⁷³, G. Zhang^{33b}, H. Zhang^{33c}, J. Zhang⁶, L. Zhang⁴⁸, R. Zhang^{33b,j}, X. Zhang^{33d},
 Z. Zhang¹¹⁷, X. Zhao⁴⁰, Y. Zhao^{33d,117}, Z. Zhao^{33b}, A. Zhemchugov⁶⁵, J. Zhong¹²⁰, B. Zhou⁸⁹,
 C. Zhou⁴⁵, L. Zhou³⁵, L. Zhou⁴⁰, M. Zhou¹⁴⁸, N. Zhou^{33f}, C.G. Zhu^{33d}, H. Zhu^{33a}, J. Zhu⁸⁹, Y. Zhu^{33b},
 X. Zhuang^{33a}, K. Zhukov⁹⁶, A. Zibell¹⁷⁴, D. Ziemińska⁶¹, N.I. Zimine⁶⁵, C. Zimmermann⁸³,
 S. Zimmermann⁴⁸, Z. Zinonos⁵⁴, M. Zinser⁸³, M. Ziolkowski¹⁴¹, L. Živković¹³, G. Zobernig¹⁷³,
 A. Zoccoli^{20a,20b}, M. zur Nedden¹⁶, G. Zurzolo^{104a,104b}, L. Zwalinski³⁰.

¹ Department of Physics, University of Adelaide, Adelaide, Australia

² Physics Department, SUNY Albany, Albany NY, United States of America

³ Department of Physics, University of Alberta, Edmonton AB, Canada

⁴ ^(a) Department of Physics, Ankara University, Ankara; ^(b) Istanbul Aydin University, Istanbul; ^(c)

- Division of Physics, TOBB University of Economics and Technology, Ankara, Turkey
- ⁵ LAPP, CNRS/IN2P3 and Université Savoie Mont Blanc, Annecy-le-Vieux, France
- ⁶ High Energy Physics Division, Argonne National Laboratory, Argonne IL, United States of America
- ⁷ Department of Physics, University of Arizona, Tucson AZ, United States of America
- ⁸ Department of Physics, The University of Texas at Arlington, Arlington TX, United States of America
- ⁹ Physics Department, University of Athens, Athens, Greece
- ¹⁰ Physics Department, National Technical University of Athens, Zografou, Greece
- ¹¹ Institute of Physics, Azerbaijan Academy of Sciences, Baku, Azerbaijan
- ¹² Institut de Física d'Altes Energies and Departament de Física de la Universitat Autònoma de Barcelona, Barcelona, Spain
- ¹³ Institute of Physics, University of Belgrade, Belgrade, Serbia
- ¹⁴ Department for Physics and Technology, University of Bergen, Bergen, Norway
- ¹⁵ Physics Division, Lawrence Berkeley National Laboratory and University of California, Berkeley CA, United States of America
- ¹⁶ Department of Physics, Humboldt University, Berlin, Germany
- ¹⁷ Albert Einstein Center for Fundamental Physics and Laboratory for High Energy Physics, University of Bern, Bern, Switzerland
- ¹⁸ School of Physics and Astronomy, University of Birmingham, Birmingham, United Kingdom
- ¹⁹ ^(a) Department of Physics, Bogazici University, Istanbul; ^(b) Department of Physics Engineering, Gaziantep University, Gaziantep; ^(c) Department of Physics, Dogus University, Istanbul, Turkey
- ²⁰ ^(a) INFN Sezione di Bologna; ^(b) Dipartimento di Fisica e Astronomia, Università di Bologna, Bologna, Italy
- ²¹ Physikalisches Institut, University of Bonn, Bonn, Germany
- ²² Department of Physics, Boston University, Boston MA, United States of America
- ²³ Department of Physics, Brandeis University, Waltham MA, United States of America
- ²⁴ ^(a) Universidade Federal do Rio De Janeiro COPPE/EE/IF, Rio de Janeiro; ^(b) Electrical Circuits Department, Federal University of Juiz de Fora (UFJF), Juiz de Fora; ^(c) Federal University of Sao Joao del Rei (UFSJ), Sao Joao del Rei; ^(d) Instituto de Fisica, Universidade de Sao Paulo, Sao Paulo, Brazil
- ²⁵ Physics Department, Brookhaven National Laboratory, Upton NY, United States of America
- ²⁶ ^(a) Transilvania University of Brasov, Brasov, Romania; ^(b) National Institute of Physics and Nuclear Engineering, Bucharest; ^(c) National Institute for Research and Development of Isotopic and Molecular Technologies, Physics Department, Cluj Napoca; ^(d) University Politehnica Bucharest, Bucharest; ^(e) West University in Timisoara, Timisoara, Romania
- ²⁷ Departamento de Física, Universidad de Buenos Aires, Buenos Aires, Argentina
- ²⁸ Cavendish Laboratory, University of Cambridge, Cambridge, United Kingdom
- ²⁹ Department of Physics, Carleton University, Ottawa ON, Canada
- ³⁰ CERN, Geneva, Switzerland
- ³¹ Enrico Fermi Institute, University of Chicago, Chicago IL, United States of America
- ³² ^(a) Departamento de Física, Pontificia Universidad Católica de Chile, Santiago; ^(b) Departamento de Física, Universidad Técnica Federico Santa María, Valparaíso, Chile
- ³³ ^(a) Institute of High Energy Physics, Chinese Academy of Sciences, Beijing; ^(b) Department of Modern Physics, University of Science and Technology of China, Anhui; ^(c) Department of Physics, Nanjing University, Jiangsu; ^(d) School of Physics, Shandong University, Shandong; ^(e) Department of Physics and Astronomy, Shanghai Key Laboratory for Particle Physics and Cosmology, Shanghai Jiao Tong University, Shanghai; ^(f) Physics Department, Tsinghua University, Beijing 100084, China
- ³⁴ Laboratoire de Physique Corpusculaire, Clermont Université and Université Blaise Pascal and CNRS/IN2P3, Clermont-Ferrand, France

- ³⁵ Nevis Laboratory, Columbia University, Irvington NY, United States of America
³⁶ Niels Bohr Institute, University of Copenhagen, Kobenhavn, Denmark
³⁷ ^(a) INFN Gruppo Collegato di Cosenza, Laboratori Nazionali di Frascati; ^(b) Dipartimento di Fisica, Università della Calabria, Rende, Italy
³⁸ ^(a) AGH University of Science and Technology, Faculty of Physics and Applied Computer Science, Krakow; ^(b) Marian Smoluchowski Institute of Physics, Jagiellonian University, Krakow, Poland
³⁹ Institute of Nuclear Physics Polish Academy of Sciences, Krakow, Poland
⁴⁰ Physics Department, Southern Methodist University, Dallas TX, United States of America
⁴¹ Physics Department, University of Texas at Dallas, Richardson TX, United States of America
⁴² DESY, Hamburg and Zeuthen, Germany
⁴³ Institut für Experimentelle Physik IV, Technische Universität Dortmund, Dortmund, Germany
⁴⁴ Institut für Kern- und Teilchenphysik, Technische Universität Dresden, Dresden, Germany
⁴⁵ Department of Physics, Duke University, Durham NC, United States of America
⁴⁶ SUPA - School of Physics and Astronomy, University of Edinburgh, Edinburgh, United Kingdom
⁴⁷ INFN Laboratori Nazionali di Frascati, Frascati, Italy
⁴⁸ Fakultät für Mathematik und Physik, Albert-Ludwigs-Universität Freiburg, Germany
⁴⁹ Section de Physique, Université de Genève, Geneva, Switzerland
⁵⁰ ^(a) INFN Sezione di Genova; ^(b) Dipartimento di Fisica, Università di Genova, Genova, Italy
⁵¹ ^(a) E. Andronikashvili Institute of Physics, Iv. Javakhishvili Tbilisi State University, Tbilisi; ^(b) High Energy Physics Institute, Tbilisi State University, Tbilisi, Georgia
⁵² II Physikalisches Institut, Justus-Liebig-Universität Giessen, Giessen, Germany
⁵³ SUPA - School of Physics and Astronomy, University of Glasgow, Glasgow, United Kingdom
⁵⁴ II Physikalisches Institut, Georg-August-Universität, Göttingen, Germany
⁵⁵ Laboratoire de Physique Subatomique et de Cosmologie, Université Grenoble-Alpes, CNRS/IN2P3, Grenoble, France
⁵⁶ Department of Physics, Hampton University, Hampton VA, United States of America
⁵⁷ Laboratory for Particle Physics and Cosmology, Harvard University, Cambridge MA, United States of America
⁵⁸ ^(a) Kirchhoff-Institut für Physik, Ruprecht-Karls-Universität Heidelberg, Heidelberg; ^(b) Physikalisches Institut, Ruprecht-Karls-Universität Heidelberg, Heidelberg; ^(c) ZITI Institut für technische Informatik, Ruprecht-Karls-Universität Heidelberg, Mannheim, Germany
⁵⁹ Faculty of Applied Information Science, Hiroshima Institute of Technology, Hiroshima, Japan
⁶⁰ ^(a) Department of Physics, The Chinese University of Hong Kong, Shatin, N.T., Hong Kong; ^(b) Department of Physics, The University of Hong Kong, Hong Kong; ^(c) Department of Physics, The Hong Kong University of Science and Technology, Clear Water Bay, Kowloon, Hong Kong, China
⁶¹ Department of Physics, Indiana University, Bloomington IN, United States of America
⁶² Institut für Astro- und Teilchenphysik, Leopold-Franzens-Universität, Innsbruck, Austria
⁶³ University of Iowa, Iowa City IA, United States of America
⁶⁴ Department of Physics and Astronomy, Iowa State University, Ames IA, United States of America
⁶⁵ Joint Institute for Nuclear Research, JINR Dubna, Dubna, Russia
⁶⁶ KEK, High Energy Accelerator Research Organization, Tsukuba, Japan
⁶⁷ Graduate School of Science, Kobe University, Kobe, Japan
⁶⁸ Faculty of Science, Kyoto University, Kyoto, Japan
⁶⁹ Kyoto University of Education, Kyoto, Japan
⁷⁰ Department of Physics, Kyushu University, Fukuoka, Japan
⁷¹ Instituto de Física La Plata, Universidad Nacional de La Plata and CONICET, La Plata, Argentina
⁷² Physics Department, Lancaster University, Lancaster, United Kingdom

- ⁷³ ^(a) INFN Sezione di Lecce; ^(b) Dipartimento di Matematica e Fisica, Università del Salento, Lecce, Italy
⁷⁴ Oliver Lodge Laboratory, University of Liverpool, Liverpool, United Kingdom
⁷⁵ Department of Physics, Jožef Stefan Institute and University of Ljubljana, Ljubljana, Slovenia
⁷⁶ School of Physics and Astronomy, Queen Mary University of London, London, United Kingdom
⁷⁷ Department of Physics, Royal Holloway University of London, Surrey, United Kingdom
⁷⁸ Department of Physics and Astronomy, University College London, London, United Kingdom
⁷⁹ Louisiana Tech University, Ruston LA, United States of America
⁸⁰ Laboratoire de Physique Nucléaire et de Hautes Energies, UPMC and Université Paris-Diderot and CNRS/IN2P3, Paris, France
⁸¹ Fysiska institutionen, Lunds universitet, Lund, Sweden
⁸² Departamento de Fisica Teorica C-15, Universidad Autonoma de Madrid, Madrid, Spain
⁸³ Institut für Physik, Universität Mainz, Mainz, Germany
⁸⁴ School of Physics and Astronomy, University of Manchester, Manchester, United Kingdom
⁸⁵ CPPM, Aix-Marseille Université and CNRS/IN2P3, Marseille, France
⁸⁶ Department of Physics, University of Massachusetts, Amherst MA, United States of America
⁸⁷ Department of Physics, McGill University, Montreal QC, Canada
⁸⁸ School of Physics, University of Melbourne, Victoria, Australia
⁸⁹ Department of Physics, The University of Michigan, Ann Arbor MI, United States of America
⁹⁰ Department of Physics and Astronomy, Michigan State University, East Lansing MI, United States of America
⁹¹ ^(a) INFN Sezione di Milano; ^(b) Dipartimento di Fisica, Università di Milano, Milano, Italy
⁹² B.I. Stepanov Institute of Physics, National Academy of Sciences of Belarus, Minsk, Republic of Belarus
⁹³ National Scientific and Educational Centre for Particle and High Energy Physics, Minsk, Republic of Belarus
⁹⁴ Department of Physics, Massachusetts Institute of Technology, Cambridge MA, United States of America
⁹⁵ Group of Particle Physics, University of Montreal, Montreal QC, Canada
⁹⁶ P.N. Lebedev Institute of Physics, Academy of Sciences, Moscow, Russia
⁹⁷ Institute for Theoretical and Experimental Physics (ITEP), Moscow, Russia
⁹⁸ National Research Nuclear University MEPhI, Moscow, Russia
⁹⁹ D.V. Skobeltsyn Institute of Nuclear Physics, M.V. Lomonosov Moscow State University, Moscow, Russia
¹⁰⁰ Fakultät für Physik, Ludwig-Maximilians-Universität München, München, Germany
¹⁰¹ Max-Planck-Institut für Physik (Werner-Heisenberg-Institut), München, Germany
¹⁰² Nagasaki Institute of Applied Science, Nagasaki, Japan
¹⁰³ Graduate School of Science and Kobayashi-Maskawa Institute, Nagoya University, Nagoya, Japan
¹⁰⁴ ^(a) INFN Sezione di Napoli; ^(b) Dipartimento di Fisica, Università di Napoli, Napoli, Italy
¹⁰⁵ Department of Physics and Astronomy, University of New Mexico, Albuquerque NM, United States of America
¹⁰⁶ Institute for Mathematics, Astrophysics and Particle Physics, Radboud University Nijmegen/Nikhef, Nijmegen, Netherlands
¹⁰⁷ Nikhef National Institute for Subatomic Physics and University of Amsterdam, Amsterdam, Netherlands
¹⁰⁸ Department of Physics, Northern Illinois University, DeKalb IL, United States of America
¹⁰⁹ Budker Institute of Nuclear Physics, SB RAS, Novosibirsk, Russia

- ¹¹⁰ Department of Physics, New York University, New York NY, United States of America
¹¹¹ Ohio State University, Columbus OH, United States of America
¹¹² Faculty of Science, Okayama University, Okayama, Japan
¹¹³ Homer L. Dodge Department of Physics and Astronomy, University of Oklahoma, Norman OK, United States of America
¹¹⁴ Department of Physics, Oklahoma State University, Stillwater OK, United States of America
¹¹⁵ Palacký University, RCPTM, Olomouc, Czech Republic
¹¹⁶ Center for High Energy Physics, University of Oregon, Eugene OR, United States of America
¹¹⁷ LAL, Université Paris-Sud and CNRS/IN2P3, Orsay, France
¹¹⁸ Graduate School of Science, Osaka University, Osaka, Japan
¹¹⁹ Department of Physics, University of Oslo, Oslo, Norway
¹²⁰ Department of Physics, Oxford University, Oxford, United Kingdom
¹²¹ ^(a) INFN Sezione di Pavia; ^(b) Dipartimento di Fisica, Università di Pavia, Pavia, Italy
¹²² Department of Physics, University of Pennsylvania, Philadelphia PA, United States of America
¹²³ National Research Centre "Kurchatov Institute" B.P.Konstantinov Petersburg Nuclear Physics Institute, St. Petersburg, Russia
¹²⁴ ^(a) INFN Sezione di Pisa; ^(b) Dipartimento di Fisica E. Fermi, Università di Pisa, Pisa, Italy
¹²⁵ Department of Physics and Astronomy, University of Pittsburgh, Pittsburgh PA, United States of America
¹²⁶ ^(a) Laboratório de Instrumentação e Física Experimental de Partículas - LIP, Lisboa; ^(b) Faculdade de Ciências, Universidade de Lisboa, Lisboa; ^(c) Department of Physics, University of Coimbra, Coimbra; ^(d) Centro de Física Nuclear da Universidade de Lisboa, Lisboa; ^(e) Departamento de Física, Universidade do Minho, Braga; ^(f) Departamento de Física Teórica y del Cosmos and CAFPE, Universidad de Granada, Granada (Spain); ^(g) Dep Física and CEFITEC of Faculdade de Ciencias e Tecnologia, Universidade Nova de Lisboa, Caparica, Portugal
¹²⁷ Institute of Physics, Academy of Sciences of the Czech Republic, Praha, Czech Republic
¹²⁸ Czech Technical University in Prague, Praha, Czech Republic
¹²⁹ Faculty of Mathematics and Physics, Charles University in Prague, Praha, Czech Republic
¹³⁰ State Research Center Institute for High Energy Physics (Protvino), NRC KI, Russia, Russia
¹³¹ Particle Physics Department, Rutherford Appleton Laboratory, Didcot, United Kingdom
¹³² ^(a) INFN Sezione di Roma; ^(b) Dipartimento di Fisica, Sapienza Università di Roma, Roma, Italy
¹³³ ^(a) INFN Sezione di Roma Tor Vergata; ^(b) Dipartimento di Fisica, Università di Roma Tor Vergata, Roma, Italy
¹³⁴ ^(a) INFN Sezione di Roma Tre; ^(b) Dipartimento di Matematica e Fisica, Università Roma Tre, Roma, Italy
¹³⁵ ^(a) Faculté des Sciences Ain Chock, Réseau Universitaire de Physique des Hautes Energies - Université Hassan II, Casablanca; ^(b) Centre National de l'Energie des Sciences Techniques Nucléaires, Rabat; ^(c) Faculté des Sciences Semlalia, Université Cadi Ayyad, LPHEA-Marrakech; ^(d) Faculté des Sciences, Université Mohamed Premier and LPTPM, Oujda; ^(e) Faculté des sciences, Université Mohammed V, Rabat, Morocco
¹³⁶ DSM/IRFU (Institut de Recherches sur les Lois Fondamentales de l'Univers), CEA Saclay (Commissariat à l'Energie Atomique et aux Energies Alternatives), Gif-sur-Yvette, France
¹³⁷ Santa Cruz Institute for Particle Physics, University of California Santa Cruz, Santa Cruz CA, United States of America
¹³⁸ Department of Physics, University of Washington, Seattle WA, United States of America
¹³⁹ Department of Physics and Astronomy, University of Sheffield, Sheffield, United Kingdom
¹⁴⁰ Department of Physics, Shinshu University, Nagano, Japan

- ¹⁴¹ Fachbereich Physik, Universität Siegen, Siegen, Germany
- ¹⁴² Department of Physics, Simon Fraser University, Burnaby BC, Canada
- ¹⁴³ SLAC National Accelerator Laboratory, Stanford CA, United States of America
- ¹⁴⁴ ^(a) Faculty of Mathematics, Physics & Informatics, Comenius University, Bratislava; ^(b) Department of Subnuclear Physics, Institute of Experimental Physics of the Slovak Academy of Sciences, Kosice, Slovak Republic
- ¹⁴⁵ ^(a) Department of Physics, University of Cape Town, Cape Town; ^(b) Department of Physics, University of Johannesburg, Johannesburg; ^(c) School of Physics, University of the Witwatersrand, Johannesburg, South Africa
- ¹⁴⁶ ^(a) Department of Physics, Stockholm University; ^(b) The Oskar Klein Centre, Stockholm, Sweden
- ¹⁴⁷ Physics Department, Royal Institute of Technology, Stockholm, Sweden
- ¹⁴⁸ Departments of Physics & Astronomy and Chemistry, Stony Brook University, Stony Brook NY, United States of America
- ¹⁴⁹ Department of Physics and Astronomy, University of Sussex, Brighton, United Kingdom
- ¹⁵⁰ School of Physics, University of Sydney, Sydney, Australia
- ¹⁵¹ Institute of Physics, Academia Sinica, Taipei, Taiwan
- ¹⁵² Department of Physics, Technion: Israel Institute of Technology, Haifa, Israel
- ¹⁵³ Raymond and Beverly Sackler School of Physics and Astronomy, Tel Aviv University, Tel Aviv, Israel
- ¹⁵⁴ Department of Physics, Aristotle University of Thessaloniki, Thessaloniki, Greece
- ¹⁵⁵ International Center for Elementary Particle Physics and Department of Physics, The University of Tokyo, Tokyo, Japan
- ¹⁵⁶ Graduate School of Science and Technology, Tokyo Metropolitan University, Tokyo, Japan
- ¹⁵⁷ Department of Physics, Tokyo Institute of Technology, Tokyo, Japan
- ¹⁵⁸ Department of Physics, University of Toronto, Toronto ON, Canada
- ¹⁵⁹ ^(a) TRIUMF, Vancouver BC; ^(b) Department of Physics and Astronomy, York University, Toronto ON, Canada
- ¹⁶⁰ Faculty of Pure and Applied Sciences, and Center for Integrated Research in Fundamental Science and Engineering, University of Tsukuba, Tsukuba, Japan
- ¹⁶¹ Department of Physics and Astronomy, Tufts University, Medford MA, United States of America
- ¹⁶² Centro de Investigaciones, Universidad Antonio Narino, Bogota, Colombia
- ¹⁶³ Department of Physics and Astronomy, University of California Irvine, Irvine CA, United States of America
- ¹⁶⁴ ^(a) INFN Gruppo Collegato di Udine, Sezione di Trieste, Udine; ^(b) ICTP, Trieste; ^(c) Dipartimento di Chimica, Fisica e Ambiente, Università di Udine, Udine, Italy
- ¹⁶⁵ Department of Physics, University of Illinois, Urbana IL, United States of America
- ¹⁶⁶ Department of Physics and Astronomy, University of Uppsala, Uppsala, Sweden
- ¹⁶⁷ Instituto de Física Corpuscular (IFIC) and Departamento de Física Atómica, Molecular y Nuclear and Departamento de Ingeniería Electrónica and Instituto de Microelectrónica de Barcelona (IMB-CNM), University of Valencia and CSIC, Valencia, Spain
- ¹⁶⁸ Department of Physics, University of British Columbia, Vancouver BC, Canada
- ¹⁶⁹ Department of Physics and Astronomy, University of Victoria, Victoria BC, Canada
- ¹⁷⁰ Department of Physics, University of Warwick, Coventry, United Kingdom
- ¹⁷¹ Waseda University, Tokyo, Japan
- ¹⁷² Department of Particle Physics, The Weizmann Institute of Science, Rehovot, Israel
- ¹⁷³ Department of Physics, University of Wisconsin, Madison WI, United States of America
- ¹⁷⁴ Fakultät für Physik und Astronomie, Julius-Maximilians-Universität, Würzburg, Germany

- ¹⁷⁵ Fachbereich C Physik, Bergische Universität Wuppertal, Wuppertal, Germany
¹⁷⁶ Department of Physics, Yale University, New Haven CT, United States of America
¹⁷⁷ Yerevan Physics Institute, Yerevan, Armenia
¹⁷⁸ Centre de Calcul de l’Institut National de Physique Nucléaire et de Physique des Particules (IN2P3), Villeurbanne, France
^a Also at Department of Physics, King’s College London, London, United Kingdom
^b Also at Institute of Physics, Azerbaijan Academy of Sciences, Baku, Azerbaijan
^c Also at Novosibirsk State University, Novosibirsk, Russia
^d Also at TRIUMF, Vancouver BC, Canada
^e Also at Department of Physics & Astronomy, University of Louisville, Louisville, KY, United States of America
^f Also at Department of Physics, California State University, Fresno CA, United States of America
^g Also at Department of Physics, University of Fribourg, Fribourg, Switzerland
^h Also at Departamento de Fisica e Astronomia, Faculdade de Ciencias, Universidade do Porto, Portugal
ⁱ Also at Tomsk State University, Tomsk, Russia
^j Also at CPPM, Aix-Marseille Université and CNRS/IN2P3, Marseille, France
^k Also at Universita di Napoli Parthenope, Napoli, Italy
^l Also at Institute of Particle Physics (IPP), Canada
^m Also at Particle Physics Department, Rutherford Appleton Laboratory, Didcot, United Kingdom
ⁿ Also at Department of Physics, St. Petersburg State Polytechnical University, St. Petersburg, Russia
^o Also at Department of Physics, The University of Michigan, Ann Arbor MI, United States of America
^p Also at Louisiana Tech University, Ruston LA, United States of America
^q Also at Institutio Catalana de Recerca i Estudis Avancats, ICREA, Barcelona, Spain
^r Also at Graduate School of Science, Osaka University, Osaka, Japan
^s Also at Department of Physics, National Tsing Hua University, Taiwan
^t Also at Department of Physics, The University of Texas at Austin, Austin TX, United States of America
^u Also at Institute of Theoretical Physics, Ilia State University, Tbilisi, Georgia
^v Also at CERN, Geneva, Switzerland
^w Also at Georgian Technical University (GTU), Tbilisi, Georgia
^x Also at Ochadai Academic Production, Ochanomizu University, Tokyo, Japan
^y Also at Manhattan College, New York NY, United States of America
^z Also at Hellenic Open University, Patras, Greece
^{aa} Also at Institute of Physics, Academia Sinica, Taipei, Taiwan
^{ab} Also at LAL, Université Paris-Sud and CNRS/IN2P3, Orsay, France
^{ac} Also at Academia Sinica Grid Computing, Institute of Physics, Academia Sinica, Taipei, Taiwan
^{ad} Also at School of Physics, Shandong University, Shandong, China
^{ae} Also at Moscow Institute of Physics and Technology State University, Dolgoprudny, Russia
^{af} Also at Section de Physique, Université de Genève, Geneva, Switzerland
^{ag} Also at International School for Advanced Studies (SISSA), Trieste, Italy
^{ah} Also at Department of Physics and Astronomy, University of South Carolina, Columbia SC, United States of America
^{ai} Also at School of Physics and Engineering, Sun Yat-sen University, Guangzhou, China
^{aj} Also at Faculty of Physics, M.V.Lomonosov Moscow State University, Moscow, Russia
^{ak} Also at National Research Nuclear University MEPhI, Moscow, Russia
^{al} Also at Department of Physics, Stanford University, Stanford CA, United States of America
^{am} Also at Institute for Particle and Nuclear Physics, Wigner Research Centre for Physics, Budapest, Hungary

an Also at University of Malaya, Department of Physics, Kuala Lumpur, Malaysia

* Deceased